

## ABSTRACT

### Advanced Kinetic Studies of Novel, Non-peptidic Thiosemicarbazone Inhibitors of Cathepsin B

Lindsey Snyder

Director: Mary Lynn Trawick, Ph.D

The lysosomal cysteine protease cathepsin B is considered to be an attractive target for the synthesis of anticancer drugs due to its over-expression in cancerous cells and its involvement in tumor formation. Among its many roles in the advancement of several pathological events including Arthritis and Alzheimer's disease, cathepsin B is primarily responsible for initiating cancer metastasis as it facilitates the degradation of the extracellular matrix. In order to impede the process of angiogenesis and to prevent the spread of cancerous cells, this study aims to identify an effective, non-toxic inhibitor of cathepsin B from a library of novel, non-peptidic thiosemicarbazone (TSC) compounds which have shown to be effective inhibitors of the cysteine protease cathepsin L. To evaluate the compounds' inhibitory effects, the concentration of the TSC inhibitors causing a 50% reduction in enzymatic activity ( $IC_{50}$  value) was determined. After an optimization of assay conditions, experiments were performed in a 96-well microplate using the substrate Z-arginyllarginyl-aminomethylcoumarin which reacts with cathepsin B and releases the fluorescent product, aminomethylcoumarin. Advanced kinetic studies of

the most potent inhibitors were performed to determine the compounds' mechanism of action. All three of the compounds studied exhibited reversible inhibition. Two of these inhibitors, a bromo-substituted, acetylated phenolic benzophenone TSC and a bromo-substituted, di-trifluoromethyl benzophenone TSC exhibited time dependent inhibition; whereas, the monohydroxy-tetramethoxy-substituted benzophenone TSC displayed classical competitive inhibition against cathepsin B activity. By developing a database consisting of TSC compounds with  $IC_{50}$  values in the low micromolar to nanomolar range, it is possible to examine the kinetics and structure-activity relationship of TSC inhibitors which could potentially be used medically to decrease tumor progression and cancer metastasis. These studies represent a collaborative project between the Trawick (biochemical) and Pinney (synthetic) Laboratories.

APPROVED BY DIRECTOR OF HONORS THESIS:

---

Dr. Mary Lynn Trawick, Department of Chemistry and  
Biochemistry

APPROVED BY THE HONORS PROGRAM:

---

Dr. Andrew Wisely, Director

DATE: \_\_\_\_\_

ADVANCED KINETIC STUDIES OF NOVEL, NON-PEPTIDIC  
THIOSEMICARBAZONE INHIBITORS OF CATHEPSIN B

A Thesis Submitted to the Faculty of  
Baylor University  
In Partial Fulfillment of the Requirements for the  
Honors Program

By  
Lindsey Snyder

Waco, TX

May 2012

## TABLE OF CONTENTS

Acknowledgments.....	v
Dedication.....	vii
List of Abbreviations.....	viii
Chapter One.....	1
Introduction.....	1
Background.....	1
Processing of Cathepsin B.....	4
Amino Acid Sequence of Cathepsin B.....	9
Structure of Cathepsin B.....	10
Mechanism of Action.....	12
Review of Literature.....	13
Types of Inhibitors.....	13
Binding of an Inhibitor to Cathepsin B.....	16
Recent Examples of Inhibitors of Cathepsin B.....	18
Project Overview.....	22
Fluorescence.....	23
Chapter Two.....	26
Materials and Methods.....	26
Materials.....	26
Protocols.....	26
Assay Conditions.....	29

Methods.....	30
Structures of Thiosemicarbazone Compounds.....	30
Cathepsin B Assay.....	33
IC <sub>50</sub> Determination .....	33
Michealis-Menten Kinetics.....	35
Time Dependence Curves.....	37
Progress Curves.....	38
Varying Pre-incubation Time.....	38
Reversibility.....	39
Protocol for Operating the Ascent Fluoroskan Microplate Reader.....	40
Fluoromax-2 Assay Conditions.....	46
Chapter Three.....	47
Results.....	47
Preliminary Kinetic Studies .....	48
Strategy for Determining Effective Inhibitors of Cathepsin B.....	51
IC <sub>50</sub> Determination of Compound <b>7</b> .....	56
IC <sub>50</sub> Determination of Compound <b>1</b> .....	58
IC <sub>50</sub> Determination of Compound <b>12</b> .....	59
IC <sub>50</sub> Determination of Compound <b>13</b> .....	60
IC <sub>50</sub> Determination of Compound <b>14</b> .....	61
Advanced Kinetics for Compound <b>12</b> .....	62
Advanced Kinetics for Compound <b>13</b> .....	70
Advanced Kinetics for Compound <b>14</b> .....	76

Conclusion.....	77
Future Work.....	79
Appendix A.....	81
Appendix B.....	86
Appendix C.....	116
References.....	123

## ACKNOWLEDGMENTS

I would like to thank my advisor, Dr. Mary Lynn Trawick, for giving me the opportunity to work in her laboratory. I am especially grateful for the guidance and advice she has given me over the past three years. I appreciate her willingness to help me throughout this process and her dedication to help me succeed.

I want to thank Amanda Charlton-Sevcik who trained me and supported me. I thoroughly enjoyed working with Amanda, and I have learned so much from her. I thank Amanda for being a great teacher and also a good friend. I am so grateful for her patience and encouragement. Thank you, Amanda, for the time you spent advising me, teaching me, and getting to know me.

I am very grateful for my family for their love and support. I want to thank my parents for their encouragement which was a continual source of motivation. I wish to thank my sister, who inspires me and who always offers reassuring words.

I thank Victoria Soeung who I've had the pleasure to work with on this project. I am grateful for Victoria's kindness, sweet spirit, and her willingness to help me. It has been a blessing to work with such a compassionate and talented individual.

I want to thank all the members of Dr. Trawick's research group who I've enjoyed getting to know over the course of my undergraduate career. I am fortunate to have learned from such a talented group. I am also appreciative of Dr. Kevin G. Pinney and his colleagues who helped in this collaborative project by synthesizing the thiosemicarbazone compounds.

I am appreciative of the professors that I've had at Baylor University who have shaped my academic career, and I am grateful for their knowledge and commitment to education.



I also thank Dr. Michelle Nemec and the Baylor Molecular Bioscience center for use of their facility and instrumentation. Finally, I thank Oxigene, Inc. for support of this research.

## DEDICATION

*To*

*My loving parents, Don and Beth*

*My wonderful sister, Holly*

*With love*

## LIST OF ABBREVIATIONS

**Z-R-R-AMC** – Z(benzyloxycarbonyl)-Arg-Arg-AMC(7-amino-4-methylcoumarin)

**AMC** - 7-amino-4-methylcoumarin

**ECM** – Extracellular matrix

**IC<sub>50</sub>** – Half maximal inhibitory concentration

**EC<sub>50</sub>** – Effective half maximal inhibitory concentration

**TSC** – Thiosemicarbazone

**DTT** – Dithiothreitol

**K<sub>m</sub>** – Concentration of substrate that leads to half-maximal velocity

**V<sub>max</sub>** – Limiting velocity as substrate concentrations get large

**RFU** – Relative fluorescence units

**Fc** – Final concentration

**Na<sub>2</sub>HPO<sub>4</sub>** - Sodium phosphate

**DMSO** – Dimethyl sulfoxide

**EDTA** – Ethylenediaminetetraacetic acid

**AB<sub>1</sub>** – Assay Buffer 1

**AB<sub>2</sub>** – Assay Buffer 2

**AB<sub>3</sub>** – Assay Buffer 3

**MW** – Molecular weight

**°C** – Degrees Celsius

**uPAR** – Urokinase-type plasminogen activator receptor

**Cmpd** - Compound

**K<sub>i</sub><sup>app</sup>** – Apparent inhibition constant

**[E]** – Enzyme concentration

**[I]** – Inhibitor concentration

**$v_i$**  – Reaction velocity with inhibitor present

**$v_0$**  – Reaction velocity without inhibitor present

**Preinc.** – Preincubation time

**Conc** – Concentration

## CHAPTER ONE

### Introduction

#### *Background*

Cancer results from the uncontrolled growth of abnormal cells by which the fundamental processes of orderly cell death and apoptosis are repressed. This unregulated cellular growth generates a mass of abnormal cells that are capable of invading surrounding tissues. The aggregation of these cells causes tumor formation and the successive dissipation of these cancerous cells stimulates the process of metastasis wherein a new cancer foci forms at a location distant from the initiation site (Coghlin and Murray, 2010). It has been reported that approximately 90% of the deaths of cancer patients are due to the formation of metastatic growths distant to the location where the tumor originated (Bialas and Kafarski, 2009). Therefore, the major player involved in cancer metastasis is tumor growth. When a tumor reaches a certain critical size, it no longer has a direct supply of oxygen and nutrients. To counteract this problem, new blood vessels form around the tumor and provide new routes for nutrient travel and thus facilitate the process of angiogenesis. Subsequently, the new blood vessels allow for easy migration of the tumor cells into the bloodstream (Baeriswyl and Christofori, 2009). If tumor development can be controlled, the potential for metastatic progression and angiogenesis can be minimized. The current treatments for tumorigenesis involve the removal of the tumor through invasive surgical procedures, and the destruction of the solid tissue mass through radiotherapy (Bialas and Kafarski, 2009). In order to prevent

tumor progression, our study seeks a therapeutic drug that can target and inhibit the enzymes involved in the process of tumorigenesis.

To understand how cancerous cells spread during the metastatic process, knowledge of the proteolytic enzymes known as proteases is required. Primarily responsible for the turnover of proteins within the cell, four classes of proteases (serine, matrix metalloproteinases, cysteine, and aspartate) have been implicated in cancer progression (Bialas and Kafarski, 2009). A remodeling of the cell's architecture is achieved through the proteases' degradation of extracellular matrix proteins such as collagen, fibronectin, and laminin (Vasijleva et al., 2007). This breakdown in the cell's outer matrix scaffold promotes the movement of cancerous cells and increases the cancer's metastatic potential. Therefore, the dysregulation of proteolytic enzymes is associated with the breakdown of normal cellular activities (Turk, 2006). A particular group of the proteolytic enzymes that is increasingly being studied are the cysteine cathepsins. There are eleven known human cysteine cathepsins that belong to the papain family of cysteine proteases (cathepsins B, C, F, H, L, K, O, S, V, X, and W) (Turk et al., 2003). Cysteine cathepsins participate in a variety of processes including bone remodeling, protein turnover, tumor progression, antigen presentation, apoptosis, and angiogenesis (Vasiljeva et al., 2007). In normal, healthy cells, the cysteine proteases are highly regulated through the activity of two of the proteases' endogenous inhibitors classified as the cystatins or stefins. These natural inhibitors aid in the maintenance of the cathepsins' normal metabolic functions of protein turnover and apoptosis. However, a disruption in a protease's regulation can lead to several pathologies. For example, an overexpression of

the lysosomal cysteine protease, cathepsin B, has been linked to cardiovascular disease, arthritis, Alzheimer's disease and cancer metastasis.

Our current study is concerned with a particular cysteine protease, cathepsin B which can be found in the lysosome of the cell and in the extracellular matrix (ECM). Once marked as "suicide bags" whose sole function was to engulf and degrade cellular material, lysosomes are now viewed as fundamental players in the fate of the cell and in tumor development (Tardy et al., 2006). Lysosomes are important components of the cell since they contain nucleases, peptidases, lipases, and proteases which are all necessary in the process of degradation and digestion of macromolecules (Kirkegaard and Jaattela, 2009). Curiously, lysosomes are both pro-oncogenic and anti-oncogenic. If the cathepsins are released intracellularly, they assist in the death of cancer cells and aid in protein turnover, but if the cathepsins are secreted in elevated concentrations outside of the cell, they can participate in the breakdown of the ECM and contribute to the progression of angiogenesis.

Ubiquitous in several types of tissues, cathepsin B acts as a multifunctional enzyme that has a major role in the degradation of the extracellular matrix (ECM) (Obermajer et al., 2008). Our study is primarily concerned with studying cathepsin B because of its association with cancer invasion and metastasis. For example, cathepsin B has been shown to be upregulated in a variety of cancers including melanoma, breast, colorectal, lung, brain, and prostate cancers (Jedeszko and Sloane, 2004). Acting as a cancer marker, a high serum level of cathepsin B is an indication of an unfavorable prognosis. During cancer development, the transformation of healthy cells to malignant cells leads to an increase in protease activity and the relocalization of cathepsin B. No longer

confined within the cell, cathepsin B participates in the degradation of the ECM. Because the ECM is an active participant in the cell's survival in that the cell cannot survive without adhesive contact, the deterioration of the ECM enables the invasion of tumor cells and can lead to cancer progression (Skrzydlewka et al., 2005). Cathepsin B's mechanism of action involves its direct attack on basement membrane protein components, and the degradation of these membrane constituents promotes the invasion and migration of malignant cells whose action serves as a prerequisite of metastasis. The breakdown of these proteins also initiates the upregulation of pro-angiogenic factors and simultaneously instigates the process of angiogenesis (Vasiljeva et al., 2007).

#### *Processing of Cathepsin B*

Like many proteases, cathepsin B is synthesized in an inactive precursor form as procathepsin B. This inactive enzyme is synthesized with a signal peptide for its production in the endoplasmic reticulum. In route to the Golgi apparatus, the prepeptide is removed and the proform is properly folded. Several post-translational modifications are performed inside the Golgi apparatus such as glycosylation (Caglic et al., 2007 and Brix et al., 2008). In its nascent state, procathepsin B is not entirely inactive in that it retains low catalytic activity (Pungercar et al., 2009). In this form, the propeptide is situated along the active site and runs in the opposite orientation as its substrate. Although the zymogen's active site is present, it is not fully activated. A representation of cathepsin B's propeptide (shown in red) and its mature part (shown in blue) is demonstrated in Figure 1.



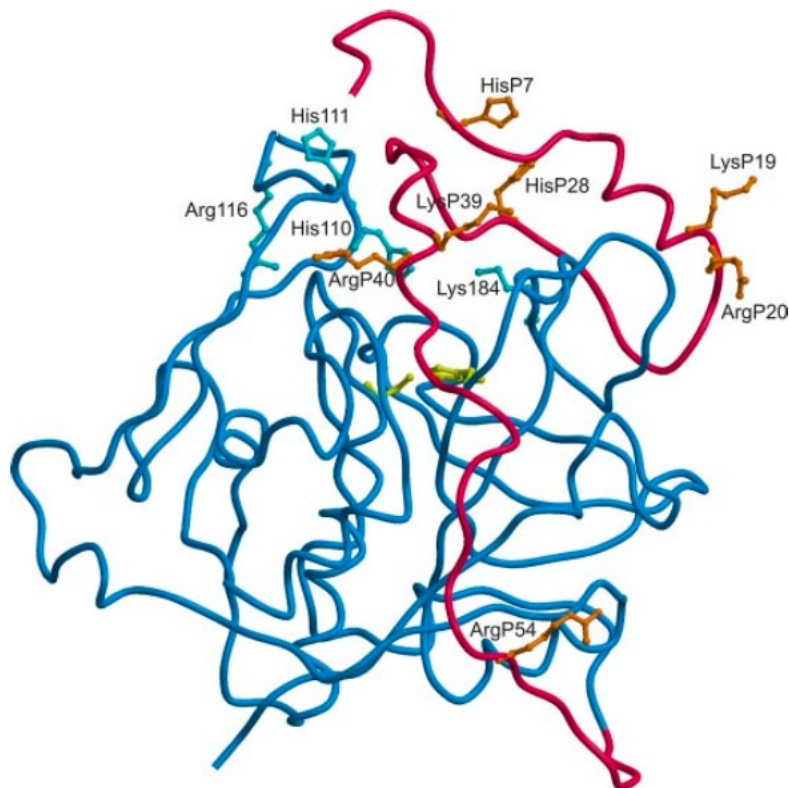


**Figure 1.** Representation of the structure of procathepsin B. The propeptide is shown in red and the mature enzyme is shown in blue. Reprinted with permission by the Copyright Permission Policy of the *Journal of Biological Chemistry*. Caglic et al., *J. Biol. Chem.* 2007, 282, 33076-33085.

After transfer to the lysosome, the processing of procathepsin B is initiated by the removal of the N-terminal propeptide that blocks the active site. The cleavage of this propeptide activates the enzyme; however, this activation step does not occur at a neutral pH since the propeptide also acts as an inhibitor. Inside the acidic milieu of the lysosome, the propeptide experiences a weaker affinity for the enzyme's mature region, and therefore, a decrease in the pH can autocatalytically generate the propeptide's cleavage from the mature part (Pungercar et al., 2009). Activation of the zymogen can also be achieved through an interaction with negatively charged glycosaminoglycans (GAGs) found on the surface of the cell (Caglic et al., 2007 and Pungercar et al., 2009).

The binding of GAGs to procathepsin B causes a conformational change that accelerates its activation by aiding in the removal of the zymogen's propeptide (Caglic et al., 2007). The electrostatic interactions between GAGs and procathepsin B make the zymogen a better substrate for cathepsin B (Caglic et al., 2007). Procathepsin B can also be activated by other cathepsins such as cathepsins D and G. Occasionally during cellular stress, cathepsin B leaks into the cytosol of the cell where it initiates apoptosis and protein turnover. Other times, cathepsin B is transported to the plasma membrane where it is secreted extracellularly (Brix et al., 2008).

Even though cathepsin B is seen as a major contributor to the degradation of the ECM, the process actually involves an elegantly orchestrated proteolytic cascade consisting of several types of proteases that act in an established sequence (Skrzydlewdka et al., 2005). During normal physiological conditions, a balance exists between cathepsin B and its endogenous inhibitors, but as was previously established, cancer development results in the overexpression of cathepsin B which triggers the proteolytic cascade depicted in Figure 2. As an upstream regulator in the proteolytic cascade, cathepsin B participates in the activation of both serine protease and metalloproteinase precursors known as pro-urokinase plasminogen activators (prouPA) and pro-matrix metalloproteinases (proMMPs). Studies have demonstrated that in cancer patients afflicted with tumorigenesis, a decreased level of the inhibitors of these proteases exists (Cavallo-Medved et al., 2005). Without the safeguard of the natural inhibitors, precursor proteases and their active forms accumulate along the tumor cell surface inside plasma membrane invaginations known as caveolae. It has been proposed that the structural protein, caveolin-1, is involved in the localization of cathepsin B and the urokinase

plasmingoen activator, uPA (Cavallo-Medved et al., 2005). By mediating the activity of these proteases, caveolin-1 promotes several proteolytic events occurring on the cell-surface (Cavallo-Medved et al., 2005). In caveolae, procathepsin B binds to the light chain of the annexin II heterotetramer, p11 (Obermajer et al., 2008 and Cavallo-Medved et al., 2005). It is suggested that p11 aids in the activation of procathepsin B and thus has an indirect role in the stimulation of cancer metastasis.

As depicted in Figure 2, in its active form, uPA, initiates the conversion of plasminogen to the active plasmin which targets and degrades the ECM. Plasmin is also capable of activating the zymogens of the matrix metalloproteinases which are directly involved in the breakdown of the ECM. Therefore, the ultimate outcome of this proteolytic cascade, which began with the activation of procathepsin B, results in a destabilization of the ECM. Without a secure scaffold, cancerous cells invade the ECM, and as the degradation process continues, the migration of these malignant cells results in cancer metastasis.

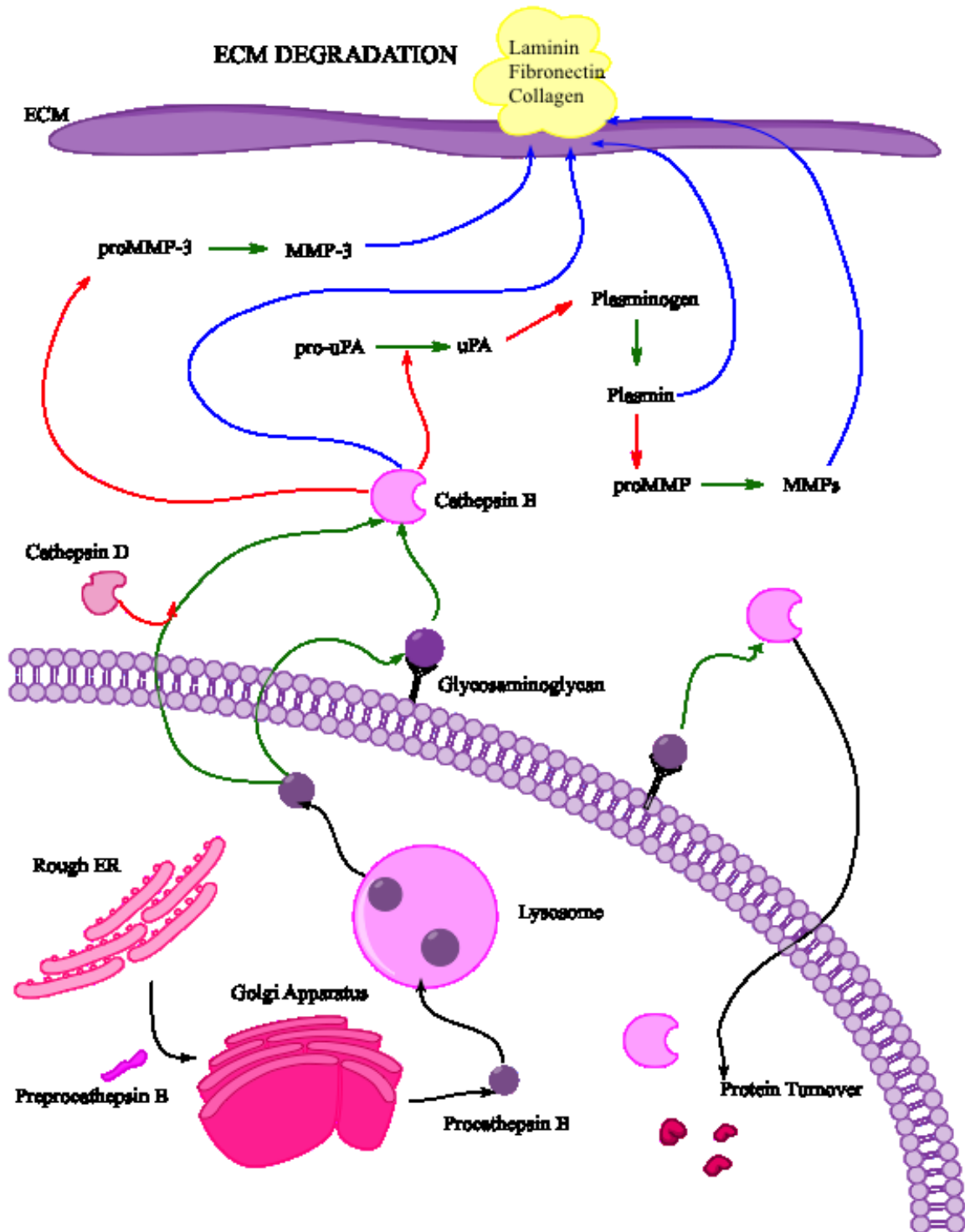


**Figure 2.** Cathepsin B role in ECM degradation recreated from Bialas et al. (CS ChemBioDraw Ultra).

Activators  
Activation Steps  
Direct degradation of ECM

In summary, several proteolytic events occur during the processing of cathepsin B to its mature form. For instance, there are multiple routes for the activation of procathepsin B. Procathepsin B can be transported from the lysosome to the cell surface where it is activated by GAGs, or if procathepsin B is situated inside the caveola, the p11 chain of the annexin II tetramer can activate procathepsin B. After the propeptide of procathepsin B is cleaved during the activation process, the protease initiates a proteolytic cascade which leads to the activation of the precursor proteins pro-uPA and plasminogen. This process results in the cathepsin's degradation of the ECM.

### *Amino Acid Sequence of Cathepsin B*

The amino acid sequence of Cathepsin B is displayed below in Figure 3. After cleavage of the propeptides, the mature cathepsin B consists of 254 amino acids.

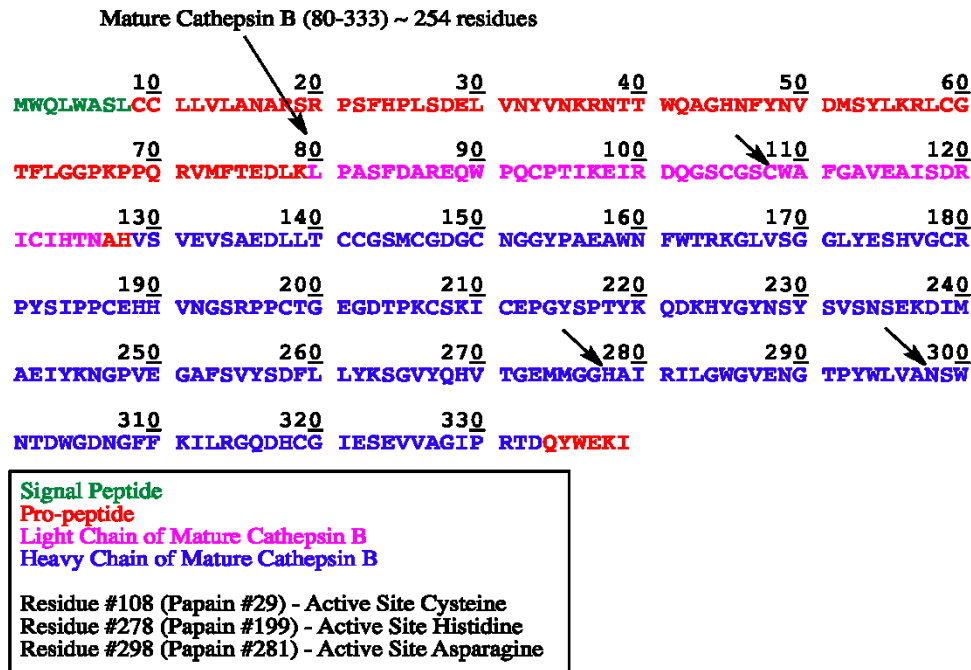


**Figure 3.** Amino acid sequence of cathepsin B (Modified from Uniprot.org)

### *Structure of Cathepsin B*

Mature cathepsin B is a 30kD bilobal protein comprised of 254 amino acid residues and has a diameter of approximately 50 Å (Musil et al., 1991). As a member of the cysteine protease family, human cathepsin B contains several cysteine residues that interact to form a total of 6 disulphide bridges which are depicted as green bonds in Figure 4 below (Musil et al., 1991). The active site of cathepsin B is characterized by a cysteine residue, and this residue, along with a histidine and an asparagine residue constitute the enzyme's catalytic triad. As shown below in Figure 4, the light chain (represented by a magenta color) is linked to the heavy chain (shown in blue) through a disulfide bond.

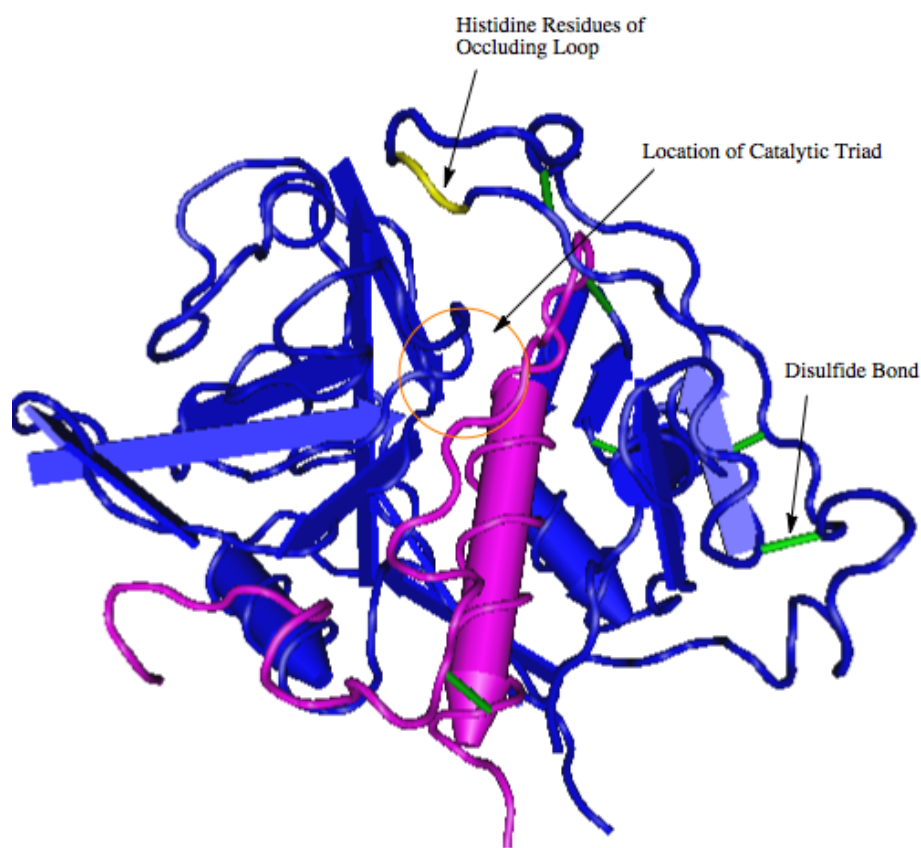


**Figure 4.** Structure of cathepsin B (National Center for Biotechnology Information).

In accordance with the cysteine proteases, cathepsin B's structure consists of a left and right domain separated by a 'V-shaped' active site slit (Turk et al., 2003). A central  $\alpha$ -helix characterizes the left domain and a  $\beta$ -barrel distinguishes the right domain. In Figure 4 above, the alpha helices are depicted as the three dimensional arrows whereas the beta sheets are represented by flat arrows.

Mammalian proteases share similar binding subsites that are numbered as S1-Sn and S1'-Sn' (Turk, 2006). Subsites refer to the surface of the protease that can bind substrate molecules (P1-Pn and P1'-Pn').

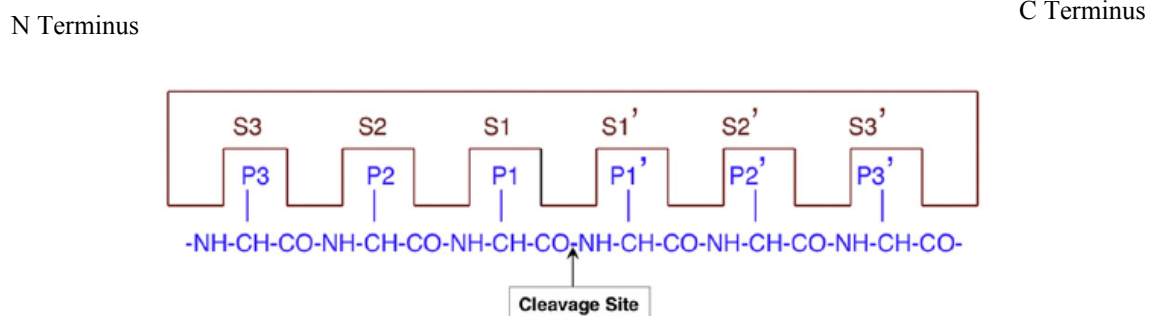


**Figure 5.** Configuration of the subsites of a protease (Hook et al., 2012). Reprinted with permission from Elsevier provided by Copyright Clearance Center, License #: 2861190750027.

Cathepsin B has a unique structure that separates it from other cysteine proteases in that it contains a flexible section consisting of approximately 20 residues which is known as the occluding loop. This loop blocks access to the active site cleft (Redzynia et al., 2008). Several important amino acids are present in the occluding loop of cathepsin B which is depicted in Figure 6. The positively charged His-111 binds to the C-terminus of an incoming substrate molecule whereas His-110 is involved in a salt bridge interaction

with Asp-22 (Redzynia et al., 2008). This salt bridge and the one between Arg-116 and Asp-224 govern the functioning of the occluding loop (Schenker et al., 2008). Because of its flexible nature, the occluding loop is responsible for the dual activity of cathepsin B in that it acts as both an exopeptidase and an endopeptidase. At low pH, the loop is in a closed conformation as two salt bridges hold it together (Schenker et al., 2008). In this closed position, cathepsin B can act as an exopeptidase. Alternatively, as the pH is raised, a residue on the loop, His-110 becomes deprotonated and the loop moves freely acting as an endopeptidase (Redzynia et al., 2008).

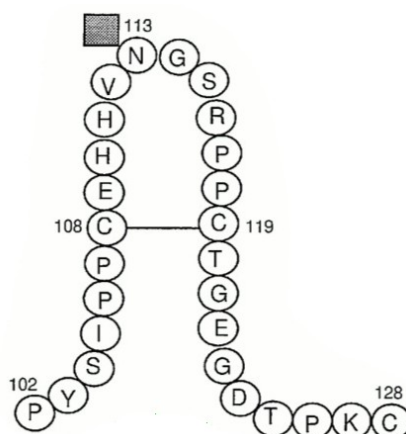


**Figure 6.** The occluding loop of Cathepsin B where the filled gray box indicates position of attachment of a N-linked oligosaccharide (Illy et al., 1997). Reprinted with permission from *The Journal of Biological Chemistry* via the Copyright Permission Policy.

### *Mechanism of Action*

A proposed mechanism of action for a cysteine protease is demonstrated below in figure 7. In this reaction, the cysteine residue is responsible for the nucleophilic attack on the protease's substrate, and the histidine residue serves as a proton donor. In the



mechanism below, the active site thiolate attacks the protease's substrate. This nucleophilic attack generates a tetrahedral intermediate which upon its collapse produces the first product of the reaction ( $\text{RNH}_2$ ). It has been proposed that in the next step, through the coupled activity of the histidine residue and the hydrolysis of the enzyme, the catalytic active site is regenerated.

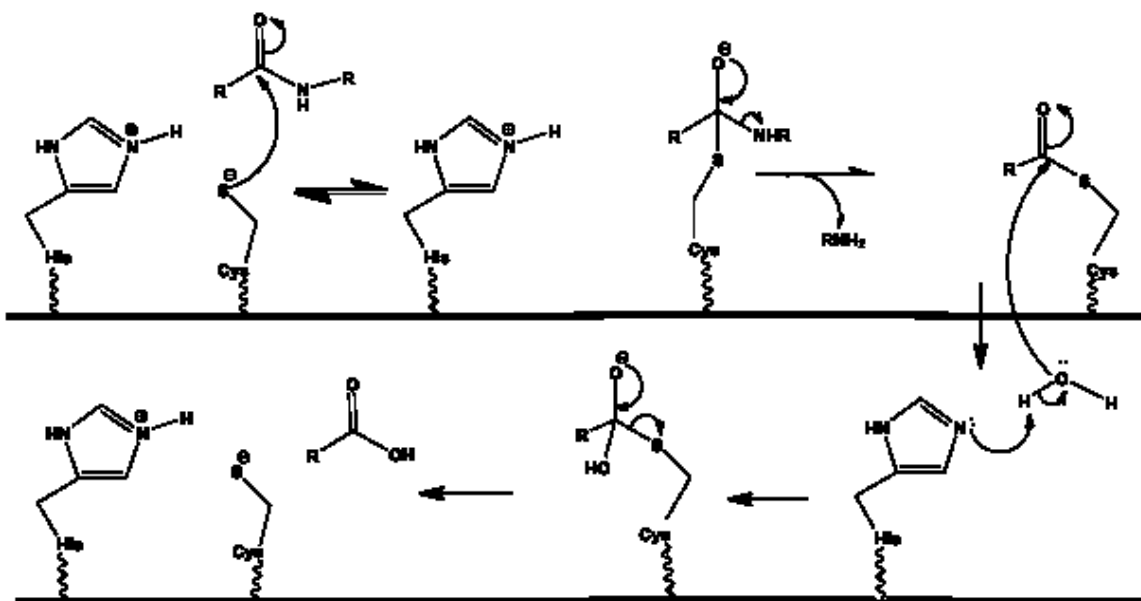


**Figure 7.** Proposed mechanism of action for a cysteine protease (ChemBioDraw)

### *Review of Literature*

Because proteases have many important functions, it is essential that they be controlled intracellularly in order to avoid destructive proteolysis. Thus, a precise balance exists between proteases and their endogenous inhibitors. If not regulated, proteolytic enzymes have the potential to harm the cell through their participation in excessive proteolysis. Because of their important role in preventing the over-activation of proteases, inhibitors have been seen as the primary “guardians” of the cell (Turk et al.,

2005). Acting as safeguards, inhibitors patrol the cell in order to impede the accidental escape of proteases in the lysosome. By effectively inhibiting proteases, inhibitors are also capable of indirectly affecting the proteolytic cascade. Therefore, most members of the protease family including cysteine and matrix metalloproteinases have their own endogenous inhibitors.

### *Different Types of Inhibitors*

According to the current literature, several different types of inhibitors exist. For example, emergency inhibitors are primarily used to target excess proteases that have escaped from the lysosome. Cells have a large supply of these inhibitors since they respond rapidly and prevent harmful proteolysis (Turk et al., 2005). The cysteine protease inhibitors called cystatins are viewed as emergency inhibitors since they protect the cell from proteases such as cathepsin B that have been accidentally released by the lysosome (Turk et al., 2005). Interestingly, like many other inhibitors, cystatins have low specificity, and since one inhibitor can bind to at least two different proteases, there is almost always an imbalance between the number of proteases and their inhibitors within the cell (Turk, 2006). Cystatins can also differentiate between exopeptidases and endopeptidases. In regards to cathepsin B and its occluding loop, cystatins must undergo structural changes before they can bind to the cathepsin's active site. Thus the binding sites of exopeptidases like cathepsin B are more difficult for inhibitors to access (Turk et al., 2005).

Because proteases and their inhibitors are housed in the same organelle, interaction between them is inevitable and must be monitored by another type of inhibitor called the

regulatory inhibitor. If not for this inhibitor, emergency inhibitors would automatically stop all protease activity. As their name suggests, regulatory inhibitors control the proteases' actions instead of simply destroying them (Turk et al., 2005). Threshold inhibitors bind rapidly to proteases and function as reinforcements in the case that many zymogens are activated at one time (Turk, 2006). Buffer-type inhibitors are reversible inhibitors that have a short stability time. In the presence of substrate, these inhibitors release enzymes so that they can bind to the substrate, but if no substrate is present, these inhibitors prevent the enzymes from being released (Turk et al., 2005). The final group of inhibitors is referred to as the delay-type inhibitors. They are irreversible inhibitors that slowly bind to proteases and only allow proteolysis to occur for a brief amount of time (Turk et al., 2005).

With medical applications being the primary concern, researchers are exploring whether large or small inhibitors are more effective for direct inhibition. Often, large inhibitors do not tightly bind to their protease targets and do not interact in a “substrate-like manner” (Turk et al., 2005). This incomplete binding creates structural strains on the enzyme-inhibitor complex. In order to avoid this potential problem, researchers are searching for ideal small molecule inhibitors that have remarkable “absorption, distribution, metabolism, excretion, and toxicology (ADMET)” (Turk, 2006). Since it is impossible to fulfill all of these requirements, there are also problems with a small molecule approach to inhibition. Small molecule inhibitors have been found to be nonspecific in that they cannot distinguish between different enzymes (Turk et al., 2005). In searching for an effective inhibitor of cathepsin B, the peptidic nature of the inhibitor is an important consideration. A nonpeptidic inhibitor is ideal because as

opposed to a compound containing peptide bonds, this type of inhibitor could more easily permeate cellular membranes.

Scientists have been studying potential cysteine protease inhibitors since the late 1970s. In 1978, Hanada et al. discovered a potent and irreversible inhibitor of these enzymes. Referred to as E-64, this inhibitor was isolated from *Aspergillus japonicus* and was found to strongly inhibit cathepsin B (Murata et al., 1991). Other derivatives of E-64 that selectively inhibit cathepsin B include a group of epoxysuccinyl peptides. Two of these novel inhibitors are referred to as CA-030 and CA-074 (Murata et al., 1991). These compounds inactivate cathepsin B through their epoxide group. It is suggested that the different substituents on CA-030 and CA-074 inactivate cathepsin B by binding to the cathepsin's occluding loop (Yamamoto et al., 2002). Unfortunately, the charged nature of the carboxylate group in CA-074 limits its use in *in vivo* studies since it cannot passively diffuse across the cell's membrane (Montaser et al., 2002). The structures of E-64, CA-030, and CA-074 are displayed in Table 1.

#### *Binding of an Inhibitor to Cathepsin B*

The typical binding motif between cathepsin B and an inhibitor is demonstrated in Figure 8. The left panel in Figure 8 displays the subsites (S1, S2, S3, S1', and S2') that are involved in the binding between a typical inhibitor and the protease's active site where the functional amino acids of cathepsin B are displayed with the stick model and the blue and red circles represent water and oxygen molecules (Watanabe et al., 2006). The right panel demonstrates the binding of an inhibitor known as CA-030 (see Table 1) to cathepsin B. In this example, the inhibitor is inserted vertically into the active site of

cathepsin B where it interacts with the enzyme's occluding loop and active-site thiolate. As demonstrated in both panels of Figure 8, each inhibitor binds with the histidine residues located in the enzyme's occluding loop. Specifically, the proline residue in CA030 binds to the occluding loop of cathepsin B through its interaction with the loop's positively charged histidine residues, His 110 and His 111. (Katunuma, 2011). Another common feature of the binding between cathepsin B and an inhibitor occurs near the S1 subsite wherein an oxyanion hole is stabilized by a glutamine residue (Gln 23 in Figure 8) which forms after the active-site thiolate's attack on its target. In order to create promising candidates for the inhibition of cathepsin B, it is essential to study the enzyme's fundamental binding mechanism. The creation of inhibition profiles like those in Figure 8 can provide insight into the specificities of binding between cathepsin B and its potential inhibitors.

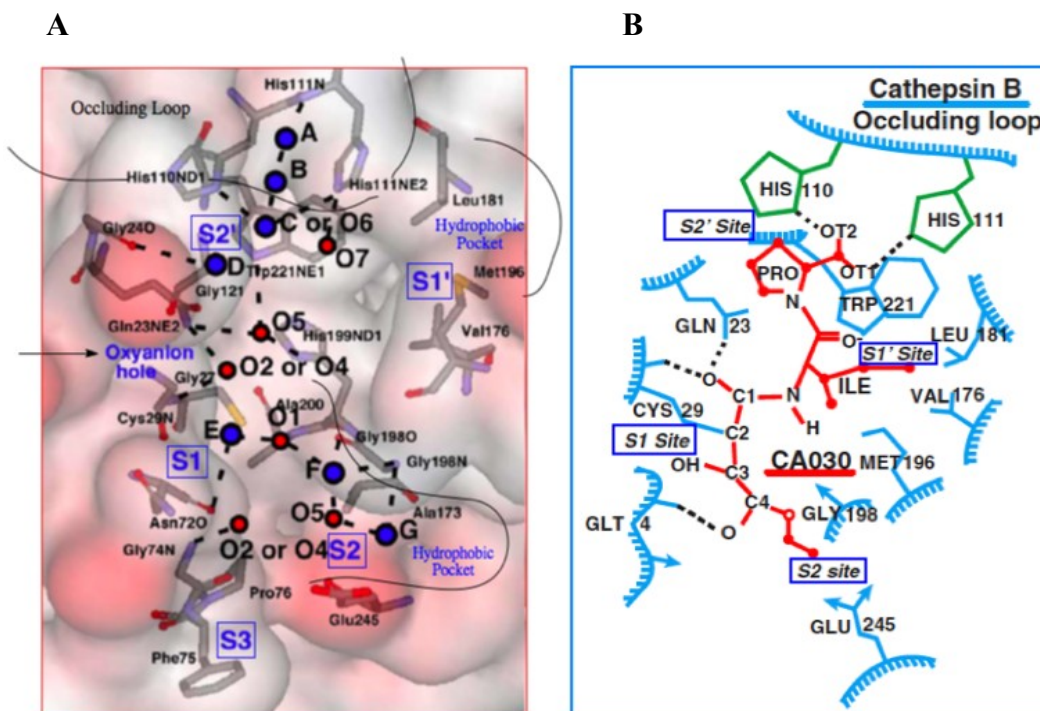


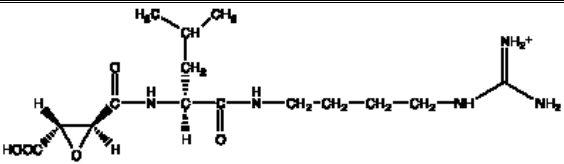
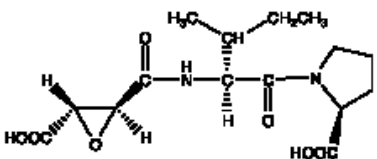
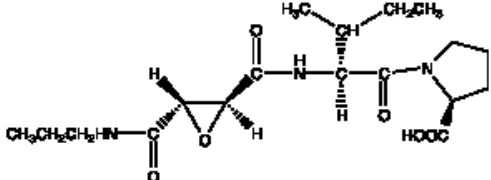
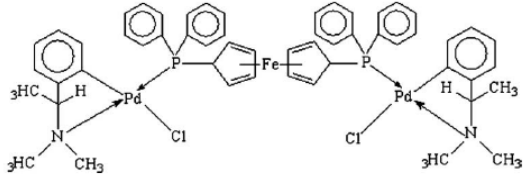
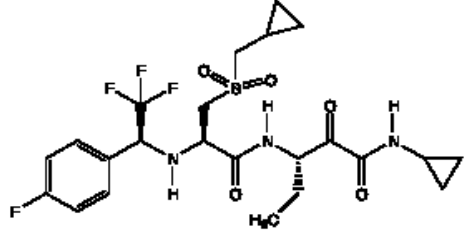
**Figure 8.** Example of typical binding between cathepsin B and an inhibitor (modified from Watanabe et al., 2006 and Katanuma, 2011). **A.** Reprinted with permission from Elsevier provided by Copyright Clearance Center, License #: 2818430228424. **B.** Reprinted with permission from *The Journal of Biological Chemistry* via the Copyright Permission Policy.

### *Recent Examples of Inhibitors of Cathepsin B*

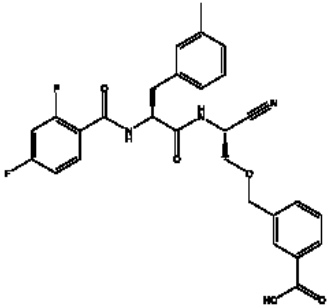
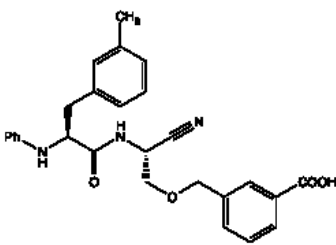
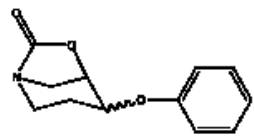
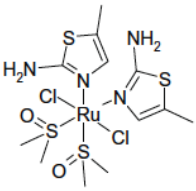
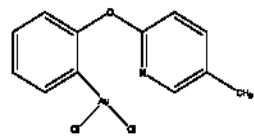
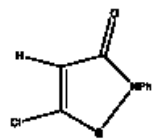
Several inhibitors of cathepsin B have been identified in recent years. The most accepted mode of inhibition requires that the inhibitor contain an electrophilic component that can bind to the enzyme's active cysteine thiol subsite (Leung-Toung et al., 2003). Often, these so called electrophilic warheads covalently bind to the enzyme and inactivate it by forming disulfide bonds (Leung-Toung et al., 2003). In the past decade, researchers have become interested in testing metallopharmaceuticals for inhibition against cathepsin B. For example, compounds containing gold (II), ruthenium (III), and tellurium (IV) have been shown to inhibit cathepsin B. (Mura et al., 2010; Zhu et al., 2011; Cunha et al., 2009). It has been hypothesized that the metals in these compounds

coordinate with the enzyme's catalytic triad thus inactivating the active site. (Mura et al., 2010). Noncompetitive inhibition has also been observed as in the case of the cathepsin B inhibitor isolated from the microorganism *Pseudomonas*. However, given that the  $IC_{50}$  value for this inhibitor was in the millimolar range, it does not appear to be an effective inhibitor of cathepsin B (Hoang et al., 2008). For successful *in vivo* toxicity studies, it is important that potential inhibitors exhibit  $IC_{50}$  values in the micromolar to nanomolar range. Several of the inhibitors displayed in Table 1 may appear to be promising therapeutic drug targets, but each needs to be extensively studied in order to access toxicity levels and bioavailability. Although a very effective inhibitor of cathepsin B, E-64 is toxic when ingested by humans and is non-specific. Therefore, there is a need to find a compound that can inhibit cathepsin B without harming the body's normal, physiological processes. With this goal in mind, the current study aims to find an inhibitor of cathepsin B among a library of thiosemicarbazone (TSC) compounds that has low toxicity.

**Table 1.** Inhibitors of Cathepsin B

Name of Compound, Reference Number	Type of Compound	Chemical Structure	IC <sub>50</sub> Value
E-64 (Yamamoto et al., 2002; Watanabe et al., 2006)	Epoxysuccinyl Peptide		40 nM
CA-030 (Yamamoto et al., 2002; Watanabe et al., 2006)	Epoxysuccinyl Peptide		120 nM
CA-074 (Yamamoto et al., 2002; Watanabe et al., 2006)	Epoxysuccinyl Peptide		38 nM
Chiral cyclopalladated complexes (Bincolleto et al., 2005)	Palladacycle compounds with biphosphinic ligands		4.5 μM
VBY-825 (Elie et al., 2010)	Covalent, reversible inhibitor		4.3 nM



Name of Compound, Reference Number	Type of Compound	Chemical Structure	IC <sub>50</sub> Value
Dipeptidyl Nitrile (Greenspan et al., 2003)	Highly Peptidic		6 nM
N-Arylamionitrile, (Greenspan et al., 2003)	Peptidomimetic Compounds		49 nM
Carbamates (Bialas and Kafarski, 2009)	Bicyclic Carbamates		5 nM
PMRu-52 (Mura et al., 2010)	Ruthenium (II) Compound		5.5 μM
Square-planar Cycloaurated Gold (III) Compounds (Zhu et al., 2011)	Gold (III) Compound		100 nM
Isothiazolone (Wisastra et al., 2011)	Isothiazolone		46 nM

### Project Overview

This study is within the general investigation of potential inhibitors of the cysteine protease, cathepsin B. The study proposes that within a specified library of thiosemicarbazone compounds (TSC), an effective inhibitor of cathepsin B exists which exhibits low toxicity (see Figure 9). This library of compounds has been previously tested against cathepsin L which is a cysteine protease classified in the same papain family as cathepsin B. In previous *in vitro* experiments, some of the TSC compounds effectively inhibited cathepsin L as evident in the  $IC_{50}$  values reported in the nanomolar to micromolar range (Kumar et al., 2010). In order to determine the efficacy of the inhibitory effects on cathepsin B, this study will analyze the  $IC_{50}$  values of the tested TSC compounds by monitoring the cathepsin B reaction through an observed increase in fluorescence as detected by a microplate reader (see Chapter II). The focus of this study is to find a TSC compound that inhibits cathepsin B while adjusting for the stability, solubility, and physiological conditions of the potential inhibitor. Furthermore, the promising inhibitors (those that display low  $IC_{50}$  values) will be more thoroughly analyzed through advanced kinetic experiments in order to elucidate the inhibitor's method of binding.

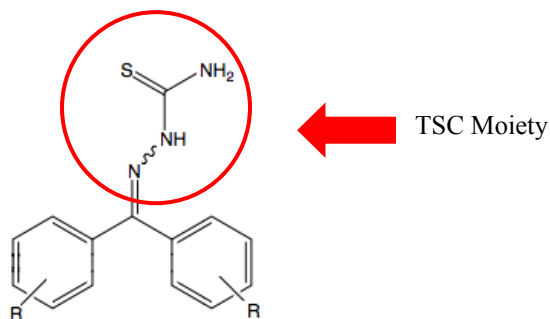


**Figure 9.** TSC moiety present on all inhibitors tested against cathepsin B

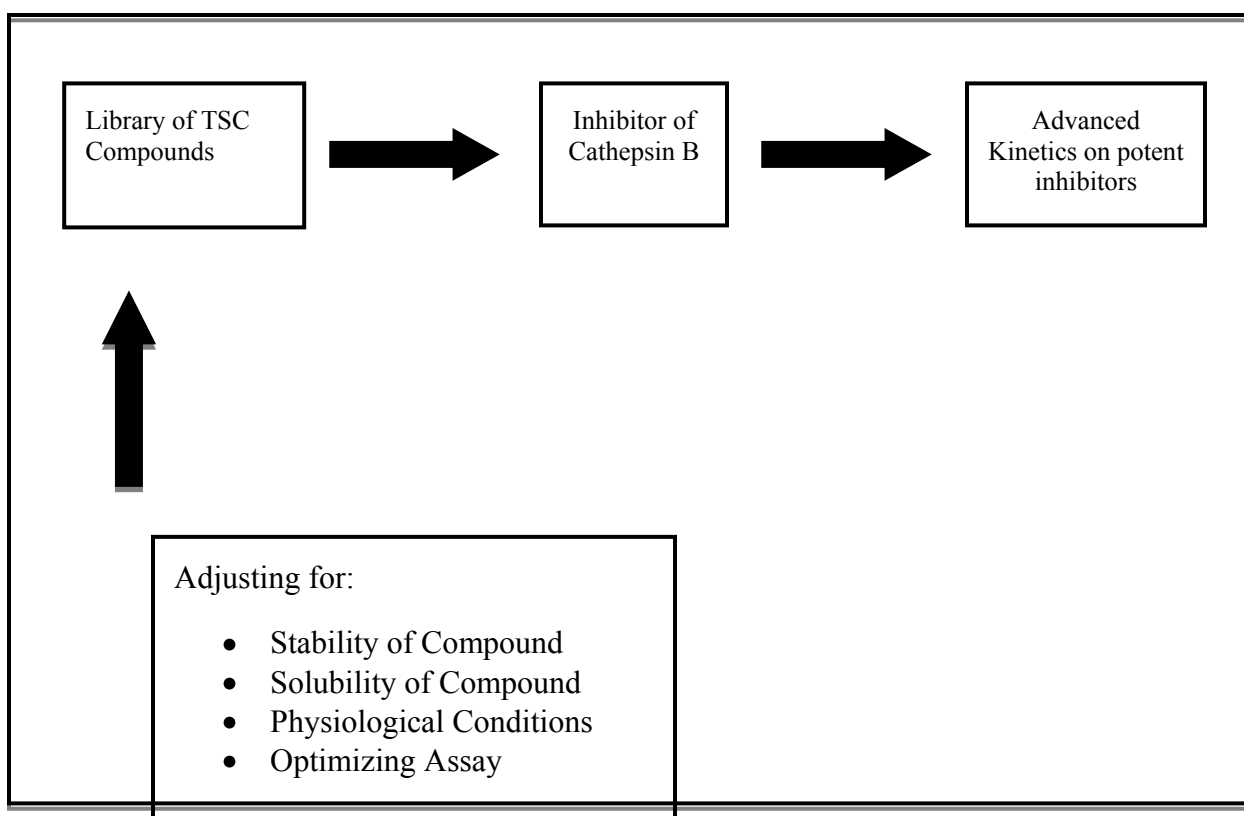


**Figure 10.** Project Overview

### *Fluorescence*

In this project, the cathepsin B reaction was monitored through the detection of a fluorescent product. Fluorescence consists of a cyclic process which involves the absorption of light from the UV-visible spectrum by a molecule, the excitation of that molecule, and the subsequent emission of light by the molecule (Tutorial on Fluorescence). Molecules can fluoresce at different intensities, and most of the building blocks of proteins and nucleic acids display relatively weak fluorescence (Atkins and de Paula, 2006). Fluorescent molecules called fluorophors move to higher energy states after being struck by photons of light. As the excited fluorophors slowly lose energy

through vibration and heat, they emit light and return to their low energy, ground states (Tutorial on Fluorescence). After initial absorption, the excited molecule enters a relaxation phase as it collides with the surrounding molecules. With each collision, the excited molecule loses a certain amount of energy. The emission energy is characteristic of the fluorophor's structure. Because the fluorophor loses energy in the process of fluorescence, its emission wavelength is longer than its excitation wavelength. Due to the differences in wavelengths, the absorbed and emitted light can be detected as different colors on the visible spectrum. Like the emission energy, the fluorescent intensity depends on the properties of the molecule (Tutorial on Fluorescence).

In order to monitor the reaction between cathepsin B and its substrate, the fluorogenic substrate Z-R-R-AMC was used in our kinetic experiments. Upon interaction with Z-R-R-AMC, cathepsin B cleaves the fluorescent product, AMC, from the substrate as shown in Figure 11. The release of AMC can be monitored fluorometrically by a microplate reader which detects the fluorescent signals in terms of relative fluorescence units, RFU. As the reaction between cathepsin B and Z-R-R-AMC progresses, an increase in fluorescence is observed. However, if a cathepsin B inhibitor is present in solution, the observed fluorescence as detected by the amount of AMC released will decrease. The decreased signal results from the inhibitor's prevention of an interaction between cathepsin B and Z-R-R-AMC. With an inhibitor bound to cathepsin B, it is more difficult for the enzyme to react with its substrate and thus less AMC is cleaved. A comparison between the amount of RFU detected during the cathepsin B/Z-R-R-AMC reaction and that of the cathepsin B/Z-R-R-AMC/inhibitor reaction can be used to determine the activity of the inhibitor.

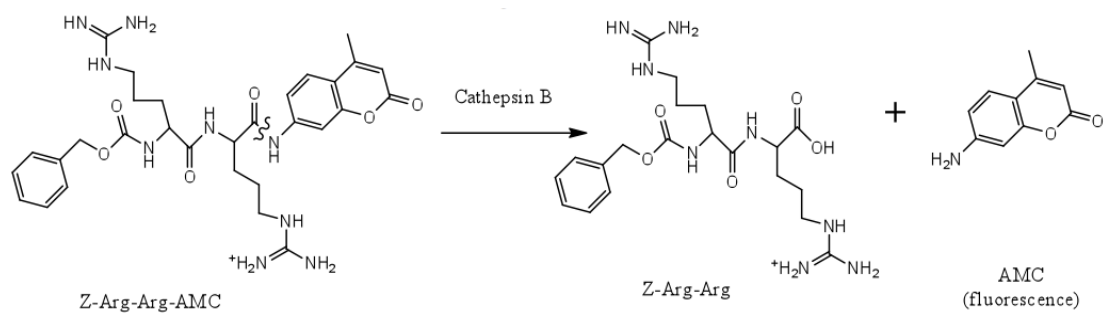


**Figure 11.** Fluorometrically monitored cleavage of Z-R-R-AMC via cathepsin B

## CHAPTER TWO

### Materials and Methods

#### *Materials*

#### *Protocols*

##### A. Preparation of 150 mM Sodium Phosphate ( $\text{Na}_2\text{HPO}_4$ ) Buffer

- Weigh 10.65 g of  $\text{Na}_2\text{HPO}_4$  (Sigma Lot #120K0125, MW 142 g/mol) with an analytical balance. Place the  $\text{Na}_2\text{HPO}_4$  in a beaker and dissolve the solid with approximately 400 mL of ultrapure water by stirring. Next, transfer solution to a 500 mL volumetric flask using a funnel. Carefully add ultrapure water to the flask until the meniscus reaches the 500 mL mark. Place parafilm over the flask and thoroughly mix the solution by inverting the flask multiple times
- Filter solution using a 0.22  $\mu\text{m}$  PES low protein binding membrane (Corning)
- Adjust pH to 6.8 using dilute phosphoric acid,  $\text{H}_3\text{PO}_4$
- Store in refrigerator and make new buffer each month

##### B. Preparation of 40 mM Ethylenediaminetetraacetic acid (EDTA)

- Weigh out 0.744 g EDTA disodium salt dihydrate (Omnipure Lot #357713034, MW 372.24 g/mol) and dissolve in 50 mL ultrapure water
- Store in refrigerator

#### C. Preparation of Assay Buffer 1 (AB<sub>1</sub>)

- Use the following amounts of 150 mM Na<sub>2</sub>HPO<sub>4</sub> buffer, 99.9% Dimethyl Sulfoxide (DMSO) (Acros Lot #A0283558, MW 78.13), and 40 mM EDTA to make a total of 15 mL: 14,217 µL buffer, 300 µL DMSO, 483 µL EDTA
- Prepare in 15 mL Falcon tube

#### D. Preparation of Assay Buffer 2 (AB<sub>2</sub>)

- Prepare on the day of experiment
- Weigh approximately 2.5 mg Dithiothreitol (DTT) (Omnipure Lot #A505256, MW 152.25 g/mol) in 15 mL Falcon tube
- Add appropriate amount of AB<sub>1</sub> according to the ratio: 5mL AB<sub>1</sub> / 2.315 mg DTT
- Vortex solution until DTT dissolves completely

#### E. Preparation of 180 µM Z(benzylozycarbonyl)-Arg-Arg-7-amino-4-methylcoumarin hydrochloride (Z-R-R-AMC)

- Prepare a 8.9 mM Z-R-R-AMC stock solution
  - To make 0.5 mL, weigh approximately 2.80 mg of Z-R-R-AMC (Bachem Lot # 1007560, MW 621.69 g/mol) in a black 1 mL tube

- Add appropriate amount of 100% DMSO according to the ratio: 11.19 mg Z-R-R-AMC / 2 mL 100% DMSO
- Vortex solution and store in refrigerator
- On the day of the experiment, for every 100  $\mu$ L of 8.9 mM Z-R-R-AMC stock, add 4.9 mL of ultrapure water to a 15 mL Falcon tube covered in foil.

F. Preparation of Assay Buffer 3 (AB<sub>3</sub>) used to make inhibitor dilutions

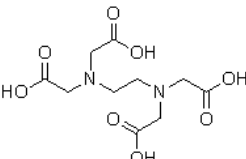
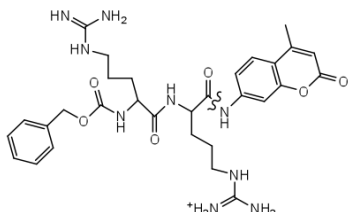
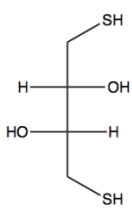
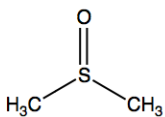
- Use the following amounts of 150 mM Na<sub>2</sub>HPO<sub>4</sub> buffer and EDTA to make a total of 10 mL: 9,678  $\mu$ L Buffer, 322  $\mu$ L EDTA

G. Preparation of Human Liver Cathepsin B (Sigma)

- Prepare cathepsin B stock solution: perform 1/20 dilution of frozen 4 nM cathepsin B (-80°C) by adding 76  $\mu$ L of 0.1% Brij (Sigma Lot #124K6100, 30% Brij 35 solution). Gently mix solution.
- On the day of the experiment, combine cathepsin B stock solution and AB<sub>2</sub> according to the ratio: 10  $\mu$ L cathepsin B and 2,476  $\mu$ L of AB<sub>2</sub>
- Store cathepsin B solution on ice



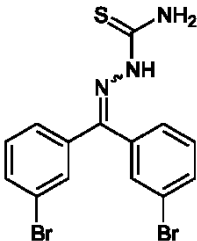
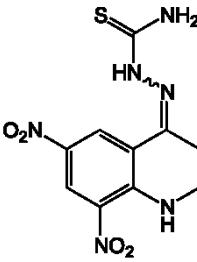
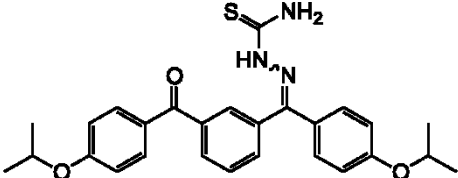
**Table 2.** Cathepsin B Assay Conditions

		Structure or Linear Formula	Molecular Weight	Significance
<b>EDTA</b>	1.25 mM		292.24 g/mol	EDTA acts as a chelating agent which binds heavy metals that might affect the enzyme's active site.
<b>Buffer</b>	150 mM	$\text{Na}_2\text{HPO}_4$	141.96 g/mol	
<b>Z-R-R-AMC</b>	60 $\mu\text{M}$		621.69 g/mol	When the substrate, Z-R-R-AMC, comes in contact with the enzyme, cathepsin B, it releases its aminomethylcoumarin (AMC) component which fluoresces.
<b>Cathepsin B</b>	2 nM		30 kD	
<b>DTT</b>	1 mM		152.25 g/mol	DTT prevents disulfide bridges from forming near the active site of cathepsin B. As a reducing agent, it also promotes the enzyme's catalytic activity.
<b>pH</b>	6.8			Similar to physiological pH.
<b>DMSO</b>	2.0%		78.13 g/mol	DMSO increases the solubility of the TSC inhibitors
<b>Brij</b>	0.1%	$\text{CH}_3(\text{CH}_2)_{10}\text{CH}_2(\text{OCH}_2\text{CH}_2)_n\text{OH}$	1199.54 g/mol	Brij prevents the aggregation of the enzyme.

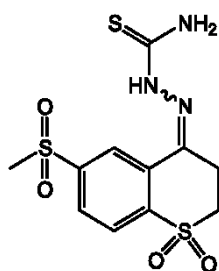
### Methods

This was a collaborative project in which the research group of Dr. Kevin G. Pinney of the Department of Chemistry and Biochemistry at Baylor University synthesized the thiosemicarbazone inhibitors that were used in the following experiments.

**Table 3.** Structures of TSC inhibitors of cathepsin B

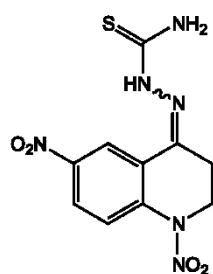
Compound	Compound Structure	MW (g/mol)
1		413.13
2		310.05
3		475.19

4



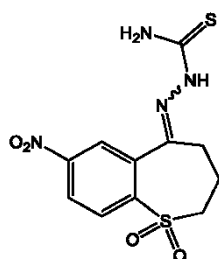
347.01

5



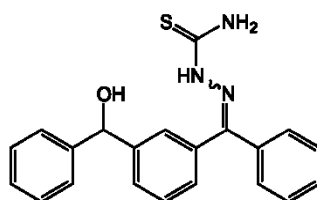
310.05

6



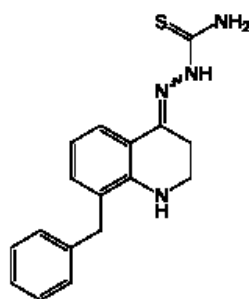
328.03

7



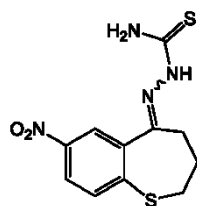
361.12

8



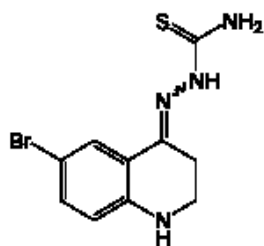
310.42

9



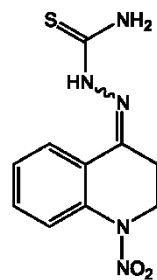
296.04

10



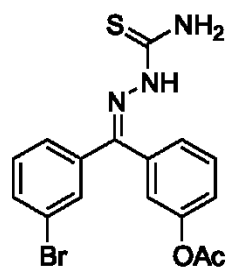
297.19

11



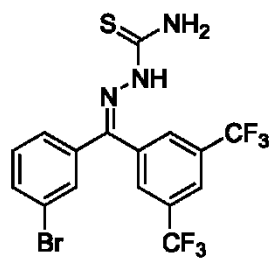
265.06

12



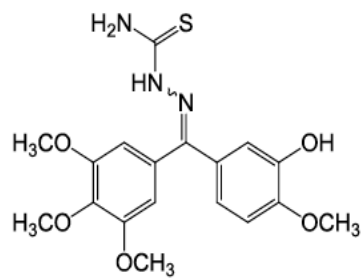
392.27

13



470.23

14



391.44

### *Cathepsin B Assay*

The fluorogenic substrate Z-arginylarginyl-aminomethylcoumarin (Z-R-R-AMC) was used in all reactions with cathepsin B. Z-R-R-AMC reacts with cathepsin B and releases the fluorescent product, aminomethylcoumarin (AMC). The cathepsin B reaction was monitored through the observance of an increase in fluorescence (AMC) as detected by a Thermo Fluoroskan Ascent FL microplate reader set at an excitation and emission wavelength of 355 nm and 460 nm respectively.

### *IC<sub>50</sub> Determination*

Inhibitors were serially diluted with 100% DMSO and assay buffer 3 to include a final concentration range of 20  $\mu$ M to 1 nM (see Table 4a and 4b). 50  $\mu$ L of a human liver Cathepsin B (Athens) solution was pre-incubated with 50  $\mu$ L of inhibitor solutions at various concentrations for 5 minutes at 37°C. To initiate the reaction, 50  $\mu$ L of the fluorogenic substrate, Z-R-R-AMC, was added to the cathepsin B-inhibitor mixture. The microplate reader ran for a total of 5 minutes and expressed the fluorescent signals in terms of relative fluorescence units (RFU) per second. In order to determine the IC<sub>50</sub> values of the various TSC inhibitors, GraphPad Prism 5.0 software was used and data was analyzed for a sigmoidal dose response (variable slope) using the equation,  $Y = \text{Bottom} + (\text{Top} - \text{Bottom}) / (1 + 10^{((\text{LogEC}_{50} - X) * \text{HillSlope}))}$  with constraints: bottom = 0, top = 1.

**Table 4A.** TSC Inhibitor Dilutions

Inhibitor Solution	Conc	Units	% DMSO	$\mu$ L prev sol.	100% DMSO	TOTAL	%DMSO
Stock (A)*	20	mM	100				100
B	2	mM	100	20	180	200	100
C	0.2	mM	100	20	180	200	100
D	0.02	mM	100	20	180	200	100
E	0.002	mM	100	20	180	200	100
F	0.0002	mM	100	20	180	200	100

\*20 mM stock (A) was prepared accordingly:

Using a glass capillary tube, ~1.0 mg of the solid inhibitor was weighed out on an analytical balance and placed in a 1.5 mL tube. Using the molecular weight of the inhibitor, the exact volume of 100% DMSO needed to make a 20 mM solution was calculated. After addition of DMSO, the inhibitor solution was vortexed.

**Table 4B.** TSC Inhibitor Dilutions Continued

Inhibitor dilutions at 35% DMSO							
Final Conc		Conc to make		$\mu$ L Solution		$\mu$ L DMSO (100%) to add	$\mu$ L AB <sub>3</sub>
20	$\mu$ M	60	$\mu$ M	A	1.5	8.5	490.0
15	$\mu$ M	45	$\mu$ M	A	1.1	8.9	490.0
10	$\mu$ M	30	$\mu$ M	B	7.5	2.5	490.0
5	$\mu$ M	15	$\mu$ M	B	3.8	6.3	490.0
1	$\mu$ M	3	$\mu$ M	C	7.5	2.5	490.0
0.5	$\mu$ M	1.5	$\mu$ M	C	3.8	6.3	490.0
0.1	$\mu$ M	0.3	$\mu$ M	D	7.5	2.5	490.0
0.05	$\mu$ M	0.15	$\mu$ M	D	3.8	6.3	490.0
0.01	$\mu$ M	0.03	$\mu$ M	E	7.5	2.5	490.0
0.001	$\mu$ M	0.003	$\mu$ M	F	7.5	2.5	490.0

## Enzyme Kinetics

### Michaelis-Menten

The assay buffer and cathepsin B solution were prepared as described for the IC<sub>50</sub> determination. Various dilutions ranging from final concentrations of 120  $\mu$ M to 10  $\mu$ M were made from an 8.92  $\mu$ M Z-R-R-AMC substrate stock solution (see Table 3). In order to prevent excess AMC fluorescence, all the substrate dilutions were made in 15 mL falcon tubes that were covered in foil. 50  $\mu$ L of the assay buffer and 50  $\mu$ L of the cathepsin B solution incubated at 37°C for 5 minutes. After addition of 50  $\mu$ L of the various substrate dilutions, the fluorescent activity was measured for 5 minutes at excitation and emission wavelengths of 355 nm and 460 nm respectively. The assay was performed in triplicate. The Michaelis-Menten curve of Z-R-R-AMC with cathepsin B was analyzed using GraphPad Prism 5.0 software by plotting the reaction velocity against the various substrate concentrations to fit the equation,  $y = (V_{\max} * X)/(K_m + X)$ .

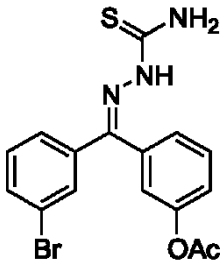
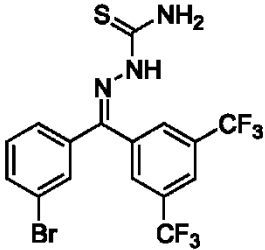
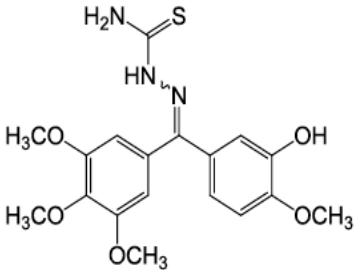
**Table 5.** Michaelis-Menten Dilutions

Final Conc ( $\mu$ M)	Conc Made ( $\mu$ M)	Stock used	Volume of Stock Needed ( $\mu$ L)	Volume of DMSO ( $\mu$ L)	Volume of H <sub>2</sub> O ( $\mu$ L)
60	180	8.92 mM	20.2	0	979.8
300	900	180 $\mu$ M	416.67	2	81.33
45	135	180 $\mu$ M	150	3	147
20	60	180 $\mu$ M	75	4.5	220.5
11	33	300 $\mu$ M	50	9	441

*Advanced Kinetics*

Experiments involving advanced kinetics were performed on the three TSC inhibitors shown in Table 6.

**Table 6.** Thiosemicarbazone Inhibitors of Cathepsin B

Compound	Compound Structure	MW
12		392.27 g/mol
13		470.23 g/mol
14		391.44 g/mol

Similar to the experiments for determining the compound's IC<sub>50</sub> values, the following advanced kinetics experiments were performed at 37°C in black 96 well Corning 3686



assay microplates with a Thermo Fluoroskan Ascent FL microplate reader set at an excitation and emission filter wavelength of 355 nm and 460 nm, respectively.

#### *Time Dependence Curves - Varying [Z-R-R-AMC]*

In order to determine if the inhibitor competes with the substrate in binding to cathepsin B, an experiment was performed in which various Z-R-R-AMC solutions with final concentrations of 60  $\mu$ M, 40  $\mu$ M, 20  $\mu$ M, 6  $\mu$ M, and 0  $\mu$ M (see Table 4) were tested with a range of inhibitor dilutions. These substrate dilutions were prepared in 15 mL falcon tubes that had been wrapped in foil. The inhibitor dilutions were made according to Table 2a and 2b as described in the procedure for the IC<sub>50</sub> determination. After 50  $\mu$ L of each of the inhibitor dilutions incubated with 50  $\mu$ L of the cathepsin B solution for 5 minutes at 37°C, 50  $\mu$ L of the various substrate concentrations were added to each of the wells yielding a total volume of 150  $\mu$ L. Following the previous conditions, the microplate measured the wells for a total of 5 minutes. Analysis was performed with GraphPad Prism 5.0 using a Nonlinear Morrison Plot to determine the inhibitor's method of binding (competitive/ slow binding) with the following constraints: [Cathepsin B] = 0.002  $\mu$ M, [Z-R-R-AMC] = 60  $\mu$ M, and a K<sub>m</sub> value from the corresponding Michaelis-Menten Curve.

**Table 7.** Dilutions for Varying [Z-R-R-AMC]

Final Conc ( $\mu$ M)	Conc Made ( $\mu$ M)	Stock used ( $\mu$ M)	Volume of Stock Needed ( $\mu$ L)	Volume of DMSO ( $\mu$ L)	Volume of H <sub>2</sub> O ( $\mu$ L)
60.4	181.19	8970	20.2	0	979.6
40.0	120.00	181	663.0	6.7	330.3
20.0	60.00	181	331.5	13.4	655.1
6.0	18.00	181	99.4	18.0	882.5
0.0	0.00	-			

### *Progress Curves*

Using the same conditions as described in the procedure for the determination of  $IC_{50}$  values, a series of 7 inhibitor dilutions were prepared ranging from 10  $\mu$ M to 0.01  $\mu$ M. 50  $\mu$ L of each of these inhibitor solutions were pipetted into 7 different wells of the Corning 3686 assay microplates. A solution of 50  $\mu$ L of assay buffer was added to the last well to serve as a control. 50  $\mu$ L of the 60  $\mu$ M (fc) (See *Materials*) Z-R-R-AMC solution was added to each of the 8 wells. Then, 50  $\mu$ L of the cathepsin B solution was also added to the 8 wells. Immediately after the addition of the enzyme, the microplate reader started its measurement of the wells. In order to achieve the maximum amount of data points, the total run time for this experiment was approximately 3,000 seconds. For the analysis, a graph displaying the relative fluorescent units against the time was constructed.

### *Varying Pre-incubation Times*

This experiment was similar to the  $IC_{50}$  determination in that 50  $\mu$ L of the inhibitor solutions (ranging from 10  $\mu$ M to 0.01  $\mu$ M) were plated with 50  $\mu$ L of the cathepsin B solution. For the first set, the inhibitor dilutions and the enzyme solution pre-incubated inside the microplate reader at 37°C for 5 minutes. For the successive sets of inhibitor dilutions and cathepsin B solutions, the pre-incubation time was varied: 15 min, 30 min, 60 min, and 120 min. After each pre-incubation time period, 50  $\mu$ L of a 60  $\mu$ M (fc) solution of the Z-R-R-AMC substrate was added to each of the wells, and then the microplate reader measured the relative fluorescence for 5 minutes. Analysis involved

determining the IC<sub>50</sub> values for each pre-incubation time and plotting a graph displaying the fractional activity vs. the pre-incubation time.

### *Reversibility*

For this experiment, the following solutions were prepared on the day of the experiment:

(1) A 40  $\mu$ M Inhibitor Solution ( $F_c = 20 \mu$ M)

-1  $\mu$ L of a 20 mM inhibitor stock solution

-9  $\mu$ L of 100% DMSO

-490.0  $\mu$ L of AB<sub>3</sub>

(2) A solution containing 10  $\mu$ L DMSO and 490.0  $\mu$ L AB<sub>3</sub> to serve as a control

(3) Appropriate amount of AB<sub>2</sub> (see *Materials*)

(4) 60  $\mu$ M Z-R-R-AMC (5000  $\mu$ L total)

-33.33  $\mu$ L of 8.9 mM Z-R-R-AMC stock solution

-1655.56  $\mu$ L AB<sub>1</sub>

-1655.56  $\mu$ L AB<sub>2</sub>

-1655.56  $\mu$ L H<sub>2</sub>O

The following 20  $\mu$ L solutions were prepared in small tubes using the solutions above:

- 3.1  $\mu$ L of 1/10 dilution of cathepsin B, 10  $\mu$ L of (1), and 6.9  $\mu$ L of (3)
- 3.1  $\mu$ L of 1/10 dilution of cathepsin B, 10  $\mu$ L of (2), and 6.9  $\mu$ L of (3)

These solutions were allowed to incubate inside the microplate reader for 1 hour at 37°C.

Then, 1.5  $\mu$ L of each of the solutions containing the inhibitor and enzyme were added to the wells of the microplate in triplicate. 148.5  $\mu$ L of solution (4) was then added to each


well. The microplate reader was programmed to shake the wells for 10 seconds and then measure the fluorescence for a total of 4 hours. For the analysis, the plots of relative fluorescence units vs. time for the control and inhibitor solutions were compared using GraphPad Prism 5.0 software.

*Protocol for Operating the Ascent Fluoroskan Microplate Reader*

1. Login to the logbook that is next to the microplate reader.
2. Remove the cover from the microplate, and turn it on by flipping the switch on the side of the instrument as illustrated below.

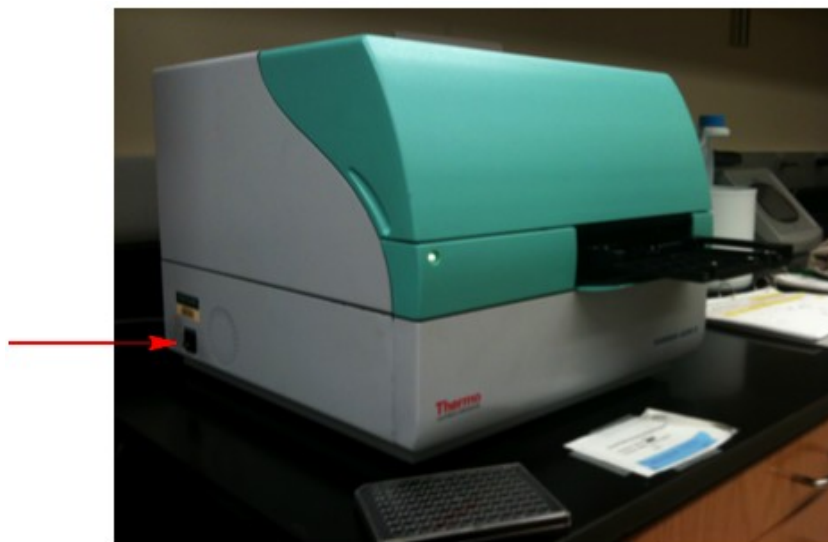


**Figure 12 .** Thermo Fluoroskan Ascent FL Microplate Reader

3. Login to the computer that is adjacent to the microplate reader.
4. On the desktop, open Ascent software by double-clicking on the icon: 
5. After the software loads, click on “Options” which is listed on the top toolbar. A screen will appear displaying the ambient temperature of the microplate. Using the sliding bar, change the temperature to 37°C and click OK.

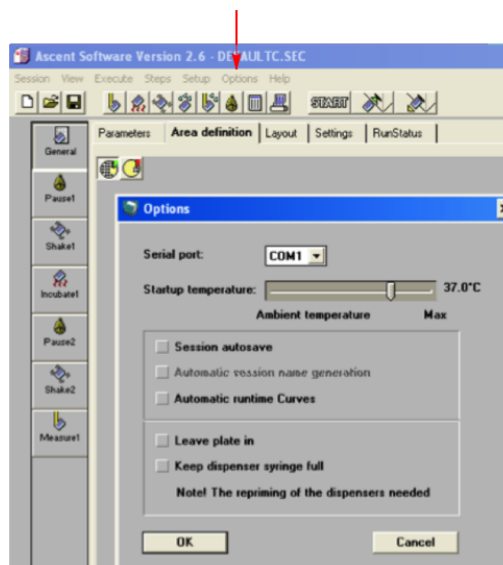


**Figure 13.** Window displaying temperature control

6. Returning to the main screen, select the “General” button located on the left column of the screen. Select “Area definition” from the list of tabs at the top of the General box. You will now select the wells which will be in use for your experiment. First, click on the circle with the bright green triangle, and then click and drag the mouse across the wells to select those that will be in use. In the figure below, the first six wells in column 2 were selected using this technique.

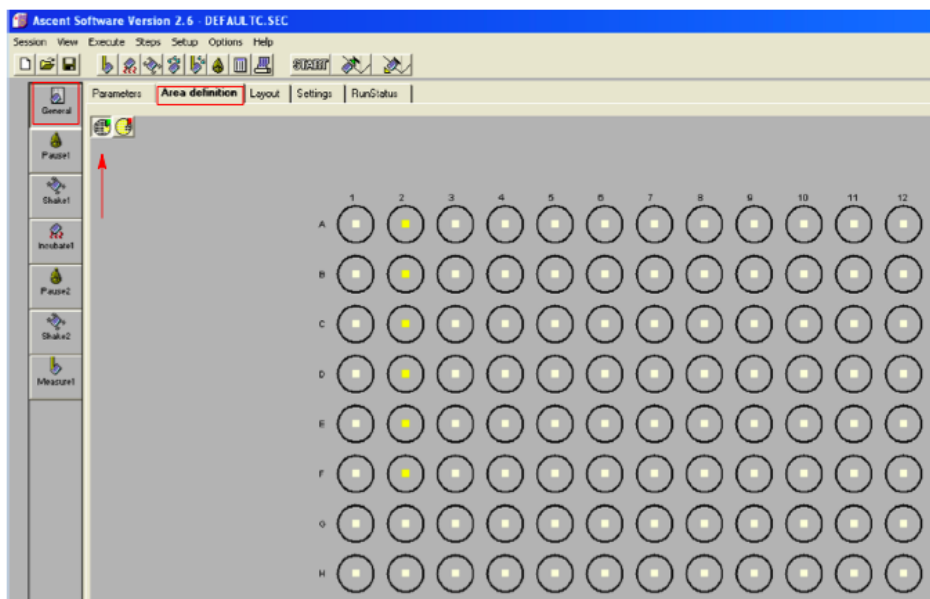


**Figure 14.** Diagram displaying selection of microplate wells

7. Select the “Settings” tab at the top of the General box. Specify how many wells the microplate will read according to the area definition already defined. In this example, because 6 wells were selected in the area definition, the microplate will “execute by...6 wells.” Use the figure below as a model to set the other specifications.

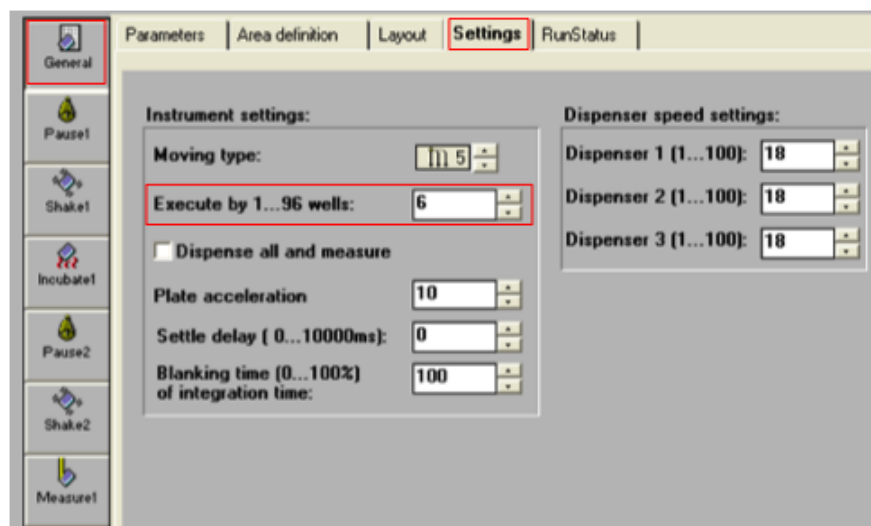


**Figure 15.** Window displaying microplate reader settings

8. You will now adjust the microplate's settings in order to accommodate the specifications of your experiment. For example, for the IC<sub>50</sub> experiments, the initial contents in the well incubated in the microplate at 37°C for 5 minutes. After the substrate was added, the microplate shook the wells for 10 seconds and measured the wells for a total of 5 minutes. To set these parameters the following steps were performed:

- The first step included a one minute pause which was inputted under the “Pause1” option on the left column of the screen.
- The second step involved a shake time of 10 seconds, a diameter of 1, and a speed of 960 rpm as shown below.

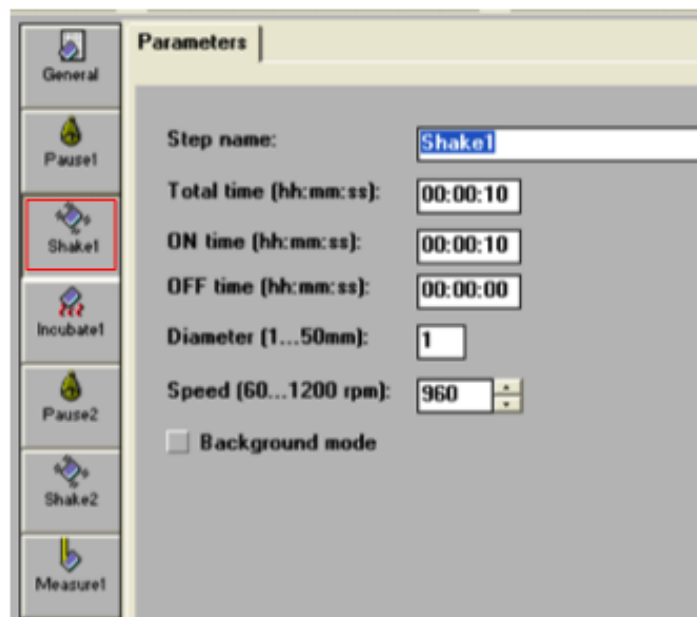


**Figure 16.** Window displaying “Shake 1”

- For the third step, an incubation time of 4 minutes and 50 seconds was inputted into the appropriate box under “Incubate1.” Using the sliding bar, the ambient temperature was also adjusted to read 37°C.

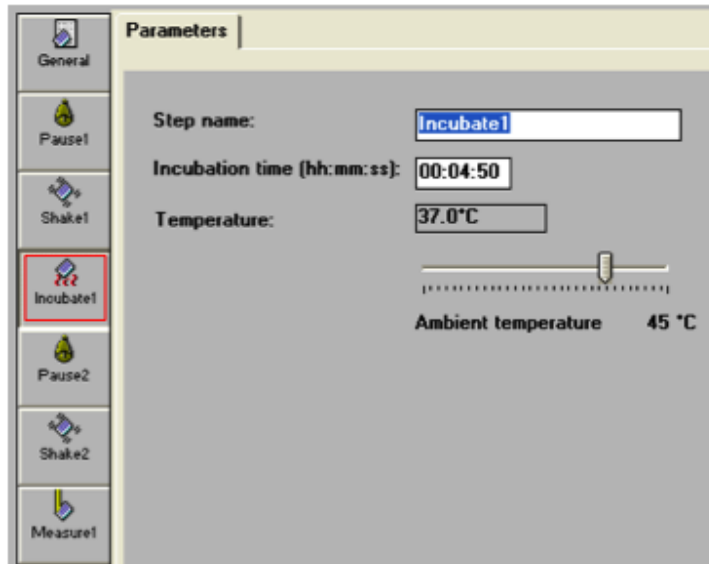


**Figure 17.** Parameters window displaying temperature control

- The fourth step involved setting the second pause as 5 minutes.
- The fifth step specified the amount of time given for the second shake which was set for 10 seconds at a diameter of 1 and an rpm of 960 (same as Shake1).
- The sixth and final step involved an adjustment of the microplate reader's measurement specifications. As shown below, the measurement method was set as "Fluorometric" and the measurement type was set as "Kinetic." The integration time, interval and measure count were set as 20, 15, and 21. These values specify how long the microplate will be given to read each well and how many times it will do so. Notice that the product of the interval and the measure count (minus 1 unit) equal the total number of seconds needed for the entire run. In this example, the microplate will run for a total of 300 seconds ( $15 \times 20$ ) or 5 minutes. For this experiment, the excitation and emission wavelengths were set as 355 nm and 460 nm.



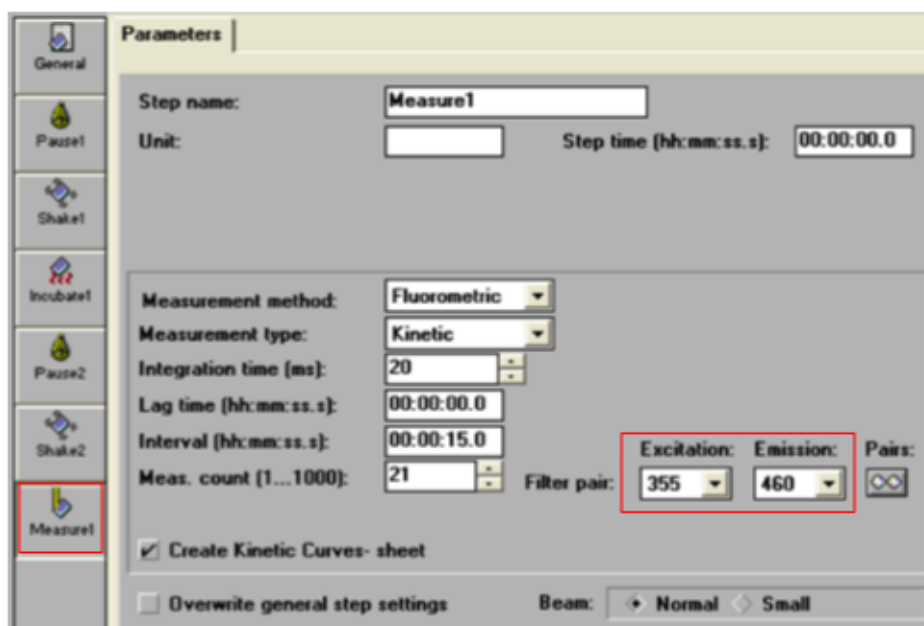


**Figure 18.** Window displaying excitation and emission wavelengths

9. Once you are ready to begin the experiment, click on the START button at the top of the screen.
10. After the experiment, it is important to save your data to an excel file before beginning the next run. The software will not save multiple runs. When finished with the microplate reader, set the temperature to 25°C and exit the program.
11. Turn off the microplate and replace the cover. Log out of the computer and indicate in the microplate logbook how many hours the instrument was on.
12. Clean your workspace before leaving.

*Assay Conditions – Fluoromax-2*

Table 8 displays the assay conditions that were used for experiments involving the fluoromax-2. The fluorimeter is more sensitive than the microplate reader.

**Table 8.** Cathepsin B Assay Conditions for the Fluoromax-2

Z-R-R-AMC	6 $\mu$ M
Cathepsin B	1.1 nM
DTT	2.7 mM
EDTA	2 mM
Brij	0.07%
Na/K Phosphate Buffer	130 mM
pH	6.0
Temperature	37°C
DMSO	2%

## CHAPTER THREE

### Results

In this collaborative project between the Dr. Mary Lynn Trawick and Dr. Kevin G. Pinney laboratories, a library of novel thiosemicarbazone compounds synthesized by Dr. Pinney and colleagues was tested for inhibition against cathepsin B. Four compounds in this study were considered potent inhibitors.  $IC_{50}$  values for these compounds were determined to assess the efficacy of the inhibitory effects. Advanced kinetic studies were performed for three of the TSC compounds in order to determine the mode of inhibition. A fluorometric assay was used to monitor the interaction of cathepsin B and the substrate Z-R-R-AMC as demonstrated in Figure 19. Upon interaction with Z-R-R-AMC, cathepsin B cleaves the fluorescent product, AMC, from the substrate. The release of AMC was monitored fluorometrically by a microplate reader set at an excitation wavelength and emission wavelength of 355 and 460 nm, respectively. The microplate detects the fluorescent signals in terms of relative fluorescence units, RFU. All data were analyzed using GraphPad Prism 5.0 software.

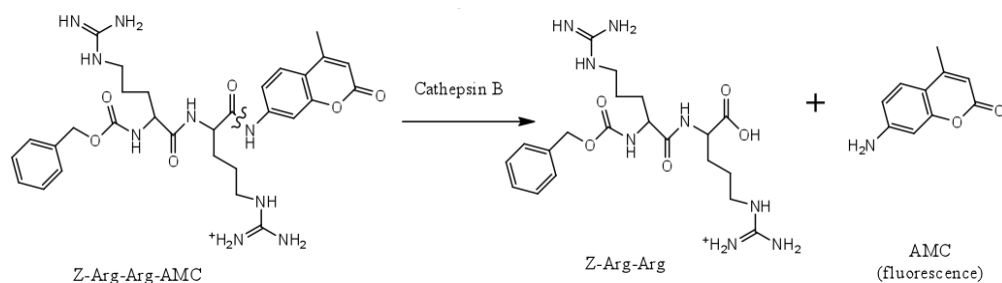


**Figure 19.** Fluorometrically monitored cleavage of Z-R-R-AMC via cathepsin

### *Cathepsin B Assay*

For the kinetic experiments, an assay modified from Wisastra et al. was used to determine the mode of inhibition of three TSC compounds. These assay conditions are summarized in Chapter II. Briefly, the assay conditions consisted of 150 mM sodium phosphate buffer (pH = 6.8), 60  $\mu$ M Z-R-R-AMC, 1.25 mM EDTA, 2 nM cathepsin B, 1 mM DTT, 2.0% DMSO, and 0.1% Brij.

### *Preliminary Kinetic Studies*

#### *AMC Standard Curve*

An AMC Standard Curve was used to determine the amount of AMC released from the substrate per minute. The amount of AMC released determines the relative fluorescence units (RFU) that are detected by the microplate reader. At higher concentrations of AMC, greater fluorescent signals are detected for the product.

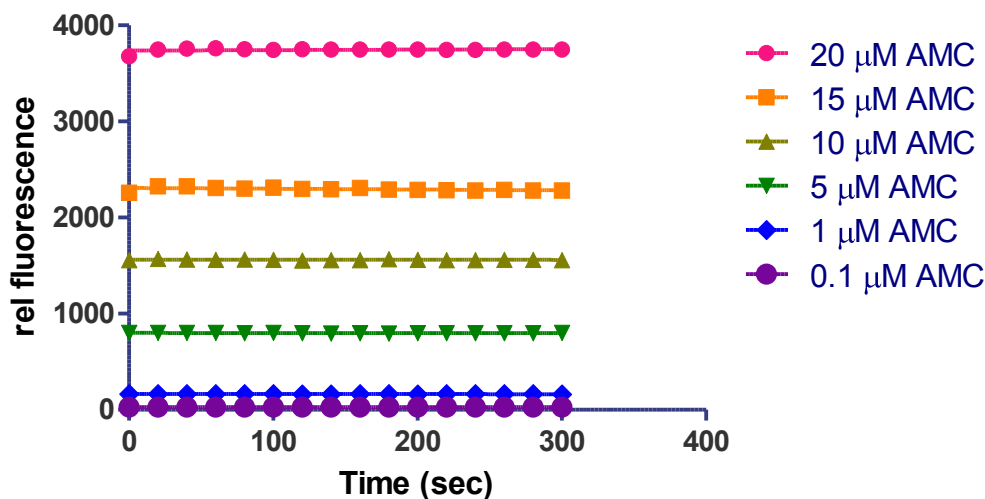


**Figure 20.** AMC at various concentrations

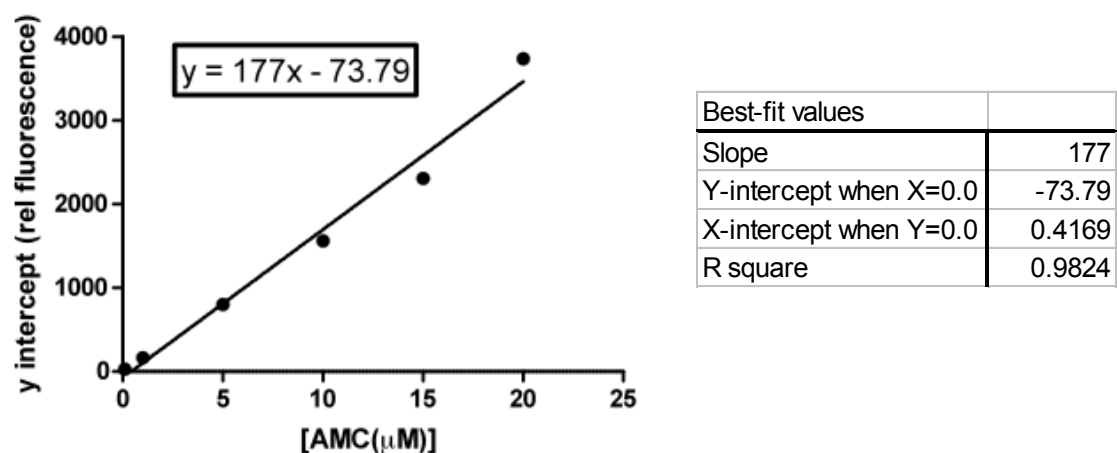


**Figure 21.** AMC standard curve

An R square value of 0.9824 confirms that a linear relationship exists between the relative fluorescence observed and the concentration of the product, AMC.

### *Michaelis-Menten Curve*

In order to determine how well cathepsin B binds to its substrate, a Michaelis-Menten curve was constructed and a  $K_m$  value was obtained. The  $K_m$  value corresponds to the substrate concentration at which the reaction is at half its maximum velocity (Voet et al., 2008).

Mathematically,  $K_m$  can be found by manipulating the equation:

$$V_0 = \frac{(V_{\max}[S])}{(K_m + [S])}$$

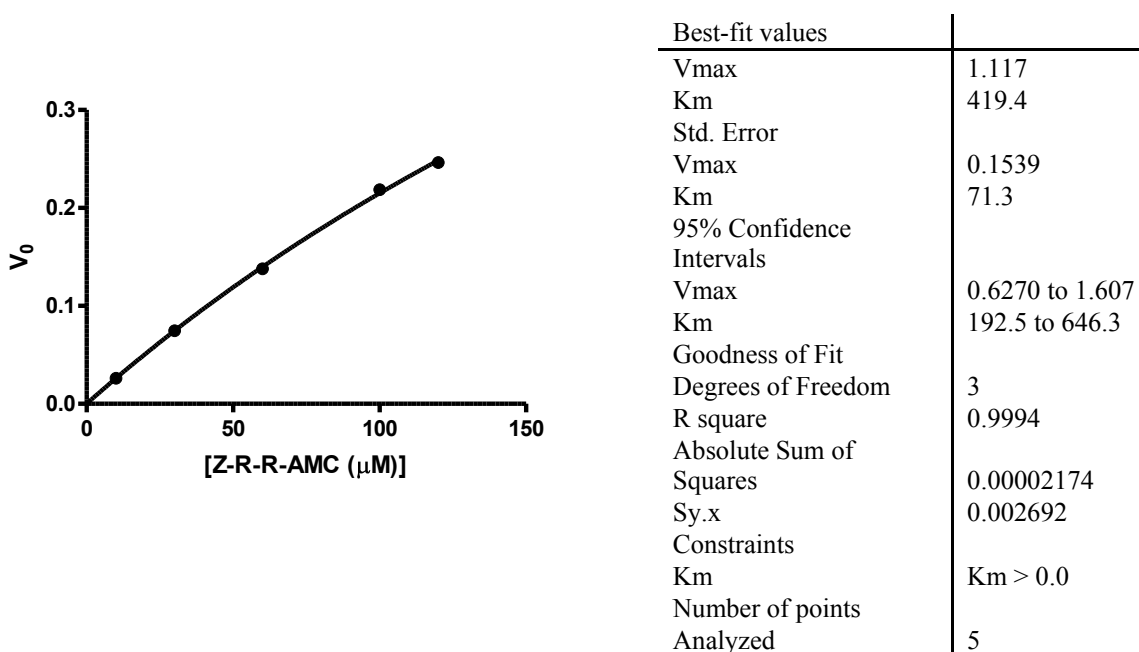
if  $[K_m] = [S]$ , then

$$V_0 = \frac{(V_{\max}[S])}{([S] + [S])}$$

$$V_0 = \frac{1}{2} V_{\max}$$

Essentially, the  $K_m$  value measures the affinity of the enzyme for the substrate and thus it depends on the formation of the enzyme-substrate (ES) complex (Voet et al., 2008). Theoretically, the  $K_m$  of a reaction is equal to a ratio of rate constants in that it represents the speed of the reaction that diminishes the ES complex divided by the speed of the reaction that causes the ES complex to appear.

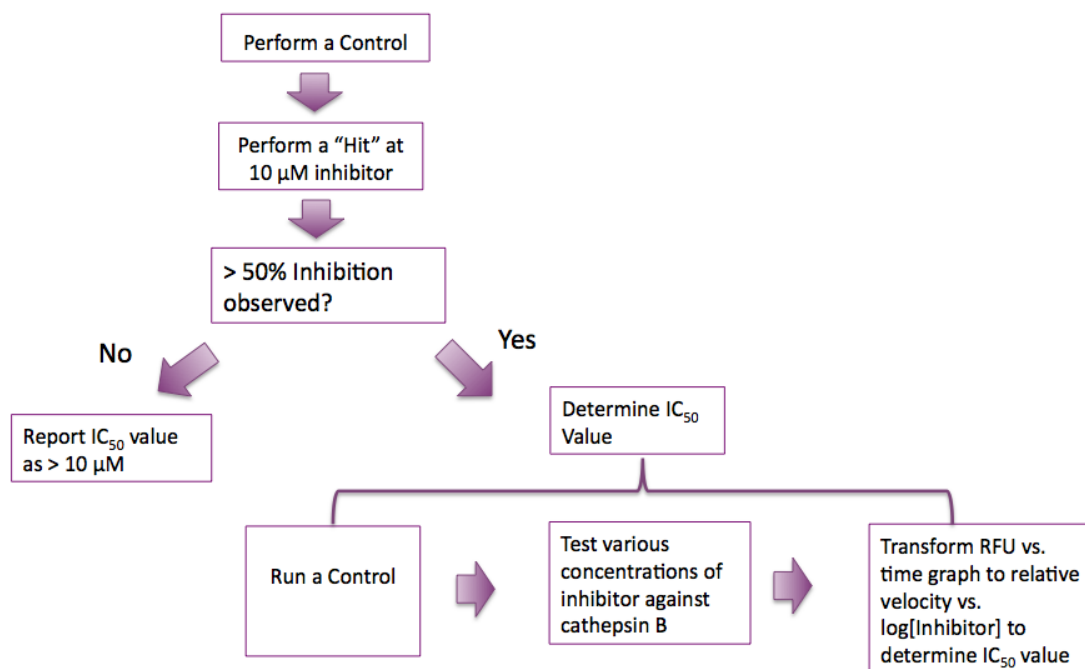
The Michaelis-Menten Curve in Figure 22 plots the initial velocity of the cathepsin B reaction against the concentration of the substrate, Z-R-R-AMC. The data were graphed using GraphPad Prism 5.0 software and a non-linear regression analysis. The Michaelis-Menten curve was analyzed using the equation,  $y = (V_{max} * X)/(K_m + X)$ . A  $K_m$  of 419.40  $\mu\text{M}$  and a  $V_{max}$  of 1.12  $\mu\text{M}/\text{sec}$  were obtained. These values were compared to those recorded in literature. Using related conditions, Caglic et al. reported a  $K_m$  value of 212  $\mu\text{M}$  (2009). Although the  $K_m$  value of 419.40  $\mu\text{M}$  obtained in this study is higher than that reported in literature, it is considered reasonable.



**Figure 22.** Michaelis-Menten Curve and Kinetics

### *Strategy for Determining Effective Inhibitors of Cathepsin B*

The following schematic in Figure 23 below demonstrates the steps by which each thiosemicarbazone compound was tested for inhibition against cathepsin B activity. The effectiveness of the inhibitors was evaluated based on the compound's  $IC_{50}$  value.

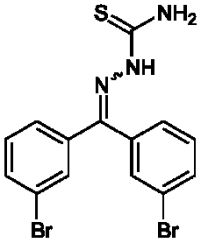
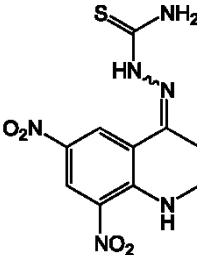
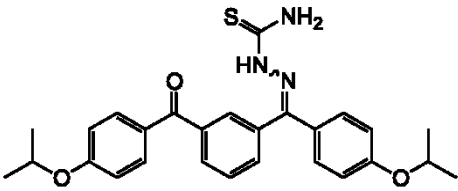
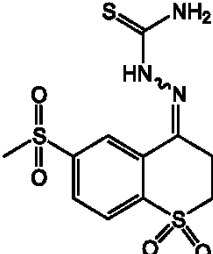


**Figure 23.** Process of  $IC_{50}$  determination

To obtain the  $IC_{50}$  value, a control was first performed by monitoring the reaction of cathepsin B and its substrate, Z-R-R-AMC. A “hit” was tested to analyze the effect of a 10  $\mu$ M inhibitor solution on the cathepsin B – substrate complex. If the tested TSC compound did not inhibit the cathepsin B reaction by 50% or more, the  $IC_{50}$  value for the compound was reported as greater than 10  $\mu$ M.

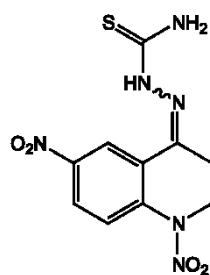
The following table displays the 14 inhibitors that were tested against cathepsin B. To test each compound, the scheme outlined in Figure 23 was followed.

**Table 12.** Structures of TSC inhibitors of cathepsin B

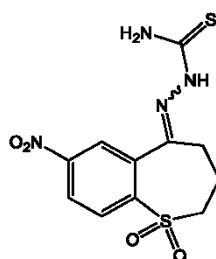
Compound	Compound Structure	IC <sub>50</sub> (μM)
1		1.10 ± 0.01
2		≥10
3		≥10
4		≥10



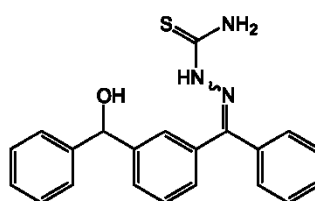
5

 $\geq 10$ 

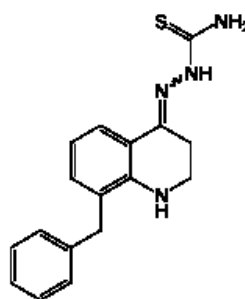
6

 $\geq 10$ 

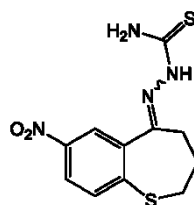
7

 $\geq 10$ 

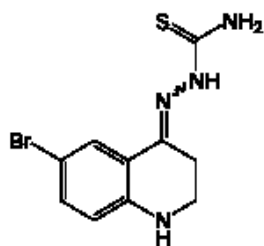
8

 $\geq 10$ 

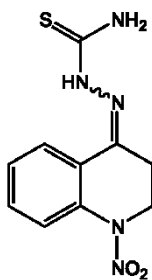
9

 $\geq 10$

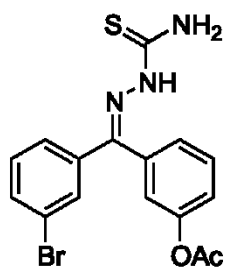
10

 $\geq 10$ 

11

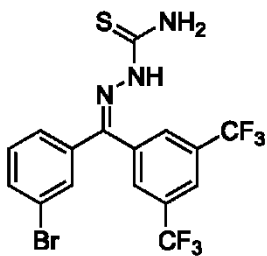
 $\geq 10$ 

12



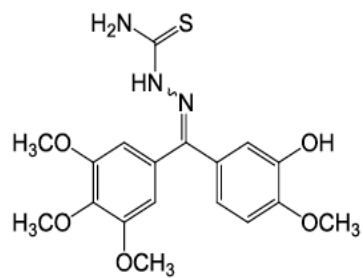
7.07

13



1.93

14



2.81

### Example of Evaluating the “Hits”

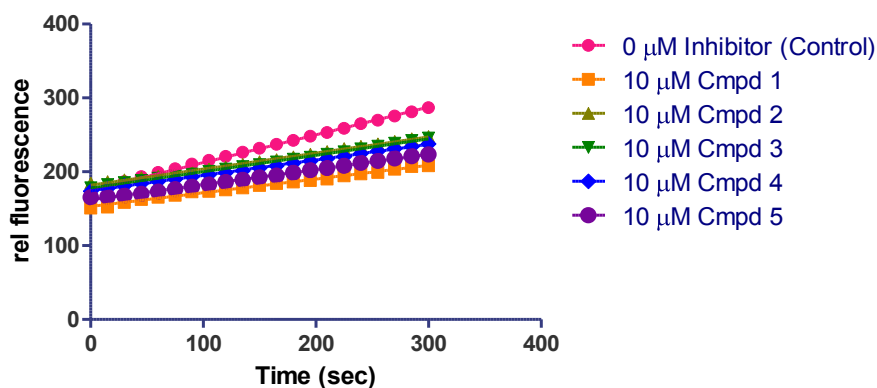


**Figure 24.** Testing the effectiveness of various TSC inhibitors against cathepsin B

In order to determine each inhibitor’s effectiveness, the slopes of the 10  $\mu$ M inhibitor solutions and those of the control were compared. A visual inspection of the graph in Figure 24 above reveals that Compounds 1-5 do not effectively inhibit cathepsin B activity. This is because the slope of the control solution as indicated by the pink circles is similar to the slopes of each of the 10  $\mu$ M inhibitor solutions. In order to quantify these results, the % inhibition of each compound was assessed (See Table 11). To determine the % inhibition, the following equation was used: % Inhibition =  $(1 - V_i/V_0) \times 100\%$ . If the percent inhibition was calculated to be  $\geq 50\%$  (as was the case for compounds **1**, **7**, **12**, **13**, and **14**) then an  $IC_{50}$  analysis was performed according to the schematic in Figure 23.

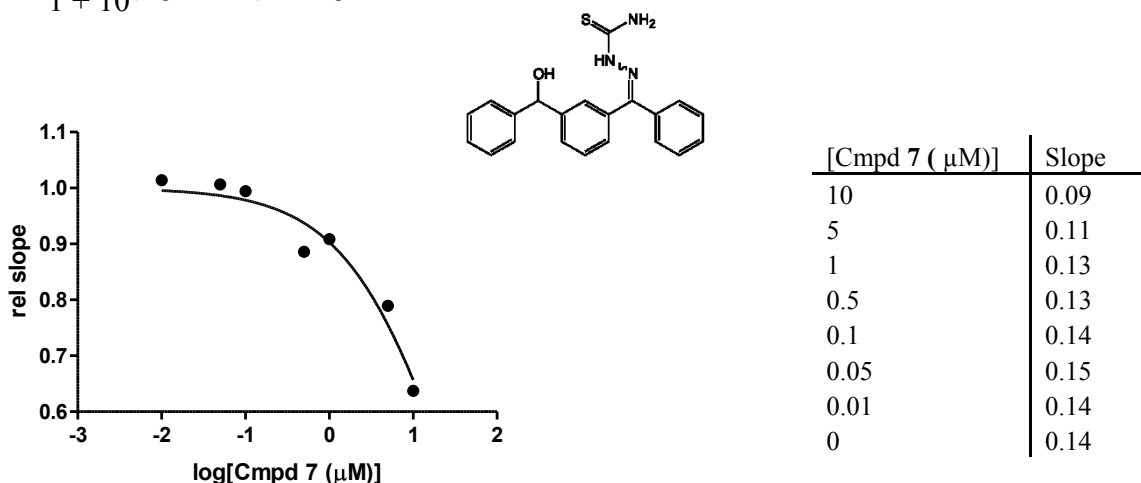
**Table 11.** Determination of the % inhibition for various inhibitors against cathepsin B

Compound	$V_0$	$V_i$	% Inhibition
1	0.3395	0.0331	90.3
2	0.3637	0.2004	44.9
3	0.3637	0.2261	37.8
4	0.3637	0.2340	35.1
5	0.3637	0.2155	40.8
6	0.3637	0.2265	37.7
7	0.3435	0.1689	50.8
8	0.2671	0.2265	15.2
9	0.2757	0.2560	7.2
10	0.2756	0.2164	21.5
11	0.2937	0.2841	4.2
12	0.2728	0.1066	60.9
13	0.2655	0.0276	89.6
14	1.5340	0.1735	88.7

### IC<sub>50</sub> Determination of Compound 7

Because compound 7 achieved a percent inhibition of 50.8, an IC<sub>50</sub> curve was constructed in order to analyze the inhibitor's potency. Cathepsin B was preincubated with each concentration of inhibitor for 5 minutes. All IC<sub>50</sub> curves were analyzed using a nonlinear regression analysis and the following Hill equation:

$$Y = \frac{(\text{Top} - \text{Bottom})}{1 + 10^{(\text{LogEC}_{50} - X) \text{ Hill Slope}}}$$



Sigmoidal dose-response (variable slope)	
Best-fit values	
Bottom	= 0.0
Top	= 1.000
LogEC50	1.412
HillSlope	-0.6861
EC50	25.79
Std. Error	
LogEC50	0.1329
HillSlope	0.1204
95% Confidence Intervals	
LogEC50	1.070 to 1.753
HillSlope	-0.9955 to -0.3766
EC50	11.74 to 56.66
Goodness of Fit	
Degrees of Freedom	5
R square	0.954
Absolute Sum of Squares	0.005254
Sy.x	0.03242
Constraints	
Bottom	Bottom = 0.0
Top	Top = 1.000
Number of points	
Analyzed	7

**Figure 25.** IC<sub>50</sub> Determination of Compound 7

For Compound **7**, a representative  $IC_{50}$  value of 25.79  $\mu M$  was obtained with an R square value of 0.95. This compound was not considered to be an effective cathepsin B inhibitor because a low  $IC_{50}$  value was not achieved. Thus, further analysis of compound **7** was not necessary and an  $IC_{50}$  value of greater than 10  $\mu M$  was reported (See Figure 23).

The  $IC_{50}$  value of compound **1**, a reference compound, was determined in order to assess the efficacy of the assay conditions.

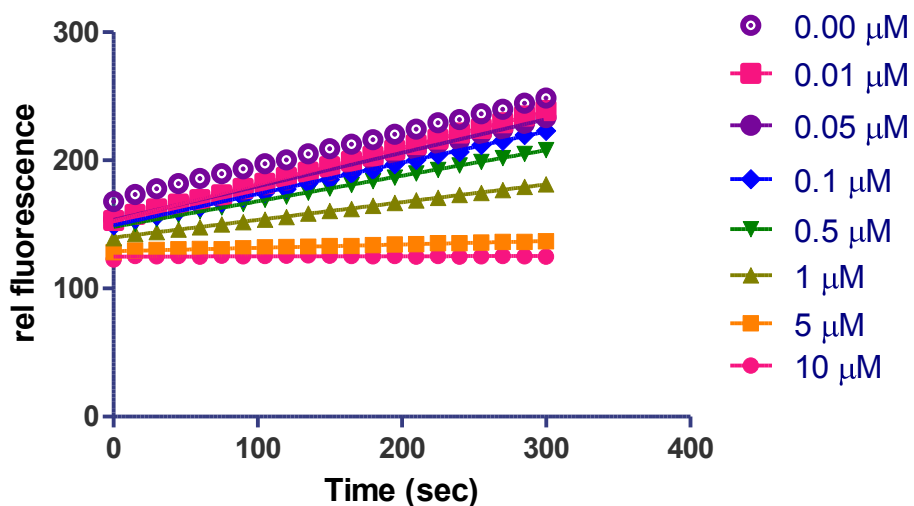
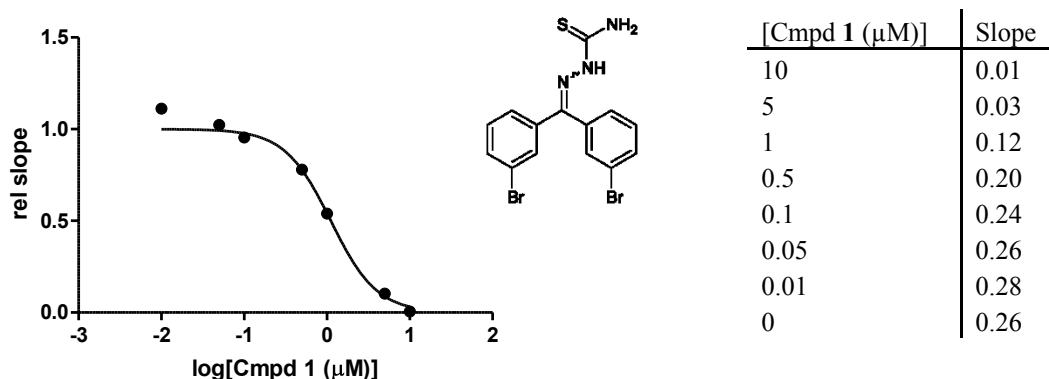


**Figure 26.** Initial kinetics for the  $IC_{50}$  determination of compound **1**

Figure 26 demonstrates that as the concentration of compound **1** increases, the reaction velocity decreases. This relationship is expected since at higher concentrations, the inhibitor will have a greater effect on the activity of cathepsin B. According to Figure 26, there is a significant decrease in the amount of fluorescence released from the 0.01  $\mu M$  inhibitor solution and the 10  $\mu M$  inhibitor solution. This decrease in velocity is also depicted as a decrease in the slopes of the two inhibitor solutions.

### IC<sub>50</sub> Determination of Compound 1

To obtain the IC<sub>50</sub> value, experiments were performed in triplicate, and cathepsin B was preincubated with each concentration of inhibitor for 5 minutes. A representative IC<sub>50</sub> value of  $1.10 \pm 0.01$   $\mu\text{M}$  was obtained for compound **1**, a di-bromobenzophenone TSC. The R square value was 0.9874 which is considered good.

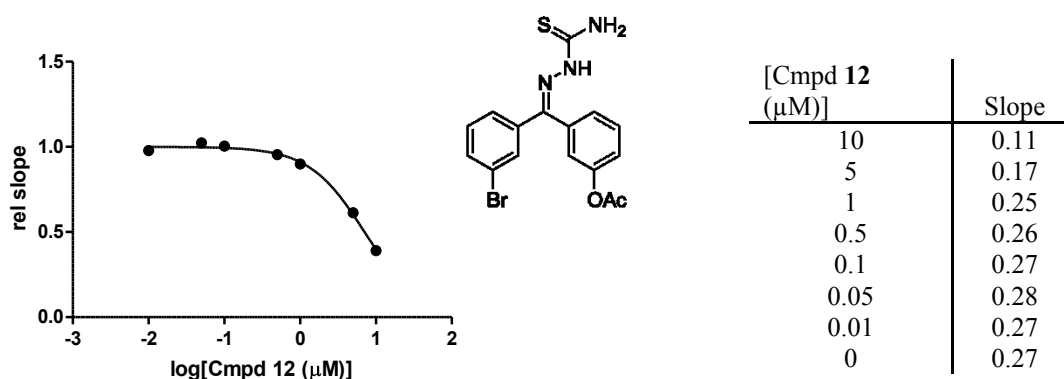


Sigmoidal dose-response (variable slope)	
Best-fit values	
Bottom	= 0.0
Top	= 1.000
LogEC50	0.04684
HillSlope	-1.559
EC50	1.10
Std. Error	
LogEC50	0.05088
HillSlope	0.2798
95% Confidence Intervals	
LogEC50	-0.08397 to 0.1777
HillSlope	-2.279 to -0.8398
EC50	0.8242 to 1.505
Goodness of Fit	
Degrees of Freedom	5
R square	0.9874
Absolute Sum of Squares	0.01497
Sy.x	0.05472
Constraints	
Bottom	Bottom = 0.0
Top	Top = 1.000
Number of points	
Analyzed	7

**Figure 27.** IC<sub>50</sub> Determination of Compound **1**

### IC<sub>50</sub> Determination of Compound 12

Cathepsin B was preincubated with each concentration of inhibitor for 5 minutes. A representative IC<sub>50</sub> value of 7.07  $\mu$ M was obtained for compound **12**, a bromo-substituted, acetylated phenolic benzophenone TSC. The R square value was 0.9954.



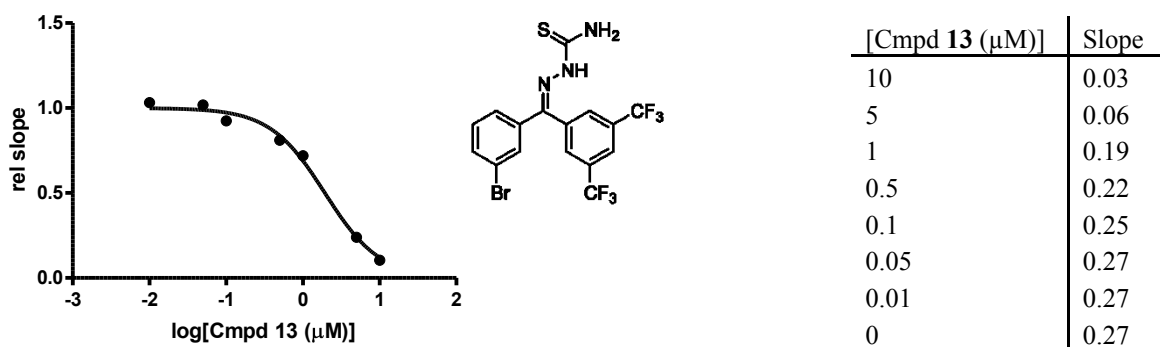
Sigmoidal dose-response (variable slope)	
Best-fit values	
Bottom	= 0.0
Top	= 1.000
LogEC50	0.8495
HillSlope	-1.186
EC50	7.07
Std. Error	
LogEC50	0.01913
HillSlope	0.08108
95% Confidence Intervals	
LogEC50	0.8003 to 0.8987
HillSlope	-1.395 to -0.9777
EC50	6.314 to 7.920
Goodness of Fit	
Degrees of Freedom	5
R square	0.9954
Absolute Sum of Squares	0.001601
Sy.x	0.0179
Constraints	
Bottom	Bottom = 0.0
Top	Top = 1.000
Number of points	
Analyzed	7

**Figure 28.** IC<sub>50</sub> determination of compound **12**

\*Note: Using the Fluoromax-2, an IC<sub>50</sub> value of 1.6  $\mu$ M was obtained for compound **12**. However, this is reasonable because the assay conditions for the Fluoromax-2 and the microplate reader were different (See Appendix 3). The final substrate concentration for the Fluoromax-2 assay was 6  $\mu$ M whereas that for the microplate assay was 60  $\mu$ M.

### IC<sub>50</sub> Determination of Compound **13**

Cathepsin B was preincubated with each concentration of inhibitor for 5 minutes. A representative IC<sub>50</sub> value of 1.93  $\mu$ M was obtained compound **13**, a di-trifluoromethyl benzophenone TSC. The R square value was 0.9954 which is considered good.



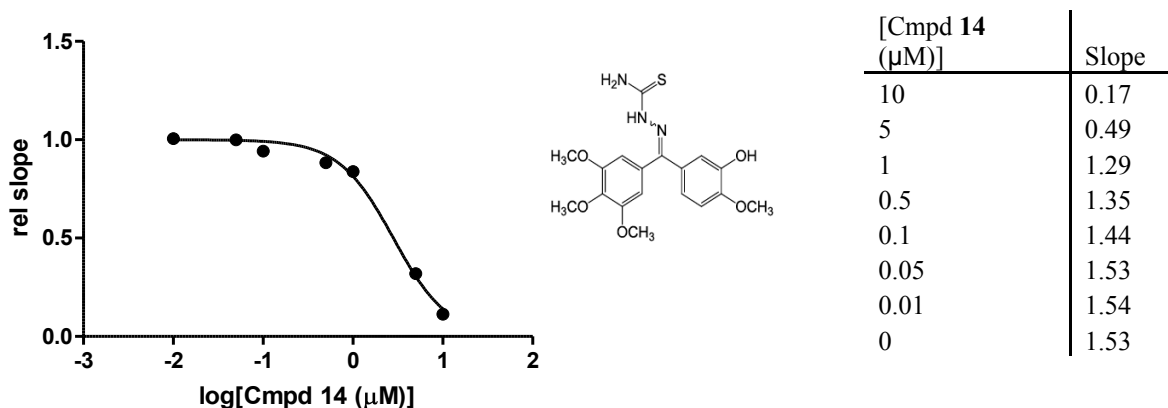
Best-fit values	
Bottom	= 0.0
Top	= 1.000
LogEC50	0.2862
HillSlope	-1.211
EC50	1.93
Std. Error	
LogEC50	0.03858
HillSlope	0.102
95% Confidence Intervals	
LogEC50	0.1870 to 0.3854
HillSlope	-1.474 to -0.9490
EC50	1.538 to 2.429
Goodness of Fit	
Degrees of Freedom	5
R square	0.9925
Absolute Sum of Squares	0.006324
Sy.x	0.03556
Constraints	
Bottom	Bottom = 0.0
Top	Top = 1.000
Number of points	
Analyzed	7

**Figure 29.** IC<sub>50</sub> determination of compound **13**



### IC<sub>50</sub> Determination of Compound **14**

Cathepsin B was preincubated with each concentration of inhibitor for 5 minutes. A representative IC<sub>50</sub> value of 2.81  $\mu$ M was obtained for compound **14**, a monohydroxy-tetramethoxy-substituted benzophenone TSC. The R square value was 0.9928.



Sigmoidal dose-response (variable slope)	
Best-fit values	
Bottom	= 0.00
Top	= 1.000
LogEC50	0.4492
HillSlope	-1.43
EC50	2.81
Std. Error	
LogEC50	0.03469
HillSlope	0.1202
95% Confidence Intervals	
LogEC50	0.3600 to 0.5384
HillSlope	-1.739 to -1.121
EC50	2.291 to 3.454
Goodness of Fit	
Degrees of Freedom	5
R square	0.9928
Absolute Sum of Squares	0.005606
Sy.x	0.03349
Constraints	
Bottom	Bottom = 0.0
Top	Top = 1.000
Number of points	
Analyzed	7

**Figure 30.** IC<sub>50</sub> determination of compound **14**

## *Determining the Mode of Action for Potent TSC Inhibitors of Cathepsin B*

### *Advanced Kinetics for Compound 12*

*Progress Curves for Compound 12.* Time dependent inhibition was considered through an analysis of a progress curve. In order to construct a progress curve for compound **12**, the microplate reader was set to measure the release of AMC over a 4 hour time period. The time dependence of the reaction was determined through an analysis of Figure 33 which depicts the reaction velocity as represented by relative fluorescence vs. time.

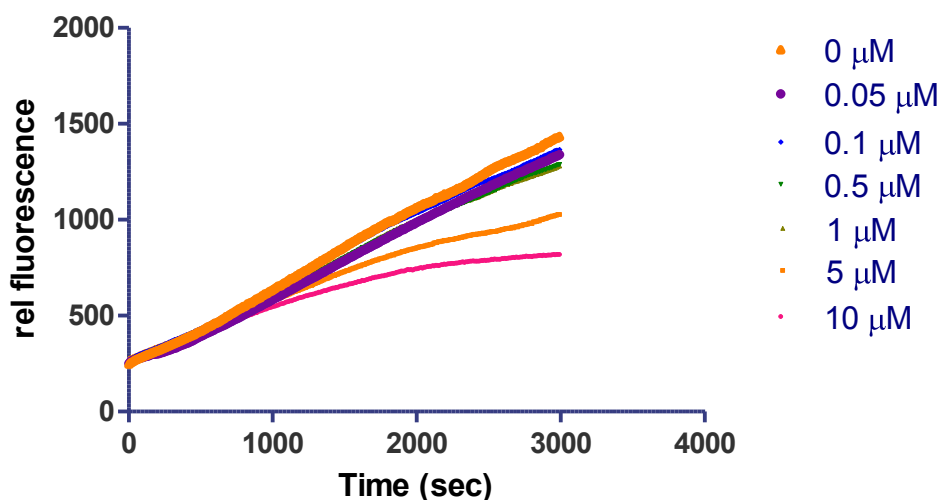
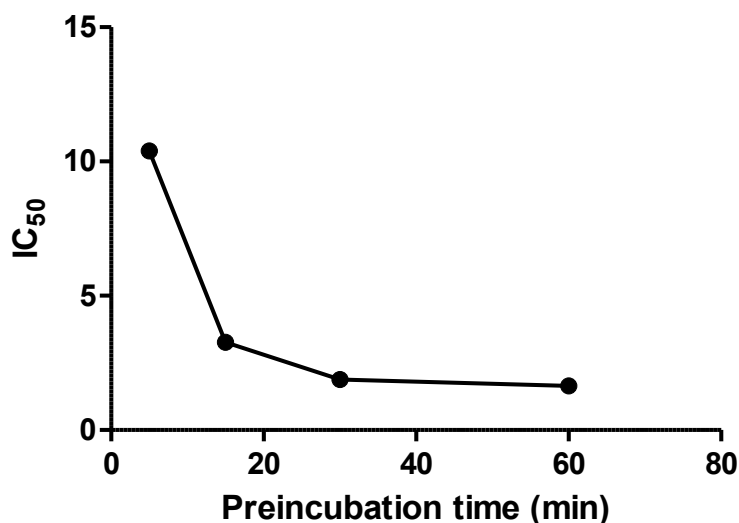


**Figure 33.** Progress Curve of compound **12**

The progress curve above demonstrates that the reaction between cathepsin B and compound **12** is time dependent in that the curve with the inhibitor initially displays a characteristic linear region followed by an approach to steady state. This pattern indicates that compound **12** binds slowly to the enzyme. According to the progress curve, the initial, uninhibited reaction is approximately linear over the 4 hour time period whereas

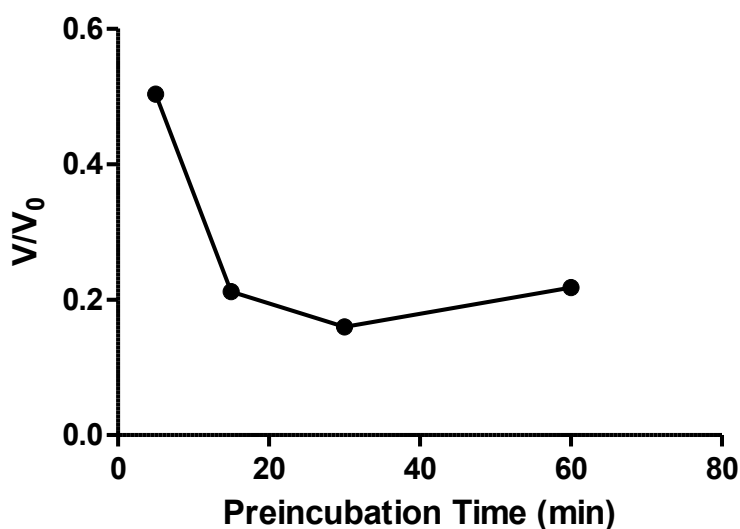
equilibrium is established between compound **12** and the enzyme in the inhibited reaction causing the curvature of the reaction progress curve represented by the bottom pink curve in Figure 33. At the start of the progress curve, the inhibited reaction curve is linear and the slope of the curve represents the enzyme's initial velocity. As time progresses, the curve deviates from linearity and a new velocity is established. Thus, this behavior suggests that compound **12** is time dependent.

*Varying Pre-incubation Time for Compound 12.* In order to confirm that compound **12** participates in time dependent inhibition, the effect of various preincubation times on the  $IC_{50}$  value was next considered. Various  $IC_{50}$  values were obtained as described in Chapter II (Methods) by altering the pre-incubation (preinc) time for which the cathepsin B solution and the dilutions of compound **12** were allowed to incubate together.



**Figure 35.**  $IC_{50}$  vs. Preincubation time for compound **12**

During the preincubation time at which compound **12** and cathepsin B are mixed together in the absence of substrate, compound **12** binds to the active site of the enzyme. If given enough time, the inhibitor will bind to most of the enzyme's active sites. As shown in Figure 35, increased incubation time results in a lower  $IC_{50}$  value. As the inhibitor and enzyme are allowed to incubate for a longer period of time, less inhibitor is required to inhibit the cathepsin B reaction by 50%.



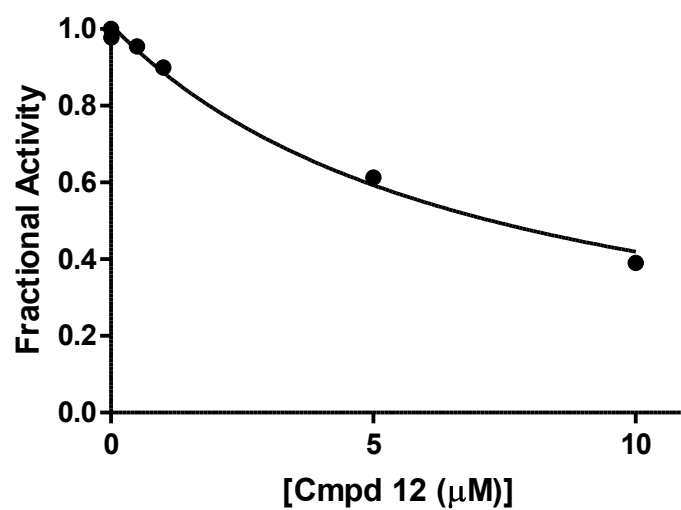
**Figure 36.** Varying preincubation time for compound **12**

Figure 36 illustrates that the steady state velocity decreases with preincubation time. Thus, compound **12** is a slow binding inhibitor. This figure demonstrates that as the preincubation time is increased, the velocity decreases, and this decrease in velocity indicates that compound **12** is inhibiting more of the cathepsin B molecules over time. Thus, lower  $IC_{50}$  values are achieved at longer preincubation times.

*Morrison Plot for Compound 12.* Because compound **12** was determined to be time-dependent, a Morrison Plot was constructed. A Morrison plot is used for analyzing slow, tight binding inhibitors or inhibitors that form a transient covalent bond with the enzyme. Analysis was performed using a Nonlinear Morrison Plot to determine the inhibitor's method of binding with the following constraints: [Cathepsin B] = 0.002  $\mu$ M, [Z-R-R-AMC] = 60  $\mu$ M, and a  $K_m$  value from the corresponding Michaelis-Menten Curve. The graph below was plotted using the classical Morrison equation,

$$\frac{v_i}{v_o} = 1 - \frac{([E] + [I] + K_i^{app}) - \sqrt{([E] + [I] + K_i^{app})^2 - 4[E][I]}}{2[E]}$$

where  $v_0$  represents the enzyme velocity with no inhibitor,  $v_i$  refers to the enzyme velocity with inhibitor,  $[E]$  represents the concentration of free enzyme,  $[I]$  represents the concentration of free inhibitor, and  $K_i^{app}$  refers to the apparent inhibition constant. The  $K_i$  was determined to be 6.13  $\mu$ M with an R squared value of 0.9918. This low  $K_i$  value suggest that compound **12** has a high affinity for cathepsin B. Furthermore, the Morrison plot indicates that the enzyme binds and dissociates slowly from the substrate because the enzyme is tied up with the inhibitor.



**Figure 34.** Morrison Plot for compound 12

**Table 14.** Morrison Plot kinetics for compound 12

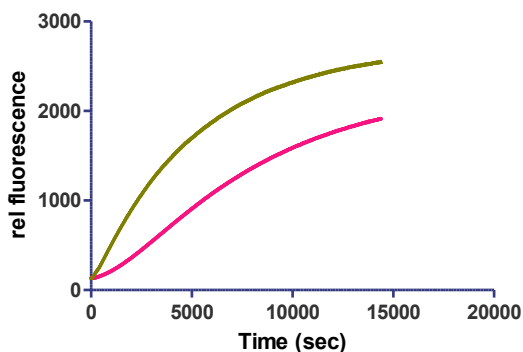
Morrison Ki	
Best-fit values	
Vo	1.012
Et	= 0.0020
Ki	6.131
S	= 60.00
Km	= 386.8
Std. Error	
Vo	0.01028
Ki	0.4214
95% Confidence Intervals	
Vo	0.9867 to 1.037
Ki	5.100 to 7.162
Goodness of Fit	
Degrees of Freedom	6
R square	0.9918
Absolute Sum of Squares	0.003049
Sy.x	0.02254
Constraints	
Et	Et = 0.0020
S	S = 60.00
Km	Km = 386.8
Number of points	
Analyzed	8

The Morrison Plot demonstrates that as the concentration of the inhibitor is increased, the fractional activity (which is determined by the ratio between the velocity of the inhibited reaction and the velocity of the uninhibited reaction) decreases. The inhibitor contributes to this decrease in velocity by impeding the activity of the enzyme. The most important region of the Morrison plot corresponds to the region in which a significant curvature is observed (Copeland, 2005). This occurs in the range at which the free inhibitor concentration approximates the free enzyme concentration. The information obtained from this region of the plot determines the value of  $K_i^{\text{app}}$ .

*Reversibility Plot for Compound 12.* To further characterize the mode of inhibition of compound **12**, reversibility was also analyzed. In order to be considered a lead compound, it is important for the inhibitor to be reversible. Irreversible inhibitors can be dangerous in that they usually form a covalent bond with their targets and permanently alter the target's active site, and this can lead to the inactivation of enzymatic activity.

The figure below demonstrates that compound **12** is a reversible inhibitor. This is evident by the recovery of the enzymatic activity after a large dilution of the cathepsin B-compound **12** complex (see Chapter II).

A



B

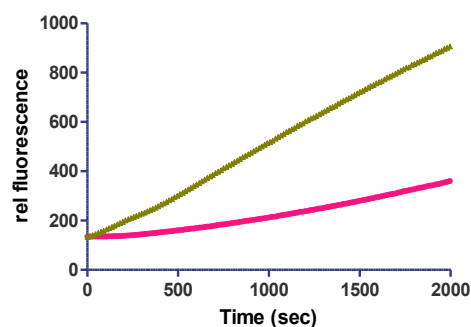


**Figure 37 A.** Reversibility of compound **12** over 4 hour time period (1 hour preincubation) **B.** Reversibility of compound **12** over approximately 30 minute time period (1 hour preincubation)

In Figure 37A and 37B, the green curve represents the control reaction which does not contain compound **12** whereas the pink curve represents the cathepsin B reaction in the presence of compound **12**. The curvilinear behavior of this progress curve suggests that the inhibition is slowly reversible. This curvature can more easily be seen in the Figure 37B which focuses on the first 2000 seconds of the reaction in Figure 37A. From this graph, the slowly reversible inhibition of compound **12** more easily visualized. The inhibited reaction displays a brief lag phase as represented by a slight curvature in the 0 to 1000 second time frame. Because of the slight upward curvature of the graph, the velocity of the reaction increases as time progresses. The curve does not approach zero RFU, so the reaction cannot be considered irreversible. As the reaction proceeds, the progress curve begins to display a linear phase which indicates slow recovery of enzyme activity.



*Test for Competitiveness: Effects of Varying [Z-R-R-AMC] on IC<sub>50</sub> Value.* In order to determine how various substrate concentrations affect the IC<sub>50</sub> value of compound **12**, 60  $\mu$ M, 40  $\mu$ M, 20  $\mu$ M, and 6  $\mu$ M Z-R-R-AMC were tested with various dilutions of compound **12** and cathepsin B. IC<sub>50</sub> curves were analyzed for each substrate concentration using the Hill equation as described previously.

**Table 13.** The Effect of Varying [Z-R-R-AMC] on IC<sub>50</sub> Value

[Z-R-R-AMC ( $\mu$ M)]	IC <sub>50</sub>
60	7.07
40	5.68
20	3.91
6	3.73

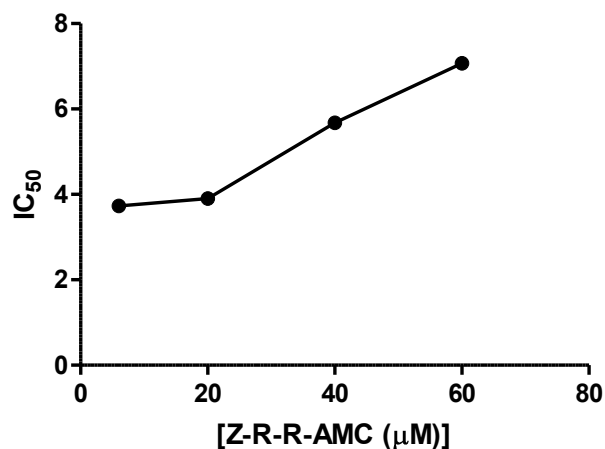


**Figure 31.** IC<sub>50</sub> vs. [substrate] for compound **12**

The data displayed in Table 13 and Figure 31 demonstrate that compound **12**, a bromo-substituted, acetylated phenolic benzophenone TSC, is competitive with respect to the substrate in that the inhibitor competes with the substrate for the free enzyme's active site. As the substrate concentration increases, more inhibitor is needed to inhibit the

cathepsin B reaction by 50%. Thus, a higher  $IC_{50}$  value is obtained as the concentration of the substrate is increased.

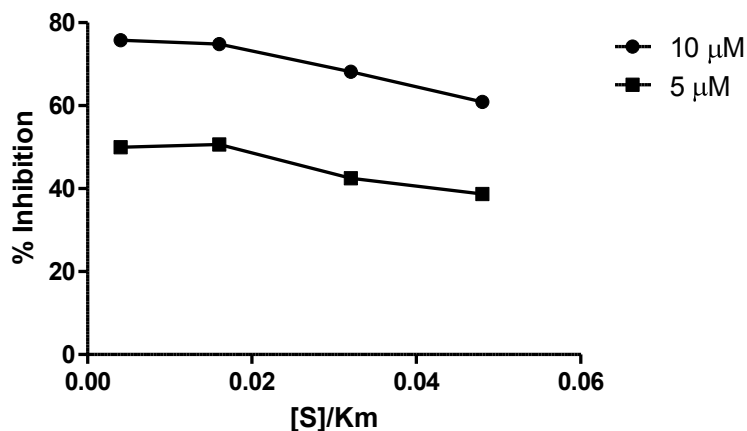


**Figure 32.** Percent Inhibition vs. [substrate]/ $K_m$  for compound **12**

Figure 32 indicates that as the substrate concentration is increased, the percent inhibition of the reaction decreases.

#### *Advanced Kinetics for Compound 13*

*Progress Curve for Compound 13.* In order to determine if compound **13** displays a time dependent mode of inhibition, a progress curve was analyzed for this inhibitor. To construct the progress curve for compound **13**, the microplate reader was set to measure the release of AMC over a 4 hour time period. The time dependence of the reaction was determined through an analysis of Figure 39 which depicts relative fluorescence vs. time.

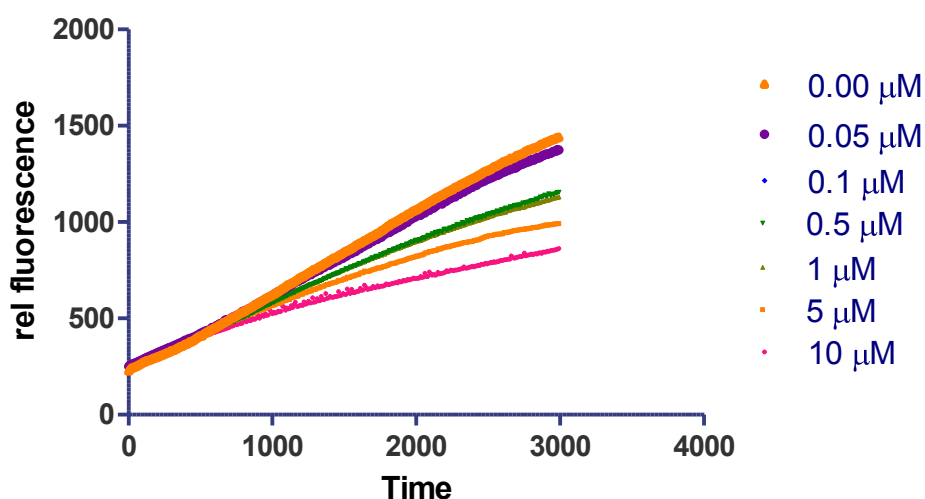


**Figure 39.** Progress Curve for compound **13**

The progress curve above demonstrates that the reaction between cathepsin B and compound **13** is time dependent in that the curve initially displays a characteristic linear region followed by an approach to steady state during the 4 hour time period.

*Varying Pre-incubation Time for Compound 13.* Once it was determined that the mode of inhibition of compound **13** is time dependent, the effect of various pre-incubation (preinc) times was considered. Various  $\text{IC}_{50}$  values were obtained as described in Chapter II (Methods) by altering the pre-incubation time for which the cathepsin B solution and the dilutions of compound **13** were allowed to incubate together.

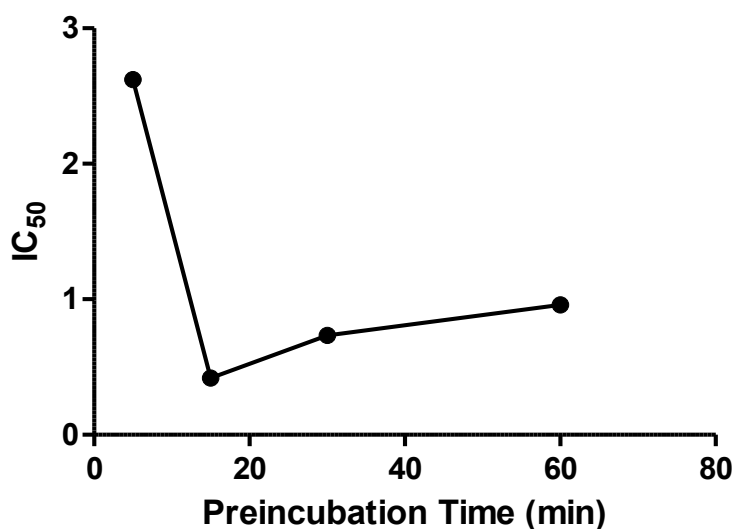


**Figure 41.** IC<sub>50</sub> vs. Preincubation time for compound **13**

Figure 41 verifies that compound **13** displays time dependent inhibition. Generally, as the time that the inhibitor interacts with the enzyme during the preincubation step increases, the smaller the IC<sub>50</sub> value becomes. Therefore, at greater preincubation times, a lower concentration of compound **13** is required to inhibit the cathepsin B reaction by 50%. This is because during a long preincubation step, the inhibitor blocks the substrate's interaction with the enzyme by binding to cathepsin B's active sites resulting in increased inhibition.

*Morrison Plot for Compound 13.* Because compound **13** was determined to be time-dependent, a Morrison Plot was constructed. Analysis was performed using a Nonlinear Morrison Plot to determine the inhibitor's method of binding with the following constraints: [Cathepsin B] = 0.002  $\mu$ M, [Z-R-R-AMC] = 60  $\mu$ M, and a  $K_m$  using the classical Morrison equation as described above. The  $K_i^{app}$  was determined to be 1.51  $\mu$ M, and the R square value was 0.9882 which is considered excellent.

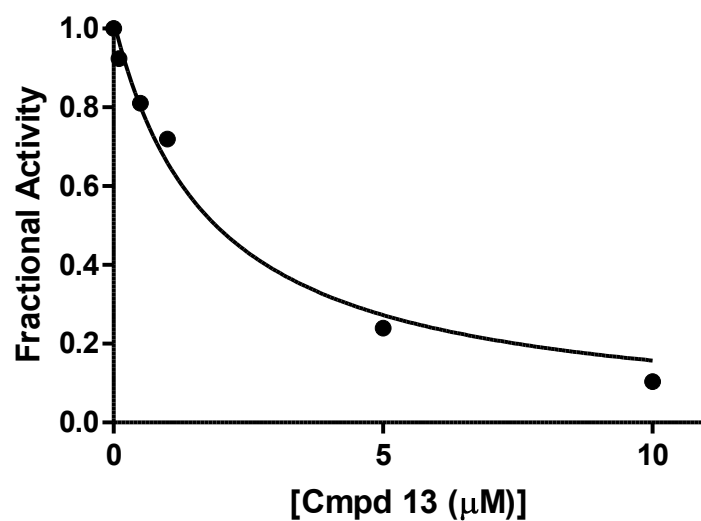


**Figure 40.** Morrison Plot for compound **13**; Preinc time of 5 minutes

**Table 16.** Morrison Plot kinetics for compound **13**

Morrison Ki	
Best-fit values	
Vo	1.022
Et	= 0.0020
Ki	1.513
S	= 60.00
Km	= 295.8
Std. Error	
Vo	0.02237
Ki	0.1976
95% Confidence Intervals	
Vo	0.9676 to 1.077
Ki	1.029 to 1.996
Goodness of Fit	
Degrees of Freedom	6
R square	0.9882
Absolute Sum of Squares	0.01092
Sy.x	0.04265
Constraints	
Et	Et = 0.0020
S	S = 60.00
Km	Km = 295.8
Number of points	
Analyzed	8

*Reversibility Plot for Compound 13.* To further understand compound **13**'s mode of inhibition, the reversibility of the enzyme-inhibitor complex was studied. Figure 43 below demonstrates the reversibility of inhibition with compound **13** as evident by the recovery of the enzymatic activity after a larger dilution of the cathepsin B-compound **1** complex (see Chapter II: Methods).

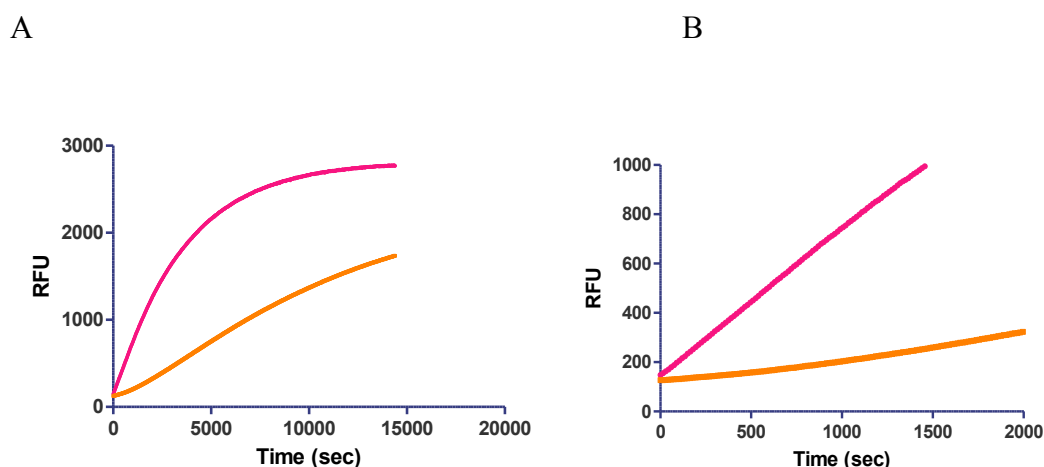


**Figure 43** **A.** Reversibility of compound **13** over a 4 hour time period (1 hour preincubation) **B.** Reversibility of compound **13** over approximately a 30 minute time period (1 hour preincubation)

In this figure, the pink curve represents the control reaction whereas the orange curve represents the cathepsin B reaction in the presence of compound **13**. The curvilinear behavior of the inhibited progress curve suggests that the inhibition is slowly reversible. This curvature can more easily be seen in the Figure 43B which focuses on the first 2000 seconds of the reaction in figure 43A. From this graph, the slowly reversible inhibition of compound **13** is more obvious. The inhibited reaction displays a slow increase in reaction velocity as indicated by the line's upward curvature. This increase in velocity

suggests that the enzyme slowly recovers its activity as the reaction progresses.

Therefore, the inhibition of cathepsin B by compound **13** is reversible.

*Test for Competitiveness: Effects of Varying [Z-R-R-AMC] on IC<sub>50</sub> Value.* In order to analyze the change in IC<sub>50</sub> values due to various substrate concentrations, 60  $\mu$ M, 40  $\mu$ M, 20  $\mu$ M, and 6  $\mu$ M Z-R-R-AMC were tested with various dilutions of compound **13** and cathepsin B. IC<sub>50</sub> curves were analyzed for each substrate concentration using the Hill equation as described previously.

**Table 15.** The Effect of Varying [Z-R-R-AMC] on IC<sub>50</sub> Value

[Z-R-R-AMC ( $\mu$ M)]	IC <sub>50</sub>
60	1.93
40	1.85
20	1.21

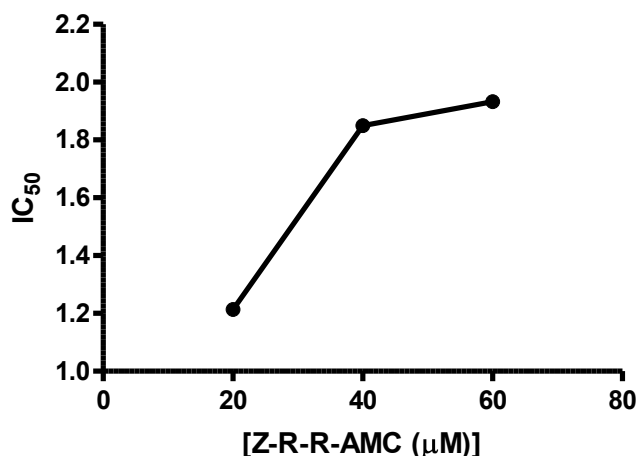


**Figure 38.** IC<sub>50</sub> vs. [substrate] for compound **13**

Like compound **12**, Table 15 and Figure 38 indicate that compound **13**, a bromo-substituted, di-trifluoromethyl benzophenone TSC, is competitive with respect to the

substrate. The competition between the substrate and compound **13** is demonstrated by the fact that the  $IC_{50}$  values increase as the substrate concentration increases, respectively.

#### *Advanced Kinetics for Compound 14*

*Test for Competitiveness: Effects of Varying [Z-R-R-AMC] on  $IC_{50}$  Value.* Taking into account some experimental variation, it appears that compound **14** competes with the substrate for the enzyme's active site (data not shown).

*Reversibility Plot for Compound 14.* As with the other compounds, the reversibility of inhibition for compound **14** was also studied. Figure 47 below demonstrates the reversibility of inhibition with compound **14** as evident by the recovery of the enzymatic activity after a large dilution of the cathepsin B-inhibitor complex (see Chapter II: Methods). Because the reaction does not proceed to zero, the inhibition is considered reversible.

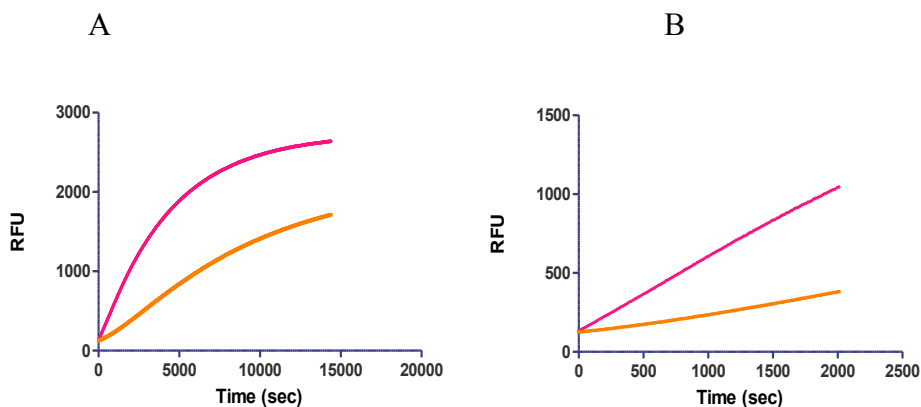


**Figure 47A.** Reversibility of compound **14** over 4 hour time period (1 hour preincubation) **B.** Reversibility of compound **14** over approximately 30 minute time period (1 hour preincubation). The data in figure 47 was collected by Victoria Soeung and reprinted with her permission.



Like compound **12** and **13**, compound **14** displays reversible inhibition as demonstrated by the different curvatures of the uninhibited and inhibited in Figure 47A. Furthermore, figure 47B more clearly demonstrates the enzyme's recovery indicating that the inhibitor forms a transient covalent bond with cathepsin B.

### *Conclusion*

Several of the non-peptidic thiosemicarbazone inhibitors synthesized by the Pinney group in a collaborative project between the Trawick and Pinney laboratories have been shown to be promising candidates for effective inhibition against cathepsin B activity in that these compounds have IC<sub>50</sub> values in the low micromolar to nanomolar range. In this study, five hits were found (compounds **1**, **7**, **12**, **13**, **14**) with compound **1** serving as the reference compound. With a representative IC<sub>50</sub> value of 25.79  $\mu$ M, compound **7** was not determined to be a lead cathepsin B inhibitor. The other three potent TSC inhibitors (compounds **12**, **13**, and **14**) were further analyzed by performing advanced kinetic experiments in order to determine a mode of inhibition. Compound **12**, a bromo-substituted, acetylated phenolic benzophenone TSC, and compound **13**, a bromo-substituted, di-trifluoromethyl benzophenone TSC exhibited time dependent, competitive inhibition with respect to the substrate. Compound **14**, a monohydroxy-tetramethoxy-substituted benzophenone TSC displayed classical competitive inhibition against cathepsin B. Furthermore, all three of these compounds displayed reversible inhibition indicating that the TSC compounds form a transient covalent bond at the active site of cathepsin B and could serve as a new type of cathepsin B inhibitor. Table 18 summarizes these findings.

**Table 18.** Summary of the advanced kinetic findings for three TSC compounds

Compound	IC <sub>50</sub> (μM) for 5 min preinc.	Time dependent	Competitive/ Uncompetitive/ Noncompetitive	Reversibility
<b>12</b>	7.07	Yes	-	Slowly reversible
<b>13</b>	1.93	Yes	-	Slowly reversible
<b>14</b>	2.81	No	Competitive	Reversible

Figure 48 below outlines the proposed mechanism of inhibition for compounds **12** and **13**. In this mechanism, the active site thiolate of the cysteine residue attacks the TSC moiety. This nucleophilic attack on the TSC substrate produces a tetrahedral intermediate which may contribute to the regeneration of the active site following the hydrolysis of cathepsin B. However, this step is not shown in figure 48 since it has not been confirmed.

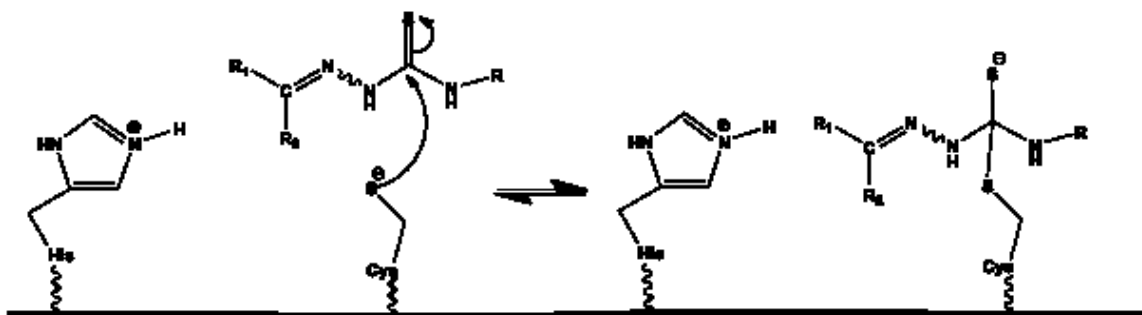


**Figure 48.** Proposed mechanism of inhibition for compounds **12** and **13**.

### *Future Work*

Future studies will involve the screening of additional thiosemicarbazone compounds for inhibition of cathepsin B activity. Also, cytotoxicity studies will be performed on the most potent inhibitors of cathepsin B including compounds **13** and **14**. These assays will be performed on normal cells as opposed to cancer cell lines in order to analyze the toxicity of the compounds. Furthermore, migration assays will be performed in cancer cells in culture to study the ability of potent TSC compounds to inhibit the invasion and migration of cancerous cells. Molecular modeling will also be used to further understand the binding of the most potent TSC inhibitors to the active site of cathepsin B. Structure-activity relationship studies of the inhibitors will also aid in understanding the binding mechanism.

## APPENDICES

## APPENDIX A

### Primary Literature Search

#### *Search terms, # of Hits*

##### *PubMed*

- Cathepsin B and cancer metastasis, 263
  - Selected articles containing “cathepsin B” in the title.
- Cathepsin B and inhibitor (limited to subset of cancer), 147
  - Selected articles with “endogenous inhibitor” and cathepsin B, “cystatin,” or “stefins” in the title.
- Cathepsin B and processing (limited to last 10 years), 133
  - Selected articles with “cathepsin B expression,” “uPA,” “processing of procathepsin B,” “cathepsin B trafficking,” or activation of cathepsin B” in the title.
- Cathepsin B and structure (limited to last 5 years), 97
  - Selected articles with “binding pocket of cathepsin B,” “crystal structure of cathepsin B,” “occluding loop,” or QSAR models and cathepsin B in the title.

##### *Scopus*

- “Cathepsin B” and cancer metastasis (limited to year 2000 to present), 233
  - Selected articles with “cathepsin B” and biomarker for cancer in the title.
- “Cathepsin B” and “cancer metastasis”, 25
  - Selected articles concerning metastatic potential and cathepsin B.
- “Cathepsin B” and processing (limited to year 2000 to present), 287
  - Selected articles concerning proteolytic networks or zymogen activation.
- “Cathepsin B” and inhibitor and cancer (limited to year 2009 to present), 99

- Selected articles with “inhibition of cathepsin B,” or cathepsin B and tumorigenesis in the title.

#### *ScienceDirect*

- “Cathepsin B” and “cancer metastasis” (limited to year 2000 to present), 327
  - Selected articles concerning the role of cathepsin B in cancer progression.
- “Cathepsin B” and inhibitor (limited to year 2011), 398
  - Selected articles concerning novel compounds as inhibitors of cathepsin B activity.
- “Procathepsin B” processing, 189
  - Selected articles with “structure of procathepsin B” in the title, or those concerning the activation of procathepsin B.

#### *Web of Science*

- Cathepsin B and cancer metastasis, 322
  - Selected articles containing “cathepsin B” in the title.
- Procathepsin B and processing, 115
  - Selected articles with “activation of cathepsin B,” or procathepsin B processing in the title.
- “Cathepsin B” and inhibitor not Cathepsin L (limited to the last 5 years), 347
  - Selected articles concerning cathepsin B inhibitors.

Science Direct

1. Performed Advanced Search:

- “Cathepsin B” in Abstract, Title, or Keywords AND Inhibitors in Abstract, Title, or Keywords; Limited to Journals
- Date Range: 2010 to Present
- 50 Hits

Selected the following articles:

- (1) Benjamin, S. Immunomodulating tellurium compounds as anti-cancer agents. *Semin. Cancer Biol.* **2012**, 22, 60-69.
- (2) Caracelli, I.; Vega-Tejido, M.; Zukerman-Schpector, J.; Cezari, M. H. S.; Lopes, J. G. S.; Juliano, L.; Santos, P. S.; Comasseto, J. V.; Cunha, R. L. O. R.; Tiekink, E. R. T. A tellurium-based cathepsin B inhibitor: Molecular structure, modelling, molecular docking and biological evaluation. *J. Mol. Struct.* **2012**, 1013, 11-18.
- (3) Mura, P.; Camalli, M.; Casini, A.; Gabbiani, C.; Messori, L. Trans –cis-cis-[RuCl<sub>2</sub>(DMSO)<sub>2</sub>(2-amino-5-methyl-thiazole)<sub>2</sub>], (PMRu52), a novel ruthenium(II) compound acting as a strong inhibitor of cathepsin B. *J. Inorg. Biochem.* **2010**, 104, 111-117.
- (4) SosiÄŒ, I.; MirkoviÄŒ, B.; Turk, S.; Å tefane, B.; Kos, J.; Gobec, S. Discovery and kinetic evaluation of 6-substituted 4-benzylthio-1,3,5-triazin-2(1H)-ones as inhibitors of cathepsin B. *Eur. J. Med. Chem.* **2011**, 46, 4648-4656.
- (5) Zhu, Y.; Cameron, B. R.; Mosi, R.; Anastassov, V.; Cox, J.; Qin, L.; Santucci, Z.; Metz, M.; Skerlj, R. T.; Fricker, S. P. Inhibition of the cathepsin cysteine proteases B and K by square-planar cycloaurated gold(III) compounds and investigation of their anti-cancer activity. *J. Inorg. Biochem.* **2011**, 105, 754-762.

2. Advanced Search:

- “Cathepsin B” in Abstract, Title, or Keywords AND Processing in Abstract, Title, or Keywords; Limited to Journals
- Date Range: 2010 to Present
- Limited to the following topics: cathepsin, cysteine protease, cell death, cathepsin b-like, protease, mmp activity, protease inhibitor, and proteasome inhibitor.
- 34 Hits

Selected the following articles:

- (1) de Bettignies, G.; Coux, O. Proteasome inhibitors: Dozens of molecules and still counting. *Biochimie* **2010**, 92, 1530-1545.
- (2) Edgington, L. E.; Verdoes, M.; Bogoy, M. Functional imaging of proteases: recent advances in the design and application of substrate-based and activity-based probes. *Curr. Opin. Chem. Biol.* **2011**, 15, 798-805.
- (3) Groth-Pedersen, L.; J            , M. Combating apoptosis and multidrug resistant cancers by targeting lysosomes. *Cancer Lett.* .
- (4) Hook, V.; Funkelstein, L.; Wegrzyn, J.; Bark, S.; Kindy, M.; Hook, G. Cysteine Cathepsins in the secretory vesicle produce active peptides: Cathepsin L generates peptide neurotransmitters and cathepsin B produces beta-amyloid of Alzheimer's disease. *Biochimica et Biophysica Acta (BBA) - Proteins & Proteomics* **2012**, 1824, 89-104.
- (5) Kaminsky, V.; Zhivotovsky, B. Proteases in autophagy. *Biochimica et Biophysica Acta (BBA) - Proteins & Proteomics* **2012**, 1824, 44-50.
- (6) Mentlein, R.; Hattermann, K.; Held-Feindt, J. Lost in disruption: Role of proteases in glioma invasion and progression. *Biochimica et Biophysica Acta (BBA) - Reviews on Cancer* **2012**, 1825, 178-185.
- (7) Repnik, U.; Stoka, V.; Turk, V.; Turk, B. Lysosomes and lysosomal cathepsins in cell death. *Biochimica et Biophysica Acta (BBA) - Proteins & Proteomics* **2012**, 1824, 22-33.
- (8) Scott, C. J.; Taggart, C. C. Biologic protease inhibitors as novel therapeutic agents. *Biochimie* **2010**, 92, 1681-1688.
- (9) Shenoy, R. T.; Sivaraman, J. Structural basis for reversible and irreversible inhibition of human cathepsin L by their respective dipeptidyl glyoxal and diazomethylketone inhibitors. *J. Struct. Biol.* **2011**, 173, 14-19.
- (10) Turk, V.; Stoka, V.; Vasiljeva, O.; Renko, M.; Sun, T.; Turk, B.; Turk, D. Cysteine cathepsins: From structure, function and regulation to new frontiers. *Biochimica et Biophysica Acta (BBA) - Proteins & Proteomics* **2012**, 1824, 68-88.
- (11) Wallin, H.; Bjarnadottir, M.; Vogel, L. K.; Wass          , J.; Ekstr      , U.; Abrahamson, M. Cystatins “ Extra- and intracellular cysteine protease inhibitors: High-level secretion and uptake of cystatin C in human neuroblastoma cells. *Biochimie* **2010**, 92, 1625-1634.



*Scopus*

1. Performed Advanced Search:

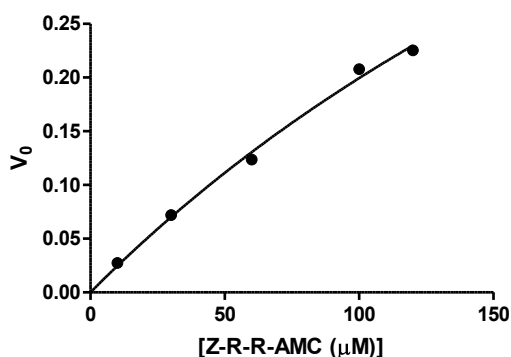
- “Cathepsin B” AND cancer metastasis in Abstract, Title, or Keywords
- Date Range: 2010 to Present
- 54 Hits

Selected the following titles:

- (1) Kasabova, M.; Saidi, A.; Naudin, C.; Sage, J.; Lecaille, F.; Lalmanach, G. Cysteine cathepsins: Markers and therapy targets in lung disorders. *Clinical Reviews in Bone and Mineral Metabolism* **2011**, *9*, 148-161.
- (2) Kolwijck, E.; Kos, J.; Obermajer, N.; Span, P. N.; Thomas, C. M. G.; Massuger, L. F. A. G.; Sweep, F. C. G. J. The balance between extracellular cathepsins and cystatin C is of importance for ovarian cancer. *Eur. J. Clin. Invest.* **2010**, *40*, 591-599.
- (3) Lokman, N. A.; Ween, M. P.; Oehler, M. K.; Ricciardelli, C. The role of annexin A2 in tumorigenesis and cancer progression. *Cancer Microenvironment* **2011**, *4*, 199-208.
- (4) Matarrese, P.; Ascione, B.; Ciarlo, L.; Vona, R.; Leonetti, C.; Scarsella, M.; Mileo, A. M.; Catricalà, C.; Paggi, M. G.; Malorni, W. Cathepsin B inhibition interferes with metastatic potential of human melanoma: An in vitro and in vivo study. *Molecular Cancer* **2010**, *9*.
- (5) Nalla, A. K.; Gorantla, B.; Gondi, C. S.; Lakka, S. S.; Rao, J. S. Targeting MMP-9, uPAR, and cathepsin B inhibits invasion, migration and activates apoptosis in prostate cancer cells. *Cancer Gene Ther.* **2010**, *17*, 599-613.

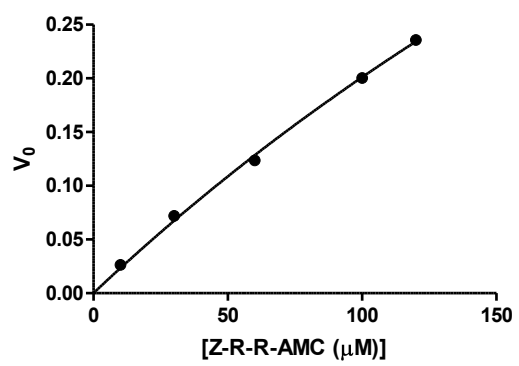
## APPENDIX B

### Michaelis-Menten Curves

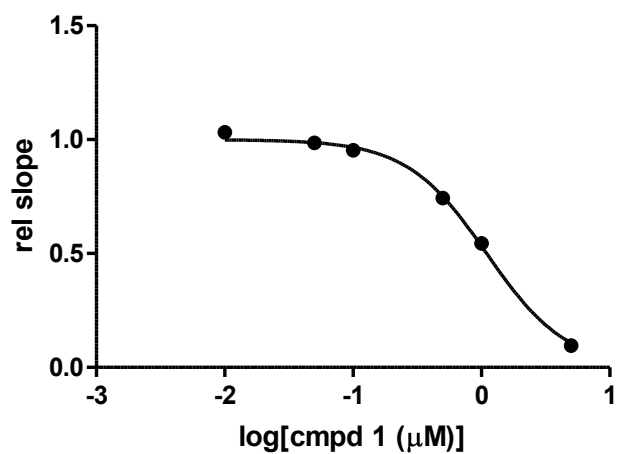


Michaelis-Menten	
Best-fit values	
Vmax	0.9615
Km	382.2
Std. Error	
Vmax	0.3408
Km	170
95% Confidence Intervals	
Vmax	-0.1230 to 2.046
Km	0.0 to 923.2
Goodness of Fit	
Degrees of Freedom	3
R square	0.9949
Absolute Sum of Squares	0.0001472
Sy.x	0.007004
Constraints	
Km	Km > 0.0
Number of points Analyzed	5

Michaelis-Menten	
Best-fit values	
Vmax	1.341
Km	566.9
Std. Error	
Vmax	0.4191
Km	208.2
95% Confidence Intervals	
Vmax	0.007153 to 2.674
Km	0.0 to 1229
Goodness of Fit	
Degrees of Freedom	3
R square	0.9982
Absolute Sum of Squares	0.00005529
Sy.x	0.004293
Constraints	
Km	Km > 0.0
Number of points	

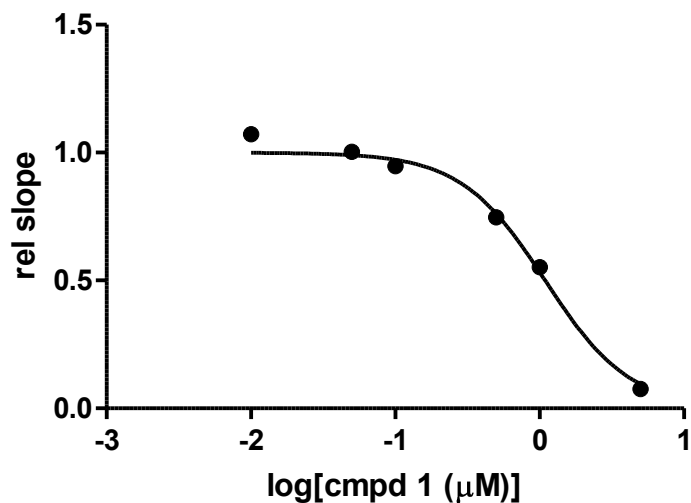


# IC<sub>50</sub> Determination of Compound 1



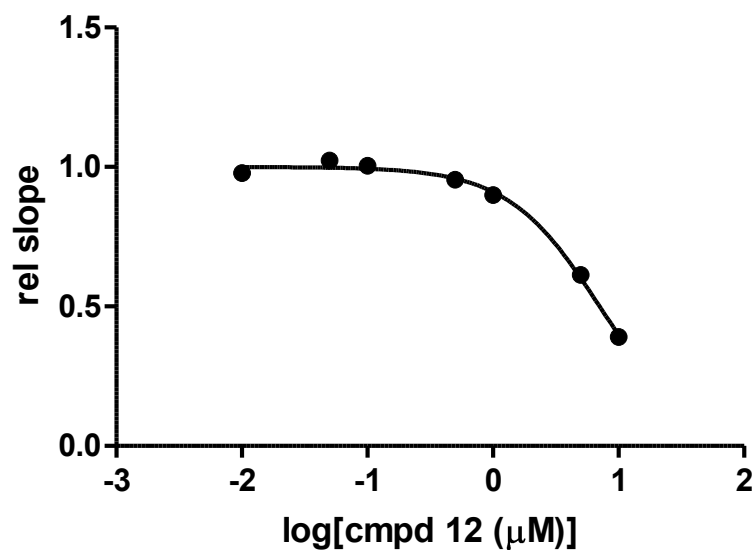
Sigmoidal dose-response (variable slope)	
Best-fit values	
Bottom	= 0.0
Top	= 1.000
LogEC50	0.04098
HillSlope	-1.396
EC50	1.099
Std. Error	
LogEC50	0.02008
HillSlope	0.09344
95% Confidence Intervals	
LogEC50	-0.01477 to 0.09674
HillSlope	-1.656 to -1.137
EC50	0.9666 to 1.249
Goodness of Fit	
Degrees of Freedom	4
R square	0.9975
Absolute Sum of Squares	0.001627
Sy.x	0.02017
Constraints	
Bottom	Bottom = 0.0
Top	Top = 1.000
Number of points	
Analyzed	6

# IC<sub>50</sub> Determination of Compound 1



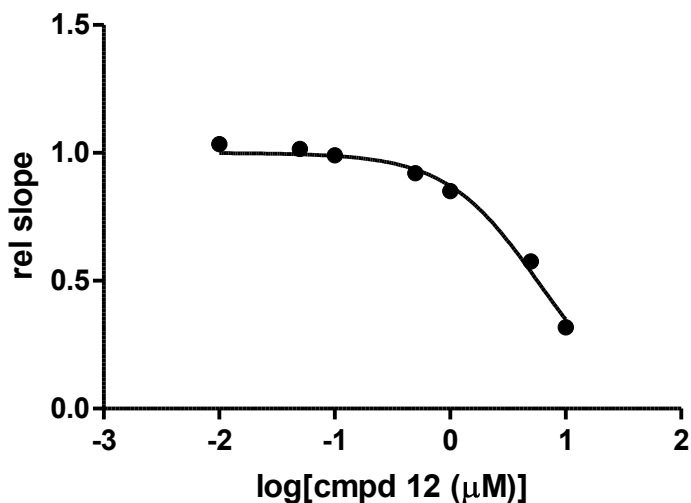
Sigmoidal dose-response (variable slope)	
Best-fit values	
Bottom	= 0.0
Top	= 1.000
LogEC50	0.03844
HillSlope	-1.483
EC50	1.093
Std. Error	
LogEC50	0.0407
HillSlope	0.2154
95% Confidence Intervals	
LogEC50	-0.07454 to 0.1514
HillSlope	-2.081 to -0.8851
EC50	0.8423 to 1.417
Goodness of Fit	
Degrees of Freedom	4
R square	0.9899
Absolute Sum of Squares	0.007089
Sy.x	0.0421
Constraints	
Bottom	Bottom = 0.0
Top	Top = 1.000
Number of points	
Analyzed	6

IC<sub>50</sub> Determination of Compound **12** with 60  $\mu$ M Z-R-R-AMC



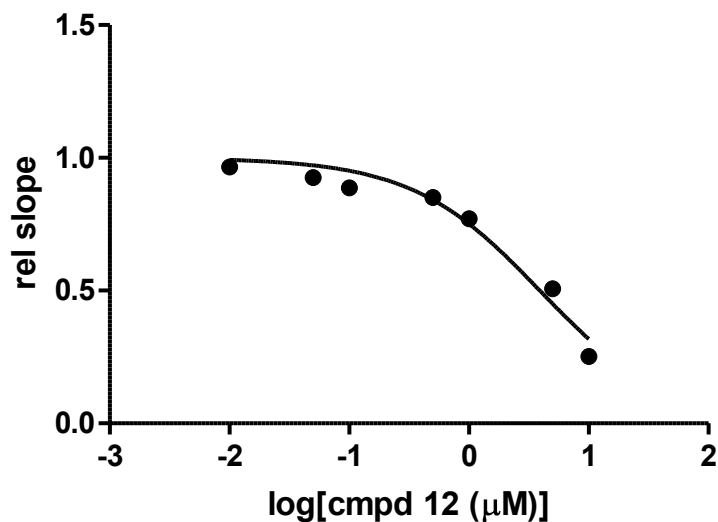
Sigmoidal dose-response (variable slope)	
Best-fit values	
Bottom	= 0.0
Top	= 1.000
LogEC50	0.8495
HillSlope	-1.186
EC50	7.072
Std. Error	
LogEC50	0.01913
HillSlope	0.08108
95% Confidence Intervals	
LogEC50	0.8003 to 0.8987
HillSlope	-1.395 to -0.9777
EC50	6.314 to 7.920
Goodness of Fit	
Degrees of Freedom	5
R square	0.9954
Absolute Sum of Squares	0.001601
Sy.x	0.0179
Constraints	
Bottom	Bottom = 0.0
Top	Top = 1.000
Number of points	
Analyzed	7

IC<sub>50</sub> Determination of Compound **12** with 40  $\mu$ M Z-R-R-AMC



Sigmoidal dose-response (variable slope)	
Best-fit values	
Bottom	= 0.0
Top	= 1.000
LogEC50	0.754
HillSlope	-1.099
EC50	5.675
Std. Error	
LogEC50	0.03445
HillSlope	0.111
95% Confidence Intervals	
LogEC50	0.6654 to 0.8425
HillSlope	-1.384 to -0.8138
EC50	4.628 to 6.959
Goodness of Fit	
Degrees of Freedom	5
R square	0.9888
Absolute Sum of Squares	0.004892
Sy.x	0.03128
Constraints	
Bottom	Bottom = 0.0
Top	Top = 1.000
Number of points	
Analyzed	7

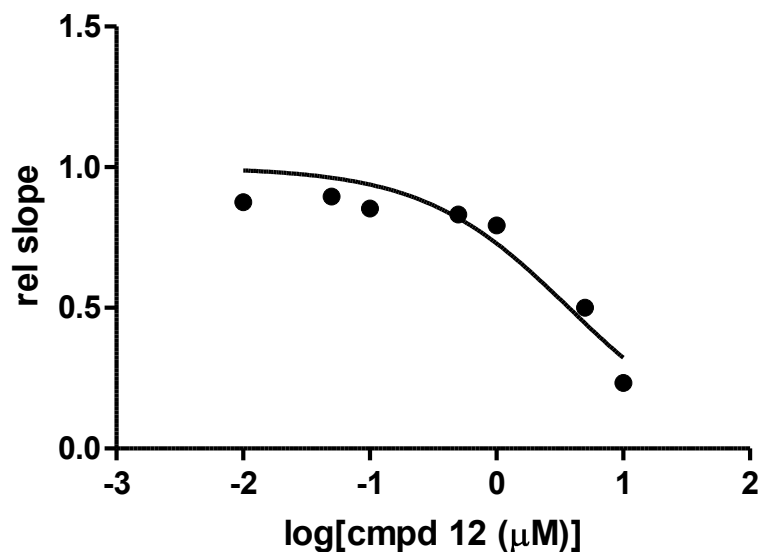
IC<sub>50</sub> Determination of Compound **12** with 20  $\mu$ M Z-R-R-AMC



Sigmoidal dose-response (variable slope)	
Best-fit values	
Bottom	= 0.0
Top	= 1.000
LogEC50	0.5917
HillSlope	-0.8118
EC50	3.905
Std. Error	
LogEC50	0.07368
HillSlope	0.1161
95% Confidence Intervals	
LogEC50	0.4022 to 0.7811
HillSlope	-1.110 to -0.5132
EC50	2.525 to 6.041
Goodness of Fit	
Degrees of Freedom	5
R square	0.9637
Absolute Sum of Squares	0.015
Sy.x	0.05478
Constraints	
Bottom	Bottom = 0.0
Top	Top = 1.000
Number of points	
Analyzed	7

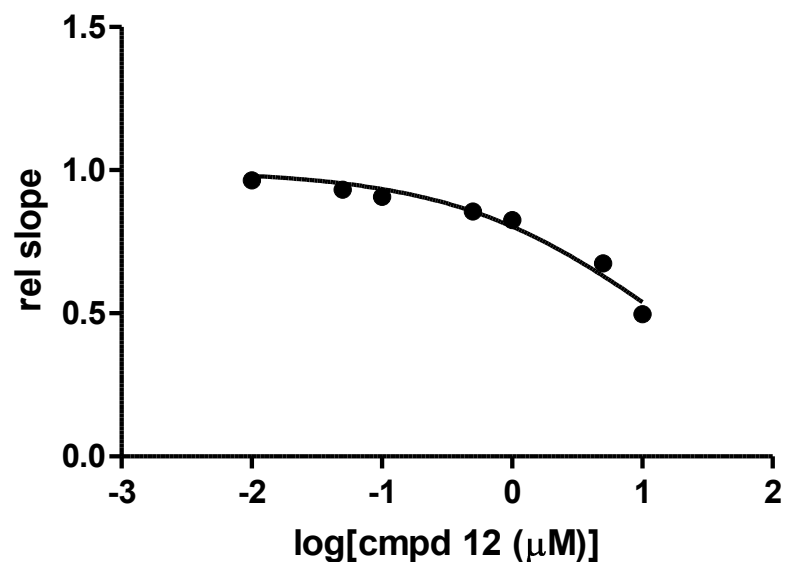


IC<sub>50</sub> Determination of Compound **12** with 6  $\mu$ M Z-R-R-AMC



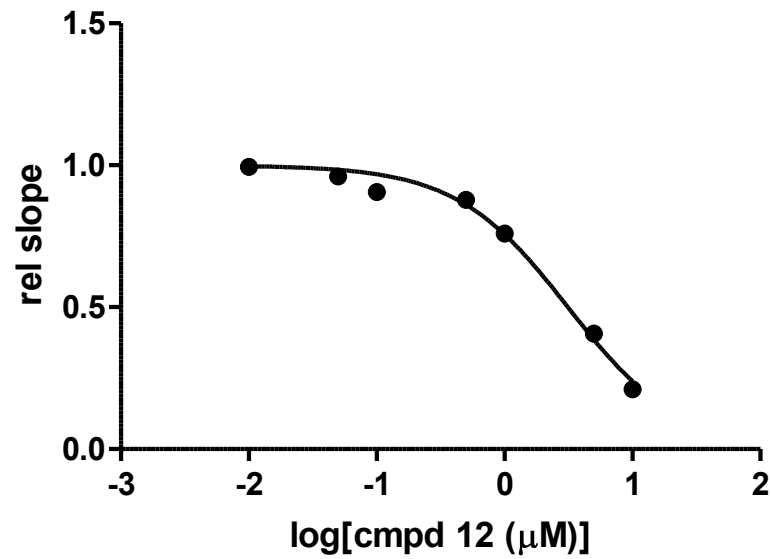
Sigmoidal dose-response (variable slope)	
Best-fit values	
Bottom	= 0.0
Top	= 1.000
LogEC50	0.5718
HillSlope	-0.7521
EC50	3.731
Std. Error	
LogEC50	0.1263
HillSlope	0.1725
95% Confidence Intervals	
LogEC50	0.2471 to 0.8966
HillSlope	-1.196 to -0.3085
EC50	1.766 to 7.882
Goodness of Fit	
Degrees of Freedom	5
R square	0.8943
Absolute Sum of Squares	0.03971
Sy.x	0.08911
Constraints	
Bottom	Bottom = 0.0
Top	Top = 1.000
Number of points	
Analyzed	7

IC<sub>50</sub> Determination of Compound **12** - 5 min Preincubation Time



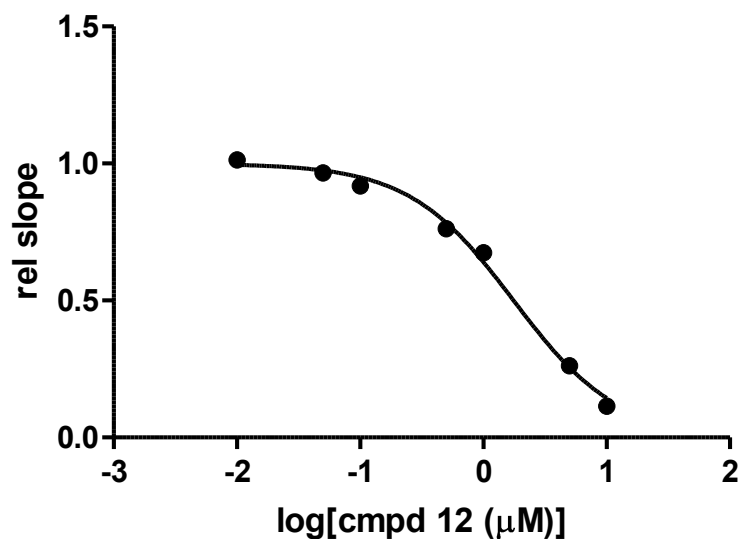
Sigmoidal dose-response (variable slope)	
Best-fit values	
Bottom	= 0.0
Top	= 1.000
LogEC50	1.128
HillSlope	-0.5414
EC50	13.42
Std. Error	
LogEC50	0.098
HillSlope	0.06562
95% Confidence Intervals	
LogEC50	0.8757 to 1.380
HillSlope	-0.7101 to -0.3727
EC50	7.511 to 23.97
Goodness of Fit	
Degrees of Freedom	5
R square	0.9655
Absolute Sum of Squares	0.005762
Sy.x	0.03395
Constraints	
Bottom	Bottom = 0.0
Top	Top = 1.000
Number of points	
Analyzed	7

# IC<sub>50</sub> Determination of Compound **12** - 15 min Preincubation Time



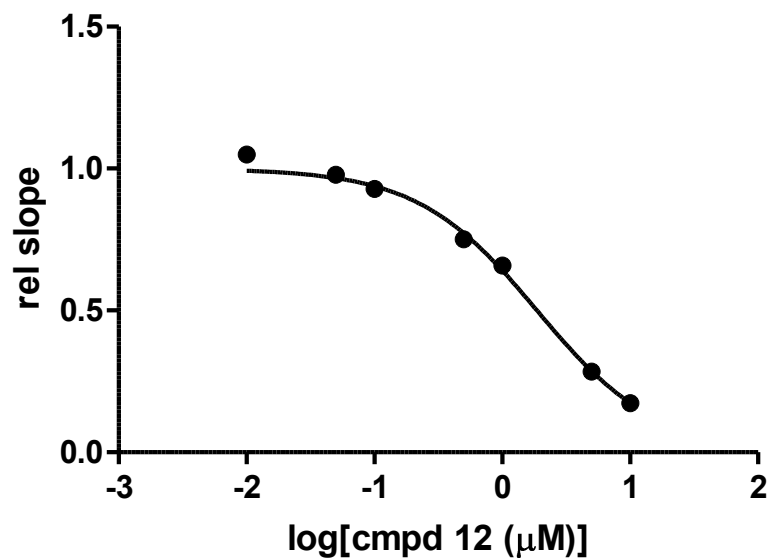
Sigmoidal dose-response (variable slope)	
Best-fit values	
Bottom	= 0.0
Top	= 1.000
LogEC50	0.4947
HillSlope	-0.994
EC50	3.124
Std. Error	
LogEC50	0.04101
HillSlope	0.08599
95% Confidence Intervals	
LogEC50	0.3893 to 0.6002
HillSlope	-1.215 to -0.7729
EC50	2.451 to 3.983
Goodness of Fit	
Degrees of Freedom	5
R square	0.9889
Absolute Sum of Squares	0.006109
Sy.x	0.03495
Constraints	
Bottom	Bottom = 0.0
Top	Top = 1.000
Number of points	
Analyzed	7

# IC<sub>50</sub> Determination of Compound **12** - 30 min Preincubation Time



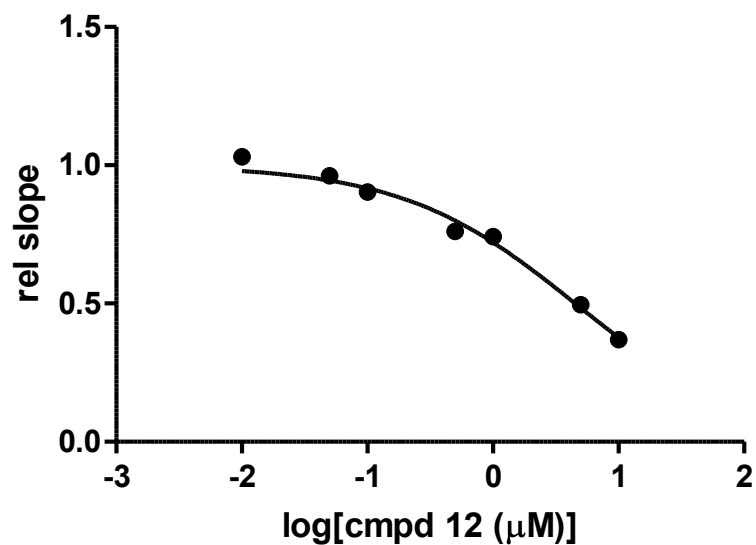
Sigmoidal dose-response (variable slope)	
Best-fit values	
Bottom	= 0.0
Top	= 1.000
LogEC50	0.2448
HillSlope	-1.025
EC50	1.757
Std. Error	
LogEC50	0.03243
HillSlope	0.06746
95% Confidence Intervals	
LogEC50	0.1614 to 0.3282
HillSlope	-1.198 to -0.8511
EC50	1.450 to 2.129
Goodness of Fit	
Degrees of Freedom	5
R square	0.9947
Absolute Sum of Squares	0.003962
Sy.x	0.02815
Constraints	
Bottom	Bottom = 0.0
Top	Top = 1.000
Number of points	
Analyzed	7

# IC<sub>50</sub> Determination of Compound **12** - 60 min Preincubation Time



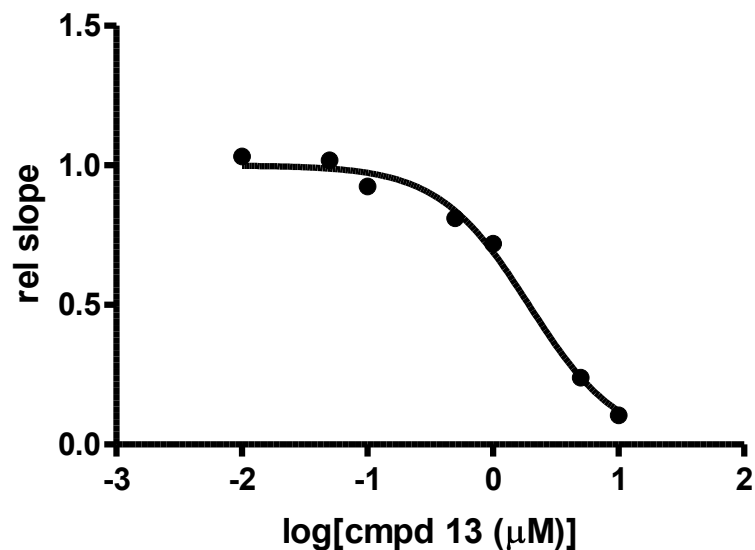
Sigmoidal dose-response (variable slope)	
Best-fit values	
Bottom	= 0.0
Top	= 1.000
LogEC50	0.2706
HillSlope	-0.9276
EC50	1.865
Std. Error	
LogEC50	0.03546
HillSlope	0.06307
95% Confidence Intervals	
LogEC50	0.1794 to 0.3618
HillSlope	-1.090 to -0.7655
EC50	1.511 to 2.300
Goodness of Fit	
Degrees of Freedom	5
R square	0.9939
Absolute Sum of Squares	0.004307
Sy.x	0.02935
Constraints	
Bottom	Bottom = 0.0
Top	Top = 1.000
Number of points	
Analyzed	7

IC<sub>50</sub> Determination of Compound **12** - 120 min Preincubation Time



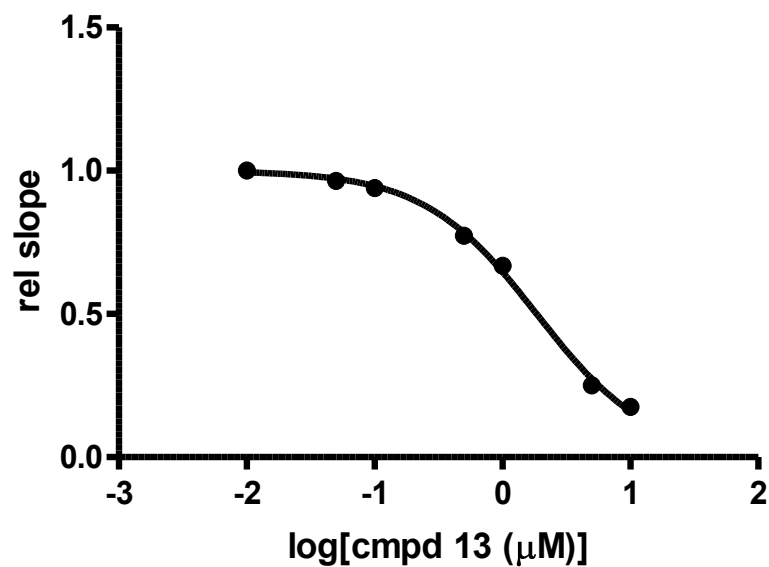
Sigmoidal dose-response (variable slope)	
Best-fit values	
Bottom	= 0.0
Top	= 1.000
LogEC50	0.6545
HillSlope	-0.6296
EC50	4.513
Std. Error	
LogEC50	0.05492
HillSlope	0.05476
95% Confidence Intervals	
LogEC50	0.5133 to 0.7957
HillSlope	-0.7704 to -0.4888
EC50	3.261 to 6.247
Goodness of Fit	
Degrees of Freedom	5
R square	0.9852
Absolute Sum of Squares	0.005263
Sy.x	0.03244
Constraints	
Bottom	Bottom = 0.0
Top	Top = 1.000
Number of points	
Analyzed	7

IC<sub>50</sub> Determination of Compound **13** with 60  $\mu$ M Z-R-R-AMC



Sigmoidal dose-response (variable slope)	
Best-fit values	
Bottom	= 0.0
Top	= 1.000
LogEC50	0.2862
HillSlope	-1.211
EC50	1.933
Std. Error	
LogEC50	0.03858
HillSlope	0.102
95% Confidence Intervals	
LogEC50	0.1870 to 0.3854
HillSlope	-1.474 to -0.9490
EC50	1.538 to 2.429
Goodness of Fit	
Degrees of Freedom	5
R square	0.9925
Absolute Sum of Squares	0.006324
Sy.x	0.03556
Constraints	
Bottom	Bottom = 0.0
Top	Top = 1.000
Number of points	
Analyzed	7

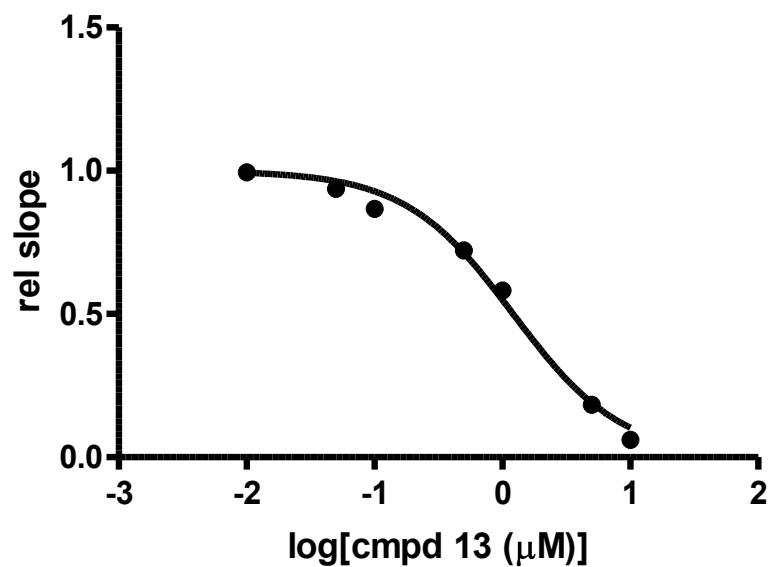
IC<sub>50</sub> Determination of Compound **13** with 40  $\mu$ M Z-R-R-AMC



Sigmoidal dose-response (variable slope)	
Best-fit values	
Bottom	= 0.0
Top	= 1.000
LogEC50	0.2671
HillSlope	-0.983
EC50	1.85
Std. Error	
LogEC50	0.02019
HillSlope	0.03928
95% Confidence Intervals	
LogEC50	0.2152 to 0.3190
HillSlope	-1.084 to -0.8820
EC50	1.641 to 2.084
Goodness of Fit	
Degrees of Freedom	5
R square	0.9979
Absolute Sum of Squares	0.001475
Sy.x	0.01718
Constraints	
Bottom	Bottom = 0.0
Top	Top = 1.000
Number of points	
Analyzed	7

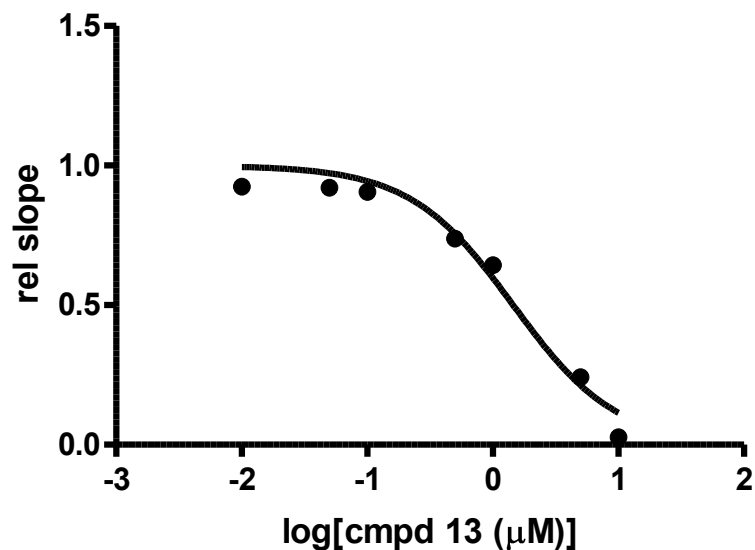


IC<sub>50</sub> Determination of Compound **13** with 20  $\mu$ M Z-R-R-AMC



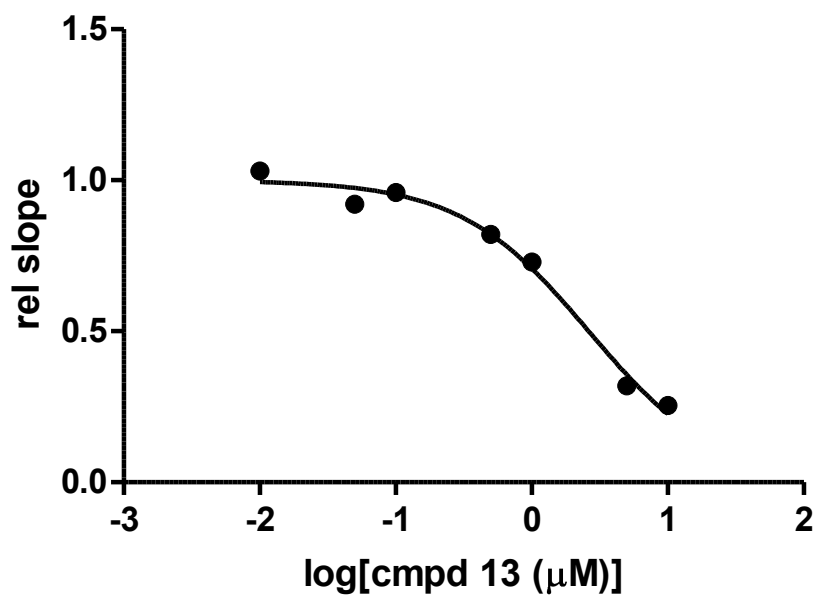
Sigmoidal dose-response (variable slope)	
Best-fit values	
Bottom	= 0.0
Top	= 1.000
LogEC50	0.08417
HillSlope	-1.026
EC50	1.214
Std. Error	
LogEC50	0.04376
HillSlope	0.0964
95% Confidence Intervals	
LogEC50	-0.02834 to 0.1967
HillSlope	-1.273 to -0.7777
EC50	0.9368 to 1.573
Goodness of Fit	
Degrees of Freedom	5
R square	0.9909
Absolute Sum of Squares	0.00748
Sy.x	0.03868
Constraints	
Bottom	Bottom = 0.0
Top	Top = 1.000
Number of points	
Analyzed	7

IC<sub>50</sub> Determination of Compound **13** with 6  $\mu$ M Z-R-R-AMC



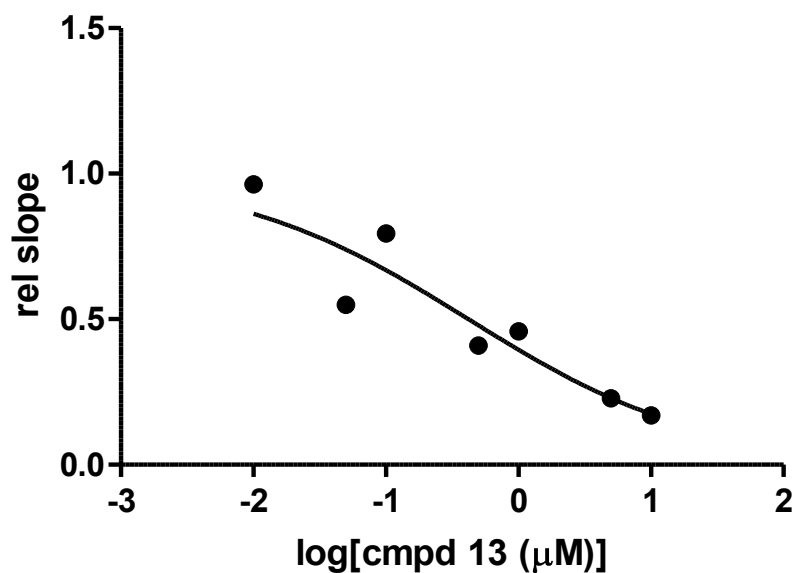
Sigmoidal dose-response (variable slope)	
Best-fit values	
Bottom	= 0.0
Top	= 1.000
LogEC50	0.162
HillSlope	-1.059
EC50	1.452
Std. Error	
LogEC50	0.07124
HillSlope	0.1605
95% Confidence Intervals	
LogEC50	-0.02113 to 0.3452
HillSlope	-1.471 to -0.6460
EC50	0.9525 to 2.214
Goodness of Fit	
Degrees of Freedom	5
R square	0.9741
Absolute Sum of Squares	0.02001
Sy.x	0.06326
Constraints	
Bottom	Bottom = 0.0
Top	Top = 1.000
Number of points	
Analyzed	7

# IC<sub>50</sub> Determination of Compound **13** - 5 min Preincubation Time



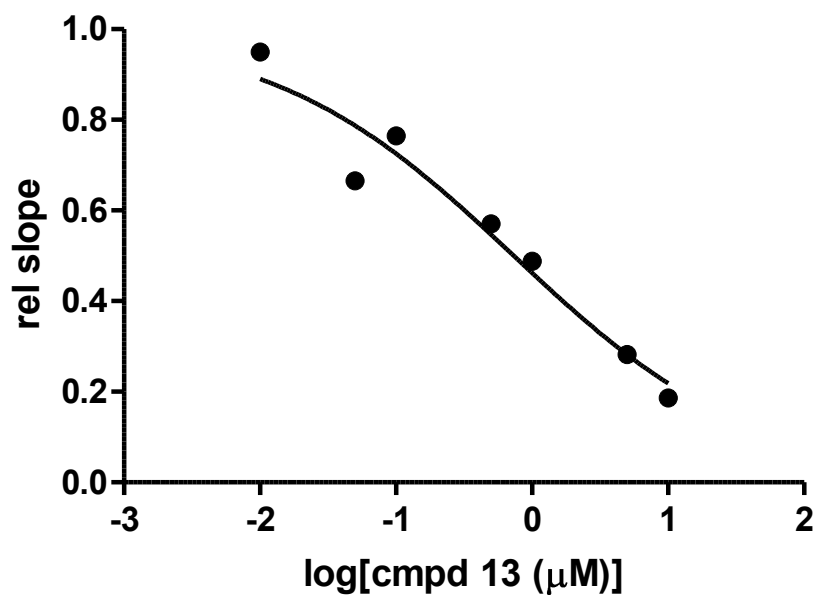
Sigmoidal dose-response (variable slope)	
Best-fit values	
Bottom	= 0.0
Top	= 1.000
LogEC50	0.4185
HillSlope	-0.918
EC50	2.621
Std. Error	
LogEC50	0.04516
HillSlope	0.081
95% Confidence Intervals	
LogEC50	0.3023 to 0.5346
HillSlope	-1.126 to -0.7097
EC50	2.006 to 3.424
Goodness of Fit	
Degrees of Freedom	5
R square	0.9883
Absolute Sum of Squares	0.006823
Sy.x	0.03694
Constraints	
Bottom	Bottom = 0.0
Top	Top = 1.000
Number of points	
Analyzed	7

IC<sub>50</sub> Determination of Compound **13** - 15 min Preincubation Time



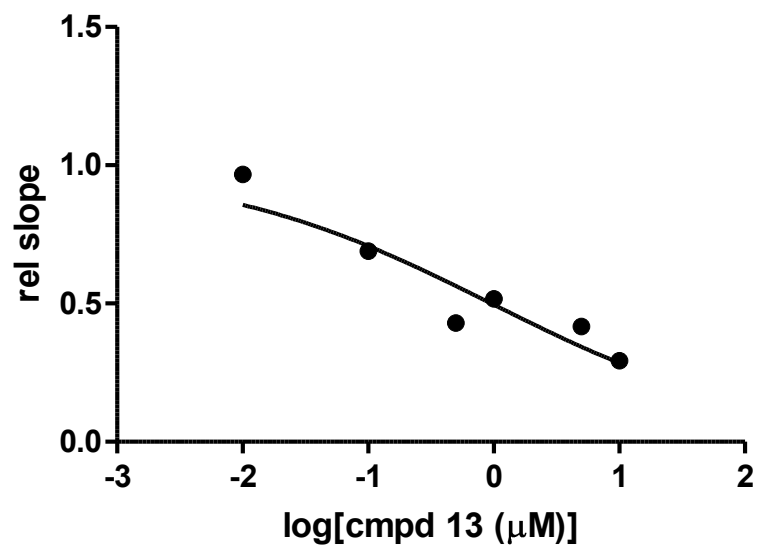
Sigmoidal dose-response (variable slope)	
Best-fit values	
Bottom	= 0.0
Top	= 1.000
LogEC50	-0.3772
HillSlope	-0.4902
EC50	0.4196
Std. Error	
LogEC50	0.2018
HillSlope	0.1244
95% Confidence Intervals	
LogEC50	-0.8961 to 0.1417
HillSlope	-0.8099 to -0.1704
EC50	0.1270 to 1.386
Goodness of Fit	
Degrees of Freedom	5
R square	0.8579
Absolute Sum of Squares	0.07048
Sy.x	0.1187
Constraints	
Bottom	Bottom = 0.0
Top	Top = 1.000
Number of points	
Analyzed	7

# IC<sub>50</sub> Determination of Compound **13** - 30 min Preincubation Time



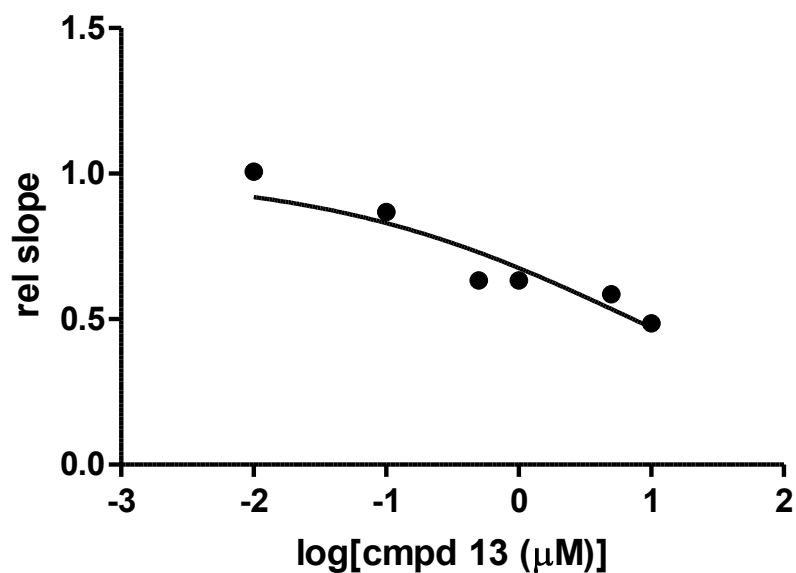
Sigmoidal dose-response (variable slope)	
Best-fit values	
Bottom	= 0.0
Top	= 1.000
LogEC50	-0.1346
HillSlope	-0.4873
EC50	0.7336
Std. Error	
LogEC50	0.1148
HillSlope	0.07059
95% Confidence Intervals	
LogEC50	-0.4297 to 0.1606
HillSlope	-0.6688 to -0.3058
EC50	0.3718 to 1.447
Goodness of Fit	
Degrees of Freedom	5
R square	0.9478
Absolute Sum of Squares	0.02227
Sy.x	0.06674
Constraints	
Bottom	Bottom = 0.0
Top	Top = 1.000
Number of points	
Analyzed	7

# IC<sub>50</sub> Determination of Compound **13** - 60 min Preincubation Time



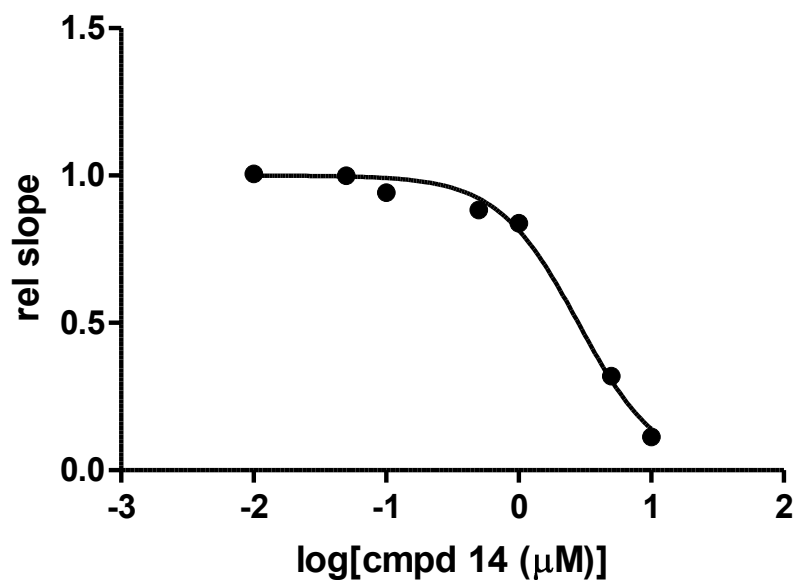
Sigmoidal dose-response (variable slope)	
Best-fit values	
Bottom	= 0.0
Top	= 1.000
LogEC50	-0.01877
HillSlope	-0.3921
EC50	0.9577
Std. Error	
LogEC50	0.2015
HillSlope	0.09891
95% Confidence Intervals	
LogEC50	-0.5782 to 0.5407
HillSlope	-0.6667 to -0.1176
EC50	0.2641 to 3.473
Goodness of Fit	
Degrees of Freedom	4
R square	0.8765
Absolute Sum of Squares	0.03611
Sy.x	0.09502
Constraints	
Bottom	Bottom = 0.0
Top	Top = 1.000
Number of points	
Analyzed	6

IC<sub>50</sub> Determination of Compound **13** - 120 min Preincubation Time



Sigmoidal dose-response (variable slope)	
Best-fit values	
Bottom	= 0.0
Top	= 1.000
LogEC50	0.8635
HillSlope	-0.3697
EC50	7.304
Std. Error	
LogEC50	0.2385
HillSlope	0.09458
95% Confidence Intervals	
LogEC50	0.2014 to 1.526
HillSlope	-0.6322 to -0.1071
EC50	1.590 to 33.55
Goodness of Fit	
Degrees of Freedom	4
R square	0.8794
Absolute Sum of Squares	0.02294
Sy.x	0.07573
Constraints	
Bottom	Bottom = 0.0
Top	Top = 1.000
Number of points	
Analyzed	6

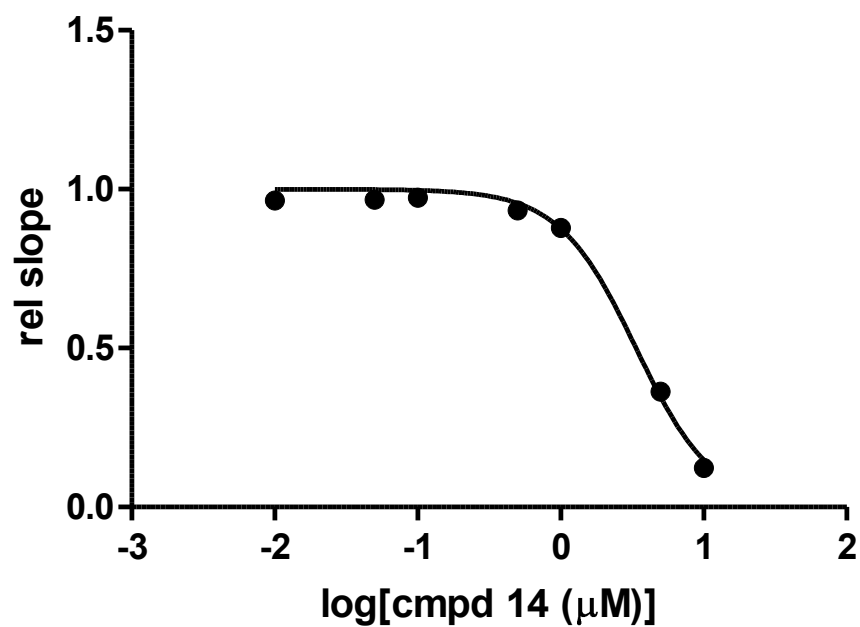
IC<sub>50</sub> Determination of Compound **14** with 60  $\mu$ M Z-R-R-AMC



Sigmoidal dose-response (variable slope)	
Best-fit values	
Bottom	= 0.0
Top	= 1.000
LogEC50	0.4492
HillSlope	-1.43
EC50	2.813
Std. Error	
LogEC50	0.03469
HillSlope	0.1202
95% Confidence Intervals	
LogEC50	0.3600 to 0.5384
HillSlope	-1.739 to -1.121
EC50	2.291 to 3.454
Goodness of Fit	
Degrees of Freedom	5
R square	0.9928
Absolute Sum of Squares	0.005606
Sy.x	0.03349
Constraints	
Bottom	Bottom = 0.0
Top	Top = 1.000
Number of points	
Analyzed	7

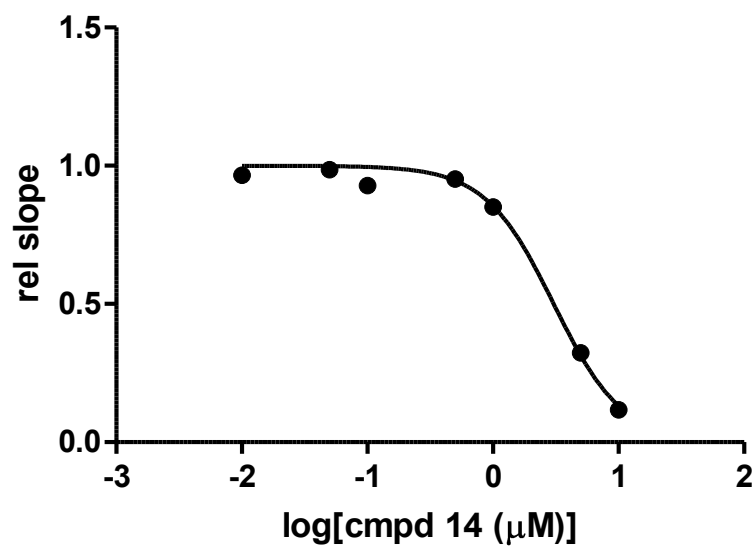


IC<sub>50</sub> Determination of Compound **14** with 40  $\mu$ M Z-R-R-AMC



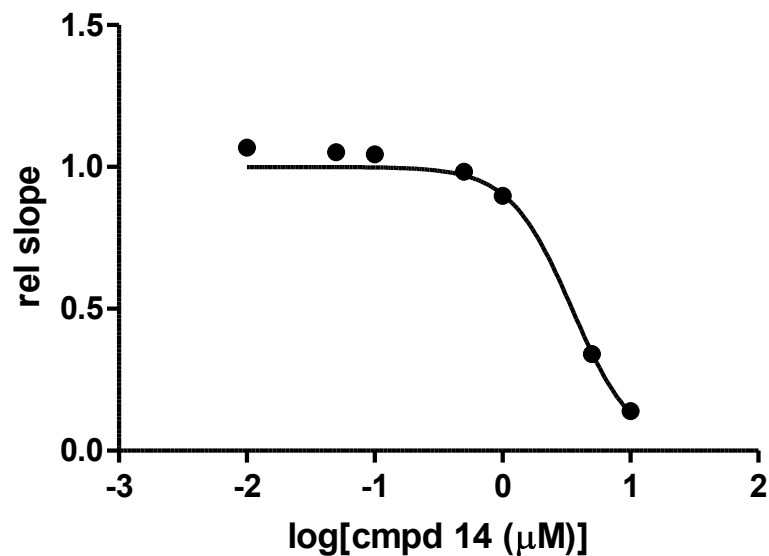
Sigmoidal dose-response (variable slope)	
Best-fit values	
Bottom	= 0.0
Top	= 1.000
LogEC50	0.5273
HillSlope	-1.608
EC50	3.367
Std. Error	
LogEC50	0.02919
HillSlope	0.136
95% Confidence Intervals	
LogEC50	0.4522 to 0.6023
HillSlope	-1.958 to -1.259
EC50	2.833 to 4.002
Goodness of Fit	
Degrees of Freedom	5
R square	0.9942
Absolute Sum of Squares	0.004276
Sy.x	0.02925
Constraints	
Bottom	Bottom = 0.0
Top	Top = 1.000
Number of points	
Analyzed	7

IC<sub>50</sub> Determination of Compound **14** with 20  $\mu$ M Z-R-R-AMC



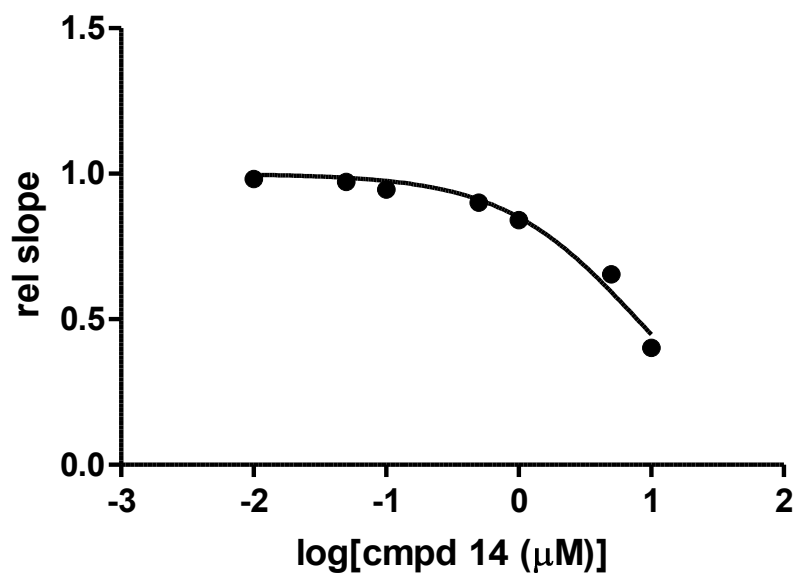
Sigmoidal dose-response (variable slope)	
Best-fit values	
Bottom	= 0.0
Top	= 1.000
LogEC50	0.4839
HillSlope	-1.586
EC50	3.047
Std. Error	
LogEC50	0.0356
HillSlope	0.1504
95% Confidence Intervals	
LogEC50	0.3923 to 0.5754
HillSlope	-1.972 to -1.199
EC50	2.468 to 3.762
Goodness of Fit	
Degrees of Freedom	5
R square	0.992
Absolute Sum of Squares	0.006155
Sy.x	0.03509
Constraints	
Bottom	Bottom = 0.0
Top	Top = 1.000
Number of points	
Analyzed	7

IC<sub>50</sub> Determination of Compound **14** with 6  $\mu$ M Z-R-R-AMC



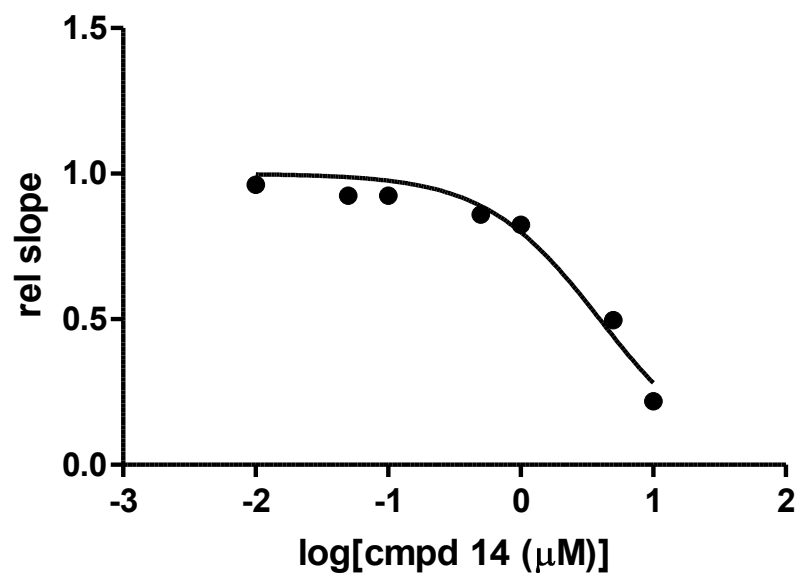
Sigmoidal dose-response (variable slope)	
Best-fit values	
Bottom	= 0.0
Top	= 1.000
LogEC50	0.5428
HillSlope	-1.787
EC50	3.49
Std. Error	
LogEC50	0.04346
HillSlope	0.2528
95% Confidence Intervals	
LogEC50	0.4311 to 0.6545
HillSlope	-2.437 to -1.137
EC50	2.698 to 4.514
Goodness of Fit	
Degrees of Freedom	5
R square	0.989
Absolute Sum of Squares	0.009685
Sy.x	0.04401
Constraints	
Bottom	Bottom = 0.0
Top	Top = 1.000
Number of points	
Analyzed	7

IC<sub>50</sub> Determination of Compound **14** - 5 min Preincubation Time



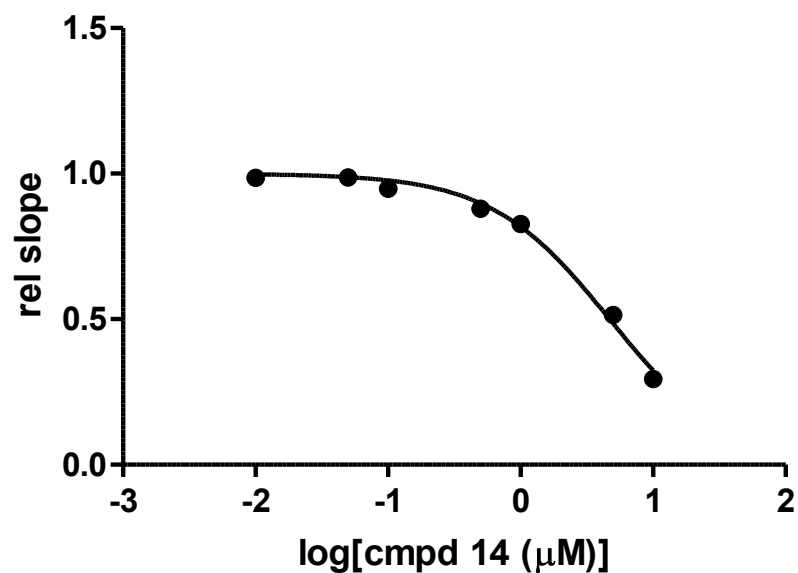
Sigmoidal dose-response (variable slope)	
Best-fit values	
Bottom	= 0.0
Top	= 1.000
LogEC50	0.8935
HillSlope	-0.8449
EC50	7.825
Std. Error	
LogEC50	0.05831
HillSlope	0.1108
95% Confidence Intervals	
LogEC50	0.7436 to 1.043
HillSlope	-1.130 to -0.5601
EC50	5.541 to 11.05
Goodness of Fit	
Degrees of Freedom	5
R square	0.9733
Absolute Sum of Squares	0.007325
Sy.x	0.03828
Constraints	
Bottom	Bottom = 0.0
Top	Top = 1.000
Number of points	
Analyzed	7

# IC<sub>50</sub> Determination of Compound **14** - 15 min Preincubation Time



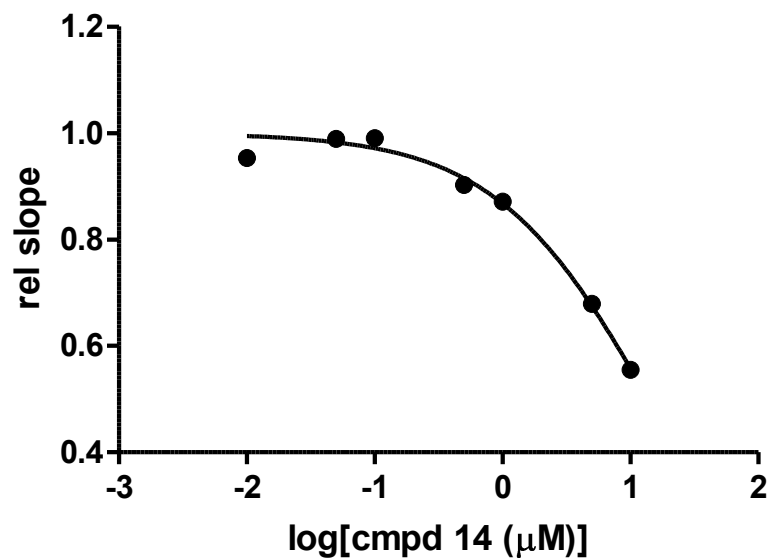
Sigmoidal dose-response (variable slope)	
Best-fit values	
Bottom	= 0.0
Top	= 1.000
LogEC50	0.5963
HillSlope	-1.007
EC50	3.947
Std. Error	
LogEC50	0.06701
HillSlope	0.1547
95% Confidence Intervals	
LogEC50	0.4240 to 0.7685
HillSlope	-1.405 to -0.6097
EC50	2.655 to 5.869
Goodness of Fit	
Degrees of Freedom	5
R square	0.9647
Absolute Sum of Squares	0.01662
Sy.x	0.05765
Constraints	
Bottom	Bottom = 0.0
Top	Top = 1.000
Number of points	
Analyzed	7

IC<sub>50</sub> Determination of Compound **14** - 30 min Preincubation Time



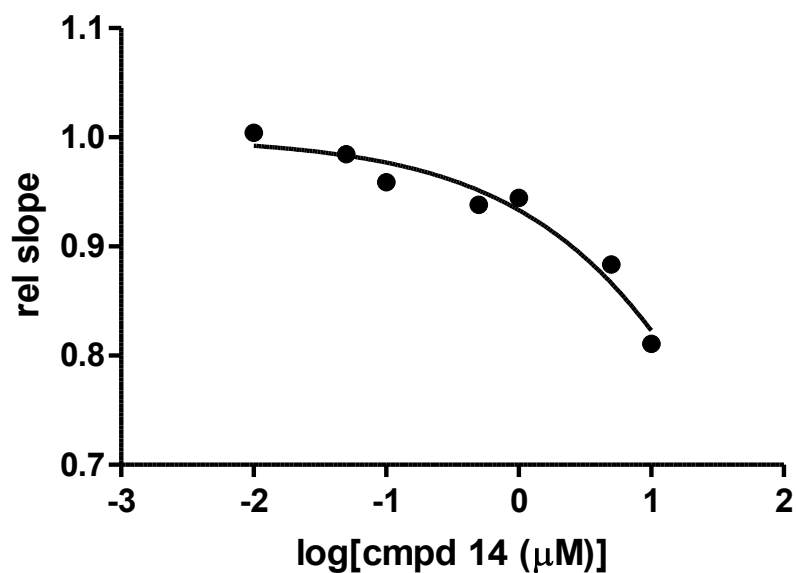
Sigmoidal dose-response (variable slope)	
Best-fit values	
Bottom	= 0.0
Top	= 1.000
LogEC50	0.6713
HillSlope	-0.9711
EC50	4.691
Std. Error	
LogEC50	0.03004
HillSlope	0.06912
95% Confidence Intervals	
LogEC50	0.5941 to 0.7485
HillSlope	-1.149 to -0.7934
EC50	3.927 to 5.604
Goodness of Fit	
Degrees of Freedom	5
R square	0.9927
Absolute Sum of Squares	0.003154
Sy.x	0.02512
Constraints	
Bottom	Bottom = 0.0
Top	Top = 1.000
Number of points	
Analyzed	7

# IC<sub>50</sub> Determination of Compound **14** - 60 min Preincubation Time



Sigmoidal dose-response (variable slope)	
Best-fit values	
Bottom	= 0.0
Top	= 1.000
LogEC50	1.142
HillSlope	-0.7153
EC50	13.86
Std. Error	
LogEC50	0.05278
HillSlope	0.06327
95% Confidence Intervals	
LogEC50	1.006 to 1.277
HillSlope	-0.8780 to -0.5526
EC50	10.14 to 18.94
Goodness of Fit	
Degrees of Freedom	5
R square	0.9864
Absolute Sum of Squares	0.002296
Sy.x	0.02143
Constraints	
Bottom	Bottom = 0.0
Top	Top = 1.000
Number of points	
Analyzed	7

IC<sub>50</sub> Determination of Compound **14** - 120 min Preincubation Time



Sigmoidal dose-response (variable slope)	
Best-fit values	
Bottom	= 0.0
Top	= 1.000
LogEC50	2.394
HillSlope	-0.479
EC50	247.6
Std. Error	
LogEC50	0.2621
HillSlope	0.07141
95% Confidence Intervals	
LogEC50	1.720 to 3.067
HillSlope	-0.6626 to -0.2954
EC50	52.47 to 1168
Goodness of Fit	
Degrees of Freedom	5
R square	0.9533
Absolute Sum of Squares	0.001209
Sy.x	0.01555
Constraints	
Bottom	Bottom = 0.0
Top	Top = 1.000
Number of points	
Analyzed	7



## APPENDIX C

### Protocol for Operating the Fluoromax-2 for Cathepsin B

#### *General guidelines for successfully operating the Fluoromax-2*

- Position 3 of cell holder is not aligned and does not give reliable results. It is recommended that you do not use position 3 when running samples.
- Never open “Grams\_32 convert.”
- Never press the F6 key.
- Never click right and left mouse at the same time.
- Once the Instrument Control Center has been opened, do not close the window or the entire program will quit.

#### *Procedure for calibrating and operating the Fluoromax-2*

1. Always turn on the lamp before you turn on the power.
2. Turn on the water bath. Set the water bath temperature to 37° Celsius.
3. Let the Fluoromax-2 warm-up for at least one hour.
4. Login to the logbook that is next to the fluorimeter. Login to the computer using the username and password that is taped to the fluorimeter. (Username: Fluoromax; Password: Fluorimeter2007)
5. Before proceeding to the next step, wait until the program disk no longer displays a green light.

6. Double click the Instrument Control Center icon that is on the desktop. Select the layout called Fluoromax-2 with 4pos sample changer. If the program asks you to emulate the software, select no and then turn the instrument off and then back on.
7. Repeat until the program does not ask you to emulate. When the program asks you if you want to bring the hardware to the last position, click yes. Wait for the program to initialize.
8. To calibrate the instrument:
  - Click on the first icon on the instrument control center window that says Run Experiment. See Figure 1 below.



Figure 1. View of Instrument Control Center  
Identification of buttons from left to right:  
Run Experiment, Run Real Time Display,  
Run Visual Setup, Run CWA.

- From the tool bar, select Collect and choose Experiment.
- When the new window appears, click on the button that says Experiment and choose the lamp file from the drop-down menu as shown in Figure 2.  
Next, click on the button that says Data File and choose the lamp file from the drop-down menu. Again, refer to Figure 2. After both lamp files have been selected, click on the Run button and click yes when asked to overwrite the file. A graph will appear.

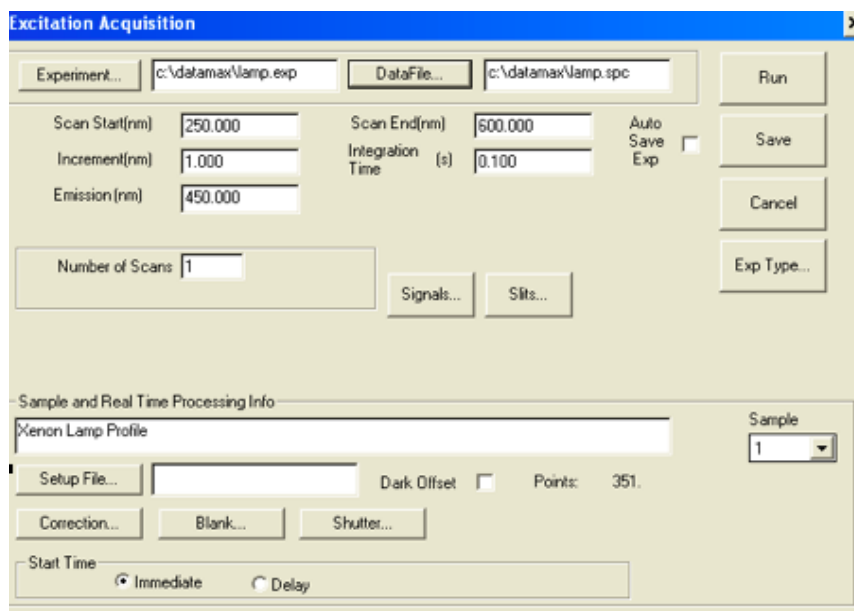


Figure 2. Window display demonstrating the selection of lamp files.

- Once the graph is finished loading, expand the graph's window in order to obtain a better view of the graph. Next, click on the maximum point on the graph which should be the point at the top of the peak. The maximum value for this excitation wavelength should be equal to  $467.0 \pm 0.5\text{nm}$ . If the value displayed on the graph is not equal to this ideal value, then return to the Instrument Control Center window and choose the second button, Run Real Time Display. Refer to Figure 1 if necessary.
- Once the Run Real Time Display window is open, enter the value that you observed on the graph into the box labeled EX1. Then, select enter.
- Go back to the Instrument Control Center window and select the third button, Run Visual Setup. When the new window appears, double click on the yellow box in the diagram. See Figure 3 below. You should observe the number you previously inputted. Next, click on calibrate and enter the number that you should observe: 467.0 and press ok. To confirm that the

value has been changed, run it again and observe the graph and the maximum point.

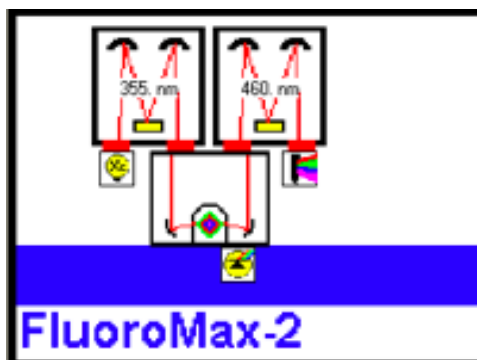


Figure 3. Diagram of the Run Visual Setup window.

- Return to the Instrument Control Center window and click on the first button, Run Experiment. As before, from the tool bar, select Collect and then choose Experiment. This time, choose files from the drop-down menus for water.exp and water.spc. See Figure 4 below.

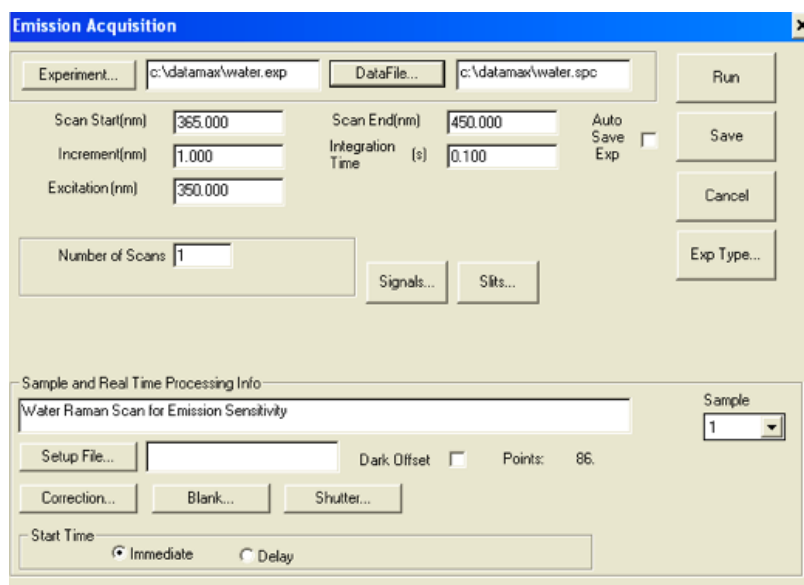


Figure 4. Window display demonstrating the selection of water files.

- Next, place some ultrapure water in a clean cuvette and set the cuvette in the appropriate position in the fluorimeter (to open fluorimeter, push in button on the face of the instrument and lift upward).

- Once the cuvette is in place, close the lid to the fluorimeter and click the Run button in the emission acquisition window. Another graph should appear. Again, click on the maximum point on the graph. The value should be  $397.0 \pm 0.5 \text{ nm}$ . If the value displayed needs to be corrected, go through the same process for calibration as mentioned above for the excitation wavelength. But, instead of entering the value that you observed on the graph in the EX1 box, enter the value in the box labeled EM1 in the Run Real Time Display window. As before, return to the Run Visual Setup window to change the calibration. Then, re-run the experiment for the water to confirm that the emission wavelength has been changed to approximately 397 nm.
- If you have not already done so, re-open the Run Visual Setup window. Click on the red box in the diagram. See Figure 3. Check that the slit widths are set to 5.0nm.

9. To run samples:

- Click on the fourth button, Run CWA (Constant Wavelength Analysis), in the Instrument Control Center window.
- In the ISA Constant Wavelength Analysis window, input the numbers 355 and 460 into the Ex. Mono and Em. Mono boxes. Next, under the acquisition parameters, add “S” to the box to the right. Then, select Kinetics and choose Define. Refer to Figure 5.

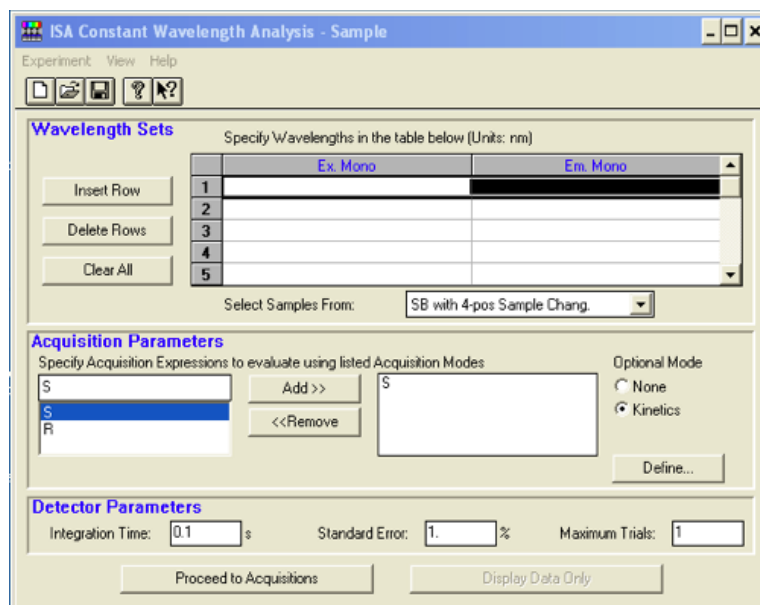


Figure 5. ISA Constant Wavelength Analysis window.

- In the Time-based Acquisition Parameters window, specify that the acquisition should be repeated every **5** seconds for a total of **300** seconds. Then, click on “Add to List.” Next, check the box that says “Minimize Sample Photobleaching” and press OK. See Figure 6.

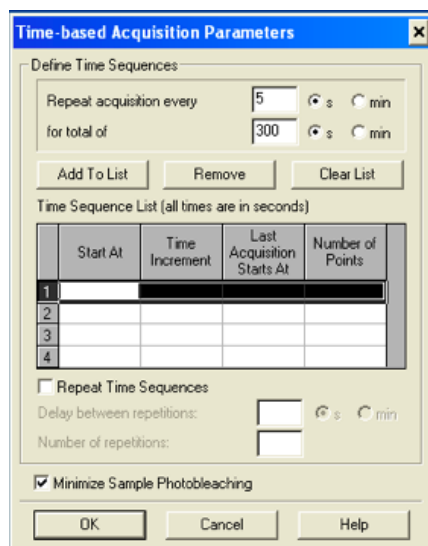


Figure 6. Time-based Acquisition Parameters window.

- Click on the “Proceed to Acquisitions” button. Next, click on “Start Acquisition.”

- In the New Sample window, label each position with a Sample ID. Check the box that says “Dark correction enabled.” An example is shown in Figure 7. See below.

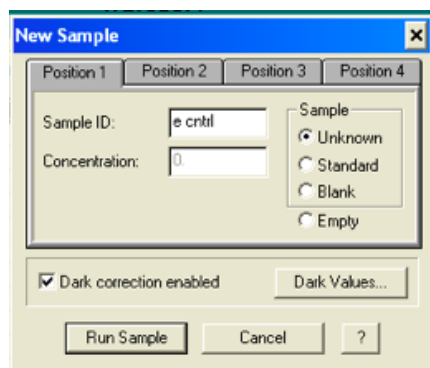


Figure 7. New Sample window

- Make sure to note that position 3 is empty. See figure 8 below.

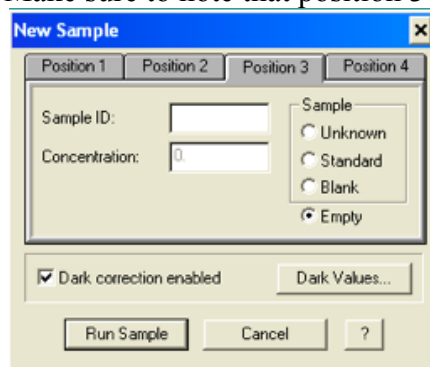


Figure 8. New Sample window displaying empty Position 3.

- When cuvettes are loaded in their proper positions, click “Run Sample.”

The instrument should begin to make noise.

10. When you are finished using the fluorimeter, save your data and exit out of the program.
11. To turn off the instrument, press power and then press lamp.
12. Turn off the water bath and log out of the book.

## REFERENCES

- Atkins, P.; de Paula, J. *Physical Chemistry for the Life Sciences*; W.H. Freeman and Company: New York, 2006; pp 567, 569.
- Baeriswyl, V., and G. Christofori. "The Angiogenic Switch in Carcinogenesis." *Seminars in cancer biology* 19.5 (2009): 329-37. *SCOPUS*. Web. 17 April 2010.
- Białas, A., and P. Kafarski. "Proteases as Anti-Cancer Targets - Molecular and Biological Basis for Development of Inhibitor-Like Drugs Against Cancer." *Anti-Cancer Agents in Medicinal Chemistry* 9.7 (2009): 728-62. *SCOPUS*. Web. 17 April 2010.
- Binoletto, C., et al. "Chiral Cyclopalladated Complexes Derived from N,N-Dimethyl-1-Phenethylamine with Bridging Bis(Diphenylphosphine)Ferrocene Ligand as Inhibitors of the Cathepsin B Activity and as Antitumoral Agents." *Bioorganic & medicinal chemistry* 13.8 (2005): 3047-55. Web.
- Brix, K., et al. "Cysteine Cathepsins: Cellular Roadmap to Different Functions." *Biochimie* 90.2 (2008): 194-207. Web.
- Caglic, D., et al. "Glycosaminoglycans Facilitate Procathepsin B Activation through Disruption of Propeptide-Mature Enzyme Interactions." *The Journal of biological chemistry* 282.45 (2007): 33076-85. Web.
- Caglic, D., et al. "Murine and Human Cathepsin B Exhibit Similar Properties: Possible Implications for Drug Discovery." *Biological chemistry* 390.2 (2009): 175-9. Web.
- Cavallo-Medved, D., et al. "Caveolin-1 Mediates the Expression and Localization of Cathepsin B, Pro-Urokinase Plasminogen Activator and their Cell-Surface Receptors in Human Colorectal Carcinoma Cells." *Journal of cell science* 118.Pt 7 (2005): 1493-503. Web.
- Coghlin, C., and G. I. Murray. "Current and Emerging Concepts in Tumour Metastasis." *The Journal of pathology* 222.1 (2010): 1-15. Web.
- Cunha, R. L. O. R., et al. "Irreversible Inhibition of Human Cathepsins B, L, S and K by Hypervalent Tellurium Compounds." *Biological chemistry* 390.11 (2009): 1205-12. *SCOPUS*. Web. 17 April 2010.
- Elie, B. T., et al. "Identification and Pre-Clinical Testing of a Reversible Cathepsin Protease Inhibitor Reveals Anti-Tumor Efficacy in a Pancreatic Cancer Model." *Biochimie* 92.11 (2010): 1618-24. Web.



- Elvin, P., and A. P. Garner. "Tumour Invasion and Metastasis: Challenges Facing Drug Discovery." *Current Opinion in Pharmacology* 5.4 SPEC. ISS. (2005): 374-81. SCOPUS. Web. 4 August 2010.
- Greenspan, P. D., et al. "N-Arylamionitriles as Bioavailable Peptidomimetic Inhibitors of Cathepsin B." *Bioorganic & medicinal chemistry letters* 13.22 (2003): 4121-4. Web.
- Hoang, V. L. T., Y. Li, and S. -K Kim. "Cathepsin B Inhibitory Activities of Phthalates Isolated from a Marine Pseudomonas Strain." *Bioorganic and Medicinal Chemistry Letters* 18.6 (2008): 2083-8. SCOPUS. Web. 4 August 2010.
- Hook, Vivian, et al. "Cysteine Cathepsins in the Secretory Vesicle Produce Active Peptides: Cathepsin L Generates Peptide Neurotransmitters and Cathepsin B Produces Beta-Amyloid of Alzheimer's Disease." *Biochimica et Biophysica Acta (BBA) - Proteins & Proteomics* 1824.1 (2012): 89-104. Web.
- Illy, C., et al. "Role of the Occluding Loop in Cathepsin B Activity." *The Journal of biological chemistry* 272.2 (1997): 1197-202. Web.
- Jedeszko, C., and B. F. Sloane. "Cysteine Cathepsins in Human Cancer." *Biological chemistry* 385.11 (2004): 1017-27. SCOPUS. Web. 4 August 2010.
- Katunuma, N. "Structure-Based Development of Specific Inhibitors for Individual Cathepsins and their Medical Applications." *Proceedings of the Japan Academy.Series B, Physical and biological sciences* 87.2 (2011): 29-39. Web.
- Kirkegaard, T., and M. Jäätelä. "Lysosomal Involvement in Cell Death and Cancer." *Biochimica et Biophysica Acta - Molecular Cell Research* 1793.4 (2009): 746-54. SCOPUS. Web. 4 August 2010.
- Kishore Kumar, G. D., et al. "Design, Synthesis, and Biological Evaluation of Potent Thiosemicarbazone Based Cathepsin L Inhibitors." *Bioorganic & medicinal chemistry letters* 20.4 (2010): 1415-9. Web.
- Leung-Toung, R., et al. "1,2,4-Thiadiazole: A Novel Cathepsin B Inhibitor." *Bioorganic & medicinal chemistry* 11.24 (2003): 5529-37. Web.
- Mohamed, M. M., and B. F. Sloane. "Cysteine Cathepsins: Multifunctional Enzymes in Cancer." *Nature Reviews Cancer* 6.10 (2006): 764-75. SCOPUS. Web. 4 August 2010.
- Montaser, M., G. Lalmanach, and L. Mach. "CA-074, but Not its Methyl Ester CA-074Me, is a Selective Inhibitor of Cathepsin B within Living Cells." *Biological chemistry* 383.7-8 (2002): 1305-8. Web.
- Mort, John S., and David J. Buttle. "Cathepsin B." *The international journal of biochemistry & cell biology* 29.5 (1997): 715-20. Web.

- Mura, P., et al. "Trans-Cis-Cis-[RuCl<sub>2</sub>(DMSO)<sub>2</sub>(2-Amino-5-Methyl-Thiazole)<sub>2</sub>], (PMRu52), a Novel Ruthenium(II) Compound Acting as a Strong Inhibitor of Cathepsin B." *Journal of inorganic biochemistry* 104.2 (2010): 111-7. Web.
- Murata, M., et al. "Novel Epoxysuccinyl Peptides: Selective Inhibitors of Cathepsin B, in Vitro." *FEBS letters* 280.2 (1991): 307-10. *SCOPUS*. Web. 4 August 2010.
- Musil, D., et al. "The Refined 2.15 Å X-Ray Crystal Structure of Human Liver Cathepsin B: The Structural Basis for its Specificity." *The EMBO journal* 10.9 (1991): 2321-30. Web.
- National Center for Biotechnology Information.  
<http://www.ncbi.nlm.nih.gov/Structure/CN3D/cn3d.shtml> (accessed October 13, 2011).
- Obermajer, N., et al. "Role of Cysteine Cathepsins in Matrix Degradation and Cell Signalling." *Connective tissue research* 49.3-4 (2008): 193-6. *SCOPUS*. Web. 17 April 2010.
- Pungercar, J. R., et al. "Autocatalytic Processing of Procathepsin B is Triggered by Proenzyme Activity." *The FEBS journal* 276.3 (2009): 660-8. Web.
- Redzynia, I., et al. "Displacement of the Occluding Loop by the Parasite Protein, Chagasin, Results in Efficient Inhibition of Human Cathepsin B." *Journal of Biological Chemistry* 283.33 (2008): 22815-25. *SCOPUS*. Web. 17 April 2010.
- Ritonja, A., et al. "Amino Acid Sequence of Human Liver Cathepsin B." *FEBS letters* 181.1 (1985): 169-72. Web.
- Schenker, P., et al. "A Double-Headed Cathepsin B Inhibitor Devoid of Warhead." *Protein Science* 17.12 (2008): 2145-55. *SCOPUS*. Web. 17 April 2010.
- Skrzydłowska, E., et al. "Proteolytic-Antiproteolytic Balance and its Regulation in Carcinogenesis." *World Journal of Gastroenterology* 11.9 (2005): 1251-66. *SCOPUS*. Web. 4 August 2010.
- Tardy, C., et al. "Lysosomes and Lysosomal Proteins in Cancer Cell Death (New Players of an Old Struggle)." *Biochimica et Biophysica Acta - Reviews on Cancer* 1765.2 (2006): 101-25. *SCOPUS*. Web. 4 August 2010.
- Turk, B., D. Turk, and G. S. Salvesen. "Regulating Cysteine Protease Activity: Essential Role of Protease Inhibitors as Guardians and Regulators." *Medicinal Chemistry Reviews - Online* 2.4 (2005): 283-97. *SCOPUS*. Web. 4 August 2010.

- Turk, B. "Targeting Proteases: Successes, Failures and Future Prospects." *Nature Reviews Drug Discovery* 5.9 (2006): 785-99. *SCOPUS*. Web. 4 August 2010.
- Turk, D., B. Turk, and V. Turk. Papain-Like Lysosomal Cysteine Proteases and their Inhibitors: Drug Discovery Targets?, 2003. *SCOPUS*. 4 August 2010.
- Tutorial on Fluorescence and Fluorescent Instrumentation. Fluorescent Microsphere Resource Center. <http://fmrc.pulmcc.washington.edu/DOCUMENTS/FMRC299.pdf> (accessed July 12, 2010).
- UniProt. <http://www.uniprot.org/uniprot/P07858> (accessed October 12, 2011).
- Vasiljeva, O., et al. "Emerging Roles of Cysteine Cathepsins in Disease and their Potential as Drug Targets." *Current pharmaceutical design* 13.4 (2007): 387-403. *SCOPUS*. Web. 4 August 2010.
- Voet, D.; Voet, J.G.; Pratt, C.W. *Fundamentals of Biochemistry*, 3<sup>rd</sup> ed.; John Wiley & Sons, Inc.: New Jersey, 2008; pp 505.
- Watanabe, D., et al. "Quantitative Evaluation of each Catalytic Subsite of Cathepsin B for Inhibitory Activity Based on Inhibitory Activity-Binding Mode Relationship of Epoxysuccinyl Inhibitors by X-Ray Crystal Structure Analyses of Complexes." *Journal of Molecular Biology* 362.5 (2006): 979-93. Web.
- Watson, C. J., and P. A. Kreuzaler. "The Role of Cathepsins in Involution and Breast Cancer." *Journal of mammary gland biology and neoplasia* 14.2 (2009): 171-9. *SCOPUS*. Web. 4 August 2010.
- Wisastra, R., et al. "Isothiazolones; Thiol-Reactive Inhibitors of Cysteine Protease Cathepsin B and Histone Acetyltransferase PCAF." *Organic & biomolecular chemistry* 9.6 (2011): 1817-22. Web.
- Yamamoto, A., et al. "Structural Basis for Development of Cathepsin B-Specific Noncovalent-Type Inhibitor: Crystal Structure of Cathepsin B-E64c Complex." *Biochimica et Biophysica Acta - Protein Structure and Molecular Enzymology* 1597.2 (2002): 244-51. *SCOPUS*. Web. 4 August 2010.
- Zhu, Y., et al. "Inhibition of the Cathepsin Cysteine Proteases B and K by Square-Planar Cycloaurated Gold(III) Compounds and Investigation of their Anti-Cancer Activity." *Journal of inorganic biochemistry* 105.5 (2011): 754-62. Web.